Université Lille I - Sciences et Technologies

Laboratoire de Mécanique de Lille (UMR CNRS 8107)

Ecole Doctorale SPI Lille Nord-de-France

Année 2014 - N° d'ordre : 41480

THESE

Pour obtenir le grade de

Docteur de l'Université Lille I - Sciences et Technologies

Discipline : Génie Civil

Présentée par

Yu ZHANG

Etude expérimentale et modélisation du comportement mécanique d'une roche tendre

Soutenue publiquement le 24 juillet 2014 devant le jury composé de

M. FS LIU, Professeur, Université d'Agriculture de Shandong, Chine, Rapporteur
M. HQ WANG, Professeur, Université du Havre, Rapporteur
M. N BURLION, Professeur, Université Lille I, Membre
M. D KONDO, Professeur, Université Paris 6, Membre
Mme. Y JIA, Maître de conférences, Université Lille I, Co-encadrant
M. JF. SHAO, Professeur, Université Lille I, Directeur de thèse

Université Lille I - Sciences et Technologies

Laboratoire de Mécanique de Lille (UMR CNRS 8107)

Ecole Doctorale SPI Lille Nord-de-France

Année 2014 - N° d'ordre : 41480

THESE

Pour obtenir le grade de

Docteur de l'Université Lille I - Sciences et Technologies

Discipline : Génie Civil

Présentée par

Yu ZHANG

Etude expérimentale et modélisation du comportement mécanique d'une roche tendre

Soutenue publiquement le 24 juillet 2014 devant le jury composé de

M. FS LIU, Professeur, Université d'Agriculture de Shandong, Chine, Rapporteur
M. HQ WANG, Professeur, Université du Havre, Rapporteur
M. N BURLION, Professeur, Université Lille I, Membre
M. D KONDO, Professeur, Université Paris 6, Membre
Mme. Y JIA, Maître de conférences, Université Lille I, Co-encadrant
M. JF. SHAO, Professeur, Université Lille I, Directeur de thèse

Remerciment

This research work was carried out in the ER4 group at the Laboratoire de Mécanique de Lille (LML). I would like to express my deepest gratitude to all those people who have helped and encouraged me in the successful completion of my doctoral study.

First and foremost, I would like to give my most sincere thanks to my supervisors, Prof. SHAO Jianfu and Dr. JIA Yun , for their guidance, kindness, stimulating discussion and continued advice permanent support over past four years. With his enormous help and supervisions, I have obtained a lot of precious research experience such as scientific thinking, knowledge in geomaterials, as well as laboratory techniques. It was truly a great pleasure and privilege to study under his mentorships.

Also I would like to express my heartfelt thanks to Dr. BIAN Hanbing, for his help, discussions, sharing, valuable suggestions as well as the time and patience they spent in reading and correcting the manuscript of this dissertation. It's such a pleasure to work in their guidance.

My special thanks go to Prof. XU Weiya from Hohai University. Prof. XU Weiya is such a virtuous, kind and generous mentor who provided me with guidance, encouragement and support for my study and my career plans. I respect and appreciate him very much.

I would like to express my thanks to Prof. Wang Huaqing and Prof. Liu Fusheng for accepting to be the reviewers of the manuscript of my thesis and the committee members of my defense. I'm so grateful for their time and precious opinions towards this thesis. I would like to sincerely thank Prof. Djimedo Kondo and Prof. Nicolas Burlion for accepting to be the committee members of my defense. I truly appreciate your time and your helpful comments.

My sincere thanks go to all my colleagues for all the help, discussions, and sharing. To Dr. SHEN Wanqing and Dr. XIE Shouyi, thanks for all the kind help and valuable advice. To LIU Zaobao, ZHENG Lifeng and LI Mingyao, it's such a pleasure to work with you in the same office for four years. Also many thanks go to LIANG Yue, CHENG Long, ZENG Tao, Liu Lin, LIU Taogen, LI Ling… It is truly my honor to work with all of you. I would like also to thank my friends, XIAO Yue,YANG Wendong,… for their friendship and big supports.

In particular, I wish to thank the China Scholarship Council (CSC), which offered me the opportunity to pursue my PhD study in France.

Finally, my parents and wife are always there for me with their supports and unconditional love throughout, for which my mere expression of gratitude does never suffice.

Résumé

Cette thèse s'inscrit dans le cadre des recherches et vise à contribuer à la compérension du comportement mécanique d'une roche tendre (i.e. cataclastique grès). La roche étudiée se trouve dans une fondation d'un barrage, situé dans le sud-ouest de la chine. L'accent de des travaux réalisés dans cette thèse a concerné le comportement à long terme du matériau étudié.

Pour caractériser le comportement mécanique et identifier les principaux paramètres qui le gouvernent, il était nécessaire d'aborder en premiére lieu avec une approche expérimentale. De nombreux essais ont été réalisé, tel que des essais de compression, des essais de fluage triaxiale et des mesures de perméabilité. On constate que la réponse mécanique du matériau dépends fortement la microstructure et les propriétés mécaniques ainsi que les contraintes appliquées. En se basant sur les résultats expérimentaux, un modèle unifiée est proposé pour décrire le comportement à court terme et à long terme du matériau étudié. Dans le modèle proposé, les principales caractéristiques observées dans les expériences sont prises en compte, en particulier des déformations irréversibles, la dépendance de la pression, la transition volumétrique entre le compaction et la dilatation ainsi que le fluage. La performance du modèle proposé est tout d'abords validé sur les essais homogènes. A la fin, une validation plus poussée de ce modèle a été réalisée dans le cadre d'applications à étudier la performance de la fondation.

Mot clés: cataclastique grès, fluage, endommagement, permeabilité, à long terme, comportement mécanique

Abstract

The short term and long term mechanical behaviors of cataclastic sandstone are investigated in this dissertation. The studied material is cored from the fault zone in the dam foundation of a hydropower station in southwestern China. The emphasis is put on the long-term behavior of studied material.

For this, conventional compression tests, multi-stage triaxial creep tests as well as the permeability measurements are performed. The mechanical behavior of studied rock is derived based on the experimental investigation. The mechanical responses of studied material are not only functions of the material properties, but are also related to applied stress. Based on the experimental investigation, a unified creep model is proposed to describe the instantaneous and time-dependent behavior of cataclastic sandstone. Main features observed in experiments are taken into account, in particular irreversible deformations, pressure dependency, volumetric transition between compaction and dilatancy and creep. The performance of the model is examined by comparing numerical simulations with test data in representative load paths. Finally, the model is applied to analyze the long term stability of a foundation of hydropower station

Keywords: Cataclastic sandstone; creep; damage; permeability; long terme; mechanical behavior

Table of content

Remerciment ..... **i**

Résumé ..... **I**

Abstract ..... **I**

Table of content ..... **i**

List of Figures ..... **i**

List of Tables ..... **i**

General introduction **1**

I. Research background and Engineering applications *1*

II. Review of research *2*

Chapter 1. Experimental investigations on strength and deformation behavior of cataclastic sandstone **6**

1.1. Introduction *6*

1.2. Physical properties of tested rock *7*

1.2.1. Starting material 7

1.2.2. Mineral composition and microstructure 8

1.2.3. Sonic wave velocity of specimen 10

1.3. Testing procedures *11*

1.3.1. Test equipment 11

1.3.2. Test procedures 11

1.4. Results for the short term test *13*

1.4.1. Hydrostatic compression test 13

1.4.2. Uniaxial compression test 14

1.4.3. Triaxial compression tests under various confining pressures 15

1.4.4. Direct shear strength 18

1.5. Discussion of triaxial compression tests *21*

1.5.1. Behavior of volumetric strain 21

1.5.2. Process of specimens failure 23

1.6. Conclusions *24*

Appendix: *26*

Chapter 2. Creep behaviors and permeability evolution of cataclastic sandstone in triaxial creep tests **28**

2.1. Introduction *28*

2.2. Permeability behavior under natural state *30*

2.3. Experimental procedures *32*

2.4. Creep deformation behavior under one-step loading procedure *34*

2.5. Creep deformation behavior under multi-step loading procedure *35*

2.5.1. Behavior of axial strain 35

2.5.2. Behavior of lateral strain 41

2.5.3. Behavior of volumetric strain 42

2.6. Permeability variations during time dependent deformation *44*

2.6.1. Permeability change with the time dependent deformation 45

2.6.2. Permeability evolution with the confining pressure and fluid flow pressure 48

2.7. Stress-strain curves during creep tests *49*

2.8. Strain rate analysis and long term strength *51*

2.8.1. creep strain rate analysis 51

2.8.2. Long term strength 54

2.9. SEM experiments and creep failure mode *56*

2.10. Conclusions *57*

Chapter 3. Numerical modeling of mechanical behaviour of cataclastic sandstone **60**

3.1. Introduction *60*

3.2. General framework *61*

3.3. Specific model for studied sandstone *65*

3.4. Identification of model's parameters *69*

3.5. Parametric study *70*

3.5.1. Influences of drained Young's modulus E_0 71

3.5.2. Influences of initial yield surface paramter α_p^0 72

3.5.3. Influences of failure surface parameter A_0 73

3.5.4. Influences of parameter η 74

3.5.5. Influences of parameter B 75

3.5.6. Influences of creep parameter γ 77

3.6. Simulation of short term laboratory tests 78

3.7. Simulation of long term laboratory tests 78

3.8. Discussion 82

3.9. Conclusions 83

Chapter 4. Study on the long-term stability of the bedrock of a hydro-power station 85

4.1. Introduction 85

4.2. General situation of the project 86

4.3. Governing equations for poroelastic coupling in saturated media 87

4.4. Numerical model and parameters 89

4.5. Numerical analysis of the stability of dam foundation 92

4.5.1. Numerical results of dam construction phase 92

4.5.2. Numerical results of water impoundment phase 96

4.5.3. Numerical results of operation phase 102

4.6. Parametric study 106

4.6.1. Influence of Young's Modulus E 107

4.6.2. Influence of parameter A 110

4.6.3. Influence of permeability parameter P_w 113

4.6.4. Influence of creep rate γ 115

4.7. Conclusion 118

Chapter 5. Conclusions and Perspectives 120

References: 123

List of Figures

Fig. 1.1 Geological distribution of cataclastic sandstone....8
Fig. 1.2 Average physical parameters of cataclastic sandstone. The error bar spans from the minimum to maximum measured values....9
Fig. 1.3 Average mineral compositions of cataclasic sandstone under X-Ray test. The error bar spans from the minimum to maximum measured values....9
Fig. 1.4 Photomicrographs of various thin sections of cataclasic sandstone....10
Fig. 1.5 Average chemical compositions of cataclasic sandstone. The error bar spans from the minimum to maximum measured values....10
Fig. 1.6 Rock servo-controlled triaxial creep equipment....12
Fig. 1.7 Self-equilibrium triaxial pressure chamber system....13
Fig. 1.8 Typical stress-strain curve for cataclasic sandstone in hydrostatic compression test....14
Fig. 1.9 Typical stress-strain curve for cataclasic sandstone in uniaxial compression test....15
Fig. 1.10 Stress strain curves under confining pressure of 1.0MPa....16
Fig. 1.11 Stress strain curves under confining pressure of 1.5MPa....17
Fig. 1.12 Stress strain curves under confining pressure of 2.0MPa....17
Fig. 1.13 Shear stress-strain behavior of cataclastic sandstones....21
Fig. 1.14 Volumetric strain curves under different confining pressures....22
Fig. 1.15 Typical complete stress-strain curve in triaxial compression test....23
Fig. 1.16 Typical failure pattern of cataclastic sandstone....24
Fig. 2.1 Triaxial creep test results under one-step loading procedure....35
Fig. 2.2 Triaxial creep test results under natural state....36
Fig. 2.3 Triaxial creep test results under 0.25 simultaneous water pressure....37
Fig. 2.4 Triaxial creep test results under 0.35 simultaneous water pressure....38
Fig. 2.5 Axial and lateral creep curves under 0.35 simultaneous water pressure....41
Fig. 2.6 Volumetric creep curves under natural state....43
Fig. 2.7 Volumetric creep curves under 0.25MPa simultaneous water pressure....43
Fig. 2.8 Volumetric creep curves under 0.35MPa simultaneous water pressure....44

Fig. 2.9 Axial strain and permeability evolution cures under CP of 1.0MPa 46
Fig. 2.10 Axial strain and permeability evolution cures under CP of 1.5MPa 47
Fig. 2.11 Axial strain and permeability evolution cures under CP of 2.0MPa.....47
Fig. 2.12 Relationship between permeability evolutions and stress 49
Fig. 2.13 Creep stress-strain curve under 0.35MPa simultaneous water pressure.....51
Fig. 2.14 Relationship between axial strain rates and time under 0.35MPa simultaneous water pressure 52
Fig. 2.15 Relationship between axial creep rates and deviatoric stress level under 0.35MPa simultaneous water pressure 53
Fig. 2.16 Relationship between steady-state creep rate and confining pressure under 0.35MPa simultaneous water pressure 53
Fig. 2.17 Relationship between steady creep rates and level stress under 0.35MPa simultaneous water pressure 55
Fig. 2.18 SEM observations for specimen after creep failure under no simultaneous water pressure 57
Fig. 2.19 SEM observations for specimen after creep failure under 0.35MPa simultaneous water pressure 57
Fig. 3.1. Illustrationof plastic yielding surface, failure surface and compaction/dilatation boundary in $p-q$ plan for studied sandstone.....66
Fig. 3.2. Influence of cohesion parameter C_0 on the failure surface 67
Fig. 3.3. Influence of frictional coefficient A_0 on the failure surface.....67
Fig. 3.4. Evolution of yield surface with plastic hardening function.....68
Fig. 3.5. Evolution of Plastic hardening function α_p versus plastic deviatoric strain γ_p 70
Fig. 3.6. Influence of elastic parameters E_0 on the strain-stress curves of triaxial compression test with the confining pressure 2MPa 71
Fig. 3.7. Influence of elastic parameters E_0 on creep deformation with the confining pressure 2MPa 72

Fig. 3.8. Influence of α_p^0 on the strain-stress curves of triaxial compression test with the confining pressure 2MPa 73
Fig. 3.9. Influence of α_p^0 on creep deformation with the confining pressure 2MPa 73
Fig. 3.10. Influence of A_0 on the strain-stress curves of triaxial compression test with the confining pressure 2MPa 74
Fig. 3.11. Influence of A_0 on creep deformation with the confining pressure 2MPa 74
Fig. 3.12. Influence of η on the volumetric deformation of triaxial compression test with the confining pressure 2MPa 75
Fig. 3.13. Influence of η on creep deformation with the confining pressure 2MPa 75
Fig. 3.14. Influences of B on the strain-stress curves with the confining pressure 2MPa 76
Fig. 3.15. Influences of B on creep deformation with the confining pressure 2MPa 77
Fig. 3.16 Influences of γ on creep deformation with the confining pressure 2MPa 77
Fig. 3.17. Simulation of triaxial tests under different confining pressures. 78
Fig. 3.18 Simulation of creep tests performed on natural samples 80
Fig. 3.19 Simulation of creep tests under the water pressure 0.25MPa 81
Fig. 3.20 Simulation of creep tests under the water pressure 0.35MPa 82
Fig. 3.21. Diminution of elastic modulus with time under water pressure 0.35MPa 83
Fig. 3.22. Variation of stationary state of microstructure evolution under various water pressures 83
Fig. 4.1 Location of Hydropower Station in southwestern China 87
Fig. 4.2 Geological distribution of deflection fractured zone 87
Fig. 4.3 Geometrical domain and boundary conditions of studied field 91
Fig. 4.4 Detail of two dimensional finite-element grid of zone studied 91
Fig. 4.5 Distribution of horizontal displacements in the foundation at the end of construction phase 93
Fig. 4.6 Evolution of horizontal displacements on the upper and lower boards and in the middle of foundation at the end of construction phase 93
Fig. 4.7 Distribution of vertical displacements in the foundation at the end of construction phase 93

Fig. 4.8 Evolution of vertical displacements on the upper and lower boards and in the middle of foundation at the end of construction phase.....94
Fig. 4.9 Distribution of horizontal stress σ_{xx} in the foundation at the end of construction phase ...94
Fig. 4.10 Evolution of horizontal stress σ_{xx} on the upper and lower boards and in the middle of foundation at the end of construction phase.....95
Fig. 4.11 Distribution of vertical stress σ_{yy} in the foundation at the end of construction phase.....95
Fig. 4.12 Evolution of vertical stress σ_{yy} on the upper and lower boards and in the middle of foundation at the end of construction phase.....95
Fig. 4.13 Distribution of hardening parameter α_p in the foundation at the end of construction phase 96
Fig. 4.14 Evolution of hardening parameter α_p on the upper and lower boards and in the middle of foundation at the end of construction phase.....96
Fig. 4.15 Distribution of liquid pressure P_w in the foundation at the end of water impoundment phase.....97
Fig. 4.16 Evolution of liquid pressure P_w on the upper and lower boards and in the middle of foundation at the end of water impoundment phase 97
Fig. 4.17 Distribution of horizontal displacement in the foundation at the end of water impoundment phase.....98
Fig. 4.18 Evolution of horizonta displacement on the upper and lower boards and in the middle of foundation at the end of water impoundment phase 98
Fig. 4.19 Distribution of vertical displacement in the foundation at the end of water impoundment phase.....99
Fig. 4.20 Evolution of vertical displacement on the upper and lower boards and in the middle of foundation at the end of water impoundment phase 99
Fig. 4.21 Distribution of horizontal stress σ_{xx} in the foundation at the end of water impoundment phase.....100

Fig. 4.22 Evolution of horizontal stress σ_{xx} on the upper and lower boards and in the middle of foundation at the end of water impoundment phase 100
Fig. 4.23 Distribution of vertical stress σ_{yy} in the foundation at the end of water impoundment phase 100
Fig. 4.24 Evolution of vertical stress σ_{yy} on the upper and lower boards and in the middle of foundation at the end of water impoundment phase 101
Fig. 4.25 Distribution of hardening parameter α_p in the foundation at the end of water impoundment phase 101
Fig. 4.26 Evolution of hardening parameter α_p on the upper and lower boards and in the middle of foundation at the end of water impoundment phase 102
Fig. 4.27 Distribution of liquid pressure P_w in the bedrock at 500 years 102
Fig. 4.28 Evolution of liquid pressure P_w on the lower line of bedrok 103
Fig. 4.29 Distribution of horizontal displacement in the bedrock at 500 years 103
Fig. 4.30 Evolution of horizontal displacement on lower line of the bedrock 104
Fig. 4.31 Distribution of vertical displacement in the bedrock at 500 year 104
Fig. 4.32 Evolution of vertical displacement on the upper line of the bedrock 104
Fig. 4.33 Distribution of horizontal stress σ_{xx} in the bedrock at 500 year 104
Fig. 4.34 Evolution of horizontal stress σ_{xx} on the lower board of the bedrock 105
Fig. 4.35 Distribution of vertical stress σ_{yy} in the bedrock at 500 year 105
Fig. 4.36 Evolution of vertical stress σ_{yy} on the upper board of the bedrok during the operation phase 106
Fig. 4.37 Distribution of hardening parameter α_p in the bedrock at 500 year 106
Fig. 4.38 Evolution of hardening parameter α_p on the upper board during the operation phase . 106
Fig. 4.39 Influence of the drained Young modulus of cataclastic sandstone on the horizontal displacement (lower line of bedrock) 108

Fig. 4.40 Influence of the drained Young modulus of cataclastic sandstone on the vertical displacement (upper liner of bedrock) 109
Fig. 4.41 Influence of the drained Young modulus of cataclastic sandstone on the horizontal stress (lower line of bedrock)..... 109
Fig. 4.42 Influence of the drained Young modulus of cataclastic sandstone on the vertical stress (upper line of bedrock)..... 110
Fig. 4.43 Influence of the drained Young modulus of cataclastic sandstone on the hardening parameter α_p (upper line of bedrock)..... 110
Fig. 4.44 Influence of the drained Young modulus of cataclastic sandstone on the liquid pressure in bedrock (lower line of bedrock)..... 110
Fig. 4.45 Influence of the parameter A on the horizontal displacement(lower line of bedrock) 111
Fig. 4.46 Influence of the parameter A on the vertical displacement (upper line of bedrock)..... 111
Fig. 4.47 Influence of the parameter A on the horizontal stress (lower line of bedrock)..... 112
Fig. 4.48 Influence of the parameter A on the verticalstress (upper line of bedrock)..... 112
Fig. 4.49 Influence of the parameter A on the hardening parameter α_p (upper line of bedrock) ... 112
Fig. 4.50 Influence of the parameter A on the liquid pressure (lower line of bedrock)..... 113
Fig. 4.51 Influence of the permeability of cataclastic sandstone on the liquid pressure (ower line of bedrock) 113
Fig. 4.52 Influence of the permeability of cataclastic sandstone on the horizontal displacement lower line of bedrock)..... 114
Fig. 4.53 Influence of the permeability of cataclastic sandstone on the vertical displacement (upper line of bedrock)..... 114
Fig. 4.54 Influence of the permeability of cataclastic sandstone on the horizontal stress (lower line of bedrock) 114
Fig. 4.55 Influence of the permeability of cataclastic sandstone on the vertical stress (upper line of bedrock) 115
Fig. 4.56 Influence of the permeability of cataclastic sandstone on the hardening parameter α_p (upper line of bedrock)..... 115

Fig. 4.57 Evolution of horizontal displacement on lower line of the bedrock under high creep rate 116
Fig. 4.58 Evolution of vertical displacement on upper line of the bedrock under high creep rate .. 117
Fig. 4.59 Evolution of liquid pressure on lower line of the bedrock under high creep rate 117
Fig. 4.60 Evolution of horizontal stress on lower line of the bedrock under high creep rate 117
Fig. 4.61 Evolution of vertical stress on upper line of the bedrock under high creep rate 118
Fig. 4.62 Evolution of hardening parameter α_p on upper line of the bedrock under high creep rate 118

List of Tables

Table 1.1 Mechanical parameters in triaxial compression tests 17
Table 1.2 Shear strength indexes under different normal force 18
Table 1.3 Stress and volumetric strain at points A and B 23
Table 1.4 Mineral compositions of cataclasic sandstone under X-Ray test 26
Table 1.5 Chemical compositions of cataclasic sandstone 26
Table 2.1 Results of permeability characteristics 31
Table 2.2 Chemical analysis of the experiment water 32
Table 2.3 Test schemes for triaxial creep test under one-step loading procedure 34
Table 2.4 Test schemes for triaxial creep test under multi-step loading procedure 34
Table 2.5 Creep strain values under natural state (mm) 39
Table 2.6 Creep strain values under 0.25MPa simultaneous water pressure (mm) 40
Table 2.7 Creep strain values under 0.35MPa simultaneous water pressure (mm) 40
Table 2.8 Threshold values for the creep tests under 0.35MPa simultaneous water pressure 42
Table 2.9 Volumetric creep strain values under natural state (mm) 44
Table 2.10 Volumetric creep strain values under 0.25MPa simultaneous water pressure (mm) 44
Table 2.11 Volumetric creep strain values under 0.35MPa simultaneous water pressure (mm) 44
Table 2.12 Long term strength for the creep tests under 0.35MPa simultaneous water pressure 56
Table 3.1. Typical values of model's parameters for studied sandstone 70
Table 4.1 Physical and elastic model's parameters for various materials of geometrical model 91
Table 4.2 Plastic model's parameters for various materials of geometrical model 92
Table 4.3 Definition of different calculations in parametric study for the cataclastic sandstone 107

General introduction

I. Research background and Engineering applications

Weak cataclastic rocks are frequently encountered in various applications of hydraulic engineering. Study of mechanical properties of such soft rocks is an important issue in the framework of stability analysis of these structures, such as dam foundation stability, reservoir subsidence, tunnel support design and hydraulic fracturing etc. (Chen et al. 2012). This dissertation is devoted to study the mechanical behavior of one weak cataclastic rock: catacalstic sandstone.

The term ‘‘cataclastic’’ is derived from the Greek word cataclase referring to purely mechanical deformation processes. The term ‘‘cataclastic rocks’’ refers to rocks wholly or partly formed by dominant cataclastic deformation processes at the progressive fracturing and commination of existing rock and mainly found associated with fault zones, i.e. tectonically fractured rocks. In general, cataclastic rocks belong to a family of sedimentary rocks. This rock is made up from stones due to the action of the erosion, carriage, sedimentation and diagenesis through decade thousands of years (Elodie and Christopher 2010; Lori and James 2012). As a result, it is characterized by a loose textual structure, a high moisture content, poor physical mechanical properties and poor cemented contacts (Burgi 1999; Habimana et al. 2002; Gudmundsson et al. 2010). As those geomechanical behaviors, cataclastic rock directly influences the safety on working site, the method and duration of construction and the long-term structural behavior. However, due to difficulties in getting undisturbed specimens and in performing laboratory tests, the short term and long term (creep) mechanical behaviors of such rocks are so far poorly understood and further experimental investigations are still needed.

The time-dependent behavior of rock is basic mechanical propertie of the rock material, which can be considered as an important base in explaining and analyzing the phenomena of geological tectonic movement, as well as predicting the long-term stability for rock engineering. Therefore, the time-dependent deformation of rock has a major impact on the long-term stability of structure (Horsrund et al. 1994). In the framework of a hydropower construction project in Southwest China (see Fig. 4.1-Fig. 4.2 in chapter 6), several tectonically fractured zones were encountered during preliminary investigations. This gives to the present study a good opportunity to investigate the

short term and long term (creep) mechanical behaviors of cataclastic sandstones.

The Li-meiwan fractured zone of deflection crosses the dam foundation of the Hydropower Station. Distribution and thickness of the fractured zone are relatively large, the width and thickness vary from 40m to 70m and from 10m to 60m respectively. It is exposed at the left bank of dam foundation. Because of multiphase tectonic actions, the fractured zone exists not only the low dip compressive rupture zone but also steep dip compressive rupture zone along the joints and faults which will have an important impact on the long-term stability of engineering structures. Cataclastic Sandstone is the main media of fractured zone and it has poor lithologic quality. Because the properties is complex and the tectonic is peculiar, comprehensive and accurate analyses to those rocks are very difficult to realize. But the mechanical behavior of such rocks would affect the stability of the entire dam foundation. Hence, based on the physical properties measurements, the creep behavior, constitutive model as well as the long-term stability of dam foundation should be investigated carefully.

II. Review of research

Joints, faults and fractured zones are often encountered in large hydropower projects. The mechanical behavior of soft rock plays an important role on the long-term stability of dam foundation, slope and underground caverns (Chen 2003; Xu et al. 2011). Therefore, their time dependent behavior is an important issue for the evaluation of structure stability and for the determination of reinforcement treatment (Horsrund et al. 1994; Tsai et al. 2008; Zhang et al. 2012; Zhang et al. 2013). As experimental test can provides a fast and direct estimation of its time dependent behavior as well as its deformation rules (Maranini and Brignoli 1999; Li and Xia 2000; Zhang et al. 2012), some uniaxial and triaxial creep results are available in the literature (Pacheco 1990; Chan 1997; Yang et al. 1999; Fabre and Pellet 2006; Brantut et al. 2013).

In general, three types of laboratory tests can be used to study the time dependent behavior of rocks, i.e., creep, relaxation, as well as loading tests at different stress or strain rates. As the creep test is easy to carry out, there are many available creep tests performed under uniaxial and triaxial loading in the literature. Moreover, the triaxial creep test can study the time-dependent behavior of rock under a stress state which is close to the in situ one. Therefore, the creep test is largely used in

the investigation the time dependent behavior of rock material (Pacheco 1990; Carter 1993; Boukharov 1995; Chan 1997; Yang 1999; Ma and Daemen 2006; Yang and Jiang 2010). However, most of these studies are devoted to describe the creep behavior of hard rocks (Ma and Daemen 2006; Xu et al. 2012). Few studies are available on the behavior of soft porous rocks (Dahou et al. 1995).

In the present study, the studied material, called cataclastic sandstone, located in the fracture zone of dam foundation in southwestern china. Because of a large scatter of geological and geomechanical properties, the mechanical behavior of cataclastic rocks is hard to be characterized. To acquire a better understanding of such kind of soft rocks, a series of laboratory test programmer and constitutive model were studied on cataclastic sandstones from a hydropower project in southwestern china. The diagram of technical route of this thesis is shown in Figure 1. It is composed of two parts. The first part is the experimental investigation, which is aimed at improving the understanding of the physical properties and mechanical behavior of cataclastic sandstone. Conventional compression tests, multi-stage triaxial creep tests as well as the permeability measurements are performed. Based the obtained experimental results, a unified constitutive model is proposed for the description of the mechanical behavior of cataclastic sandstone in the second part. The performance of proposed model is verified by simulation various laboratory tests. Finally, the proposed model will be used to analyze the stability of the foundation of hydropower station. Above all, this dissertation is decomposed into four chapters.

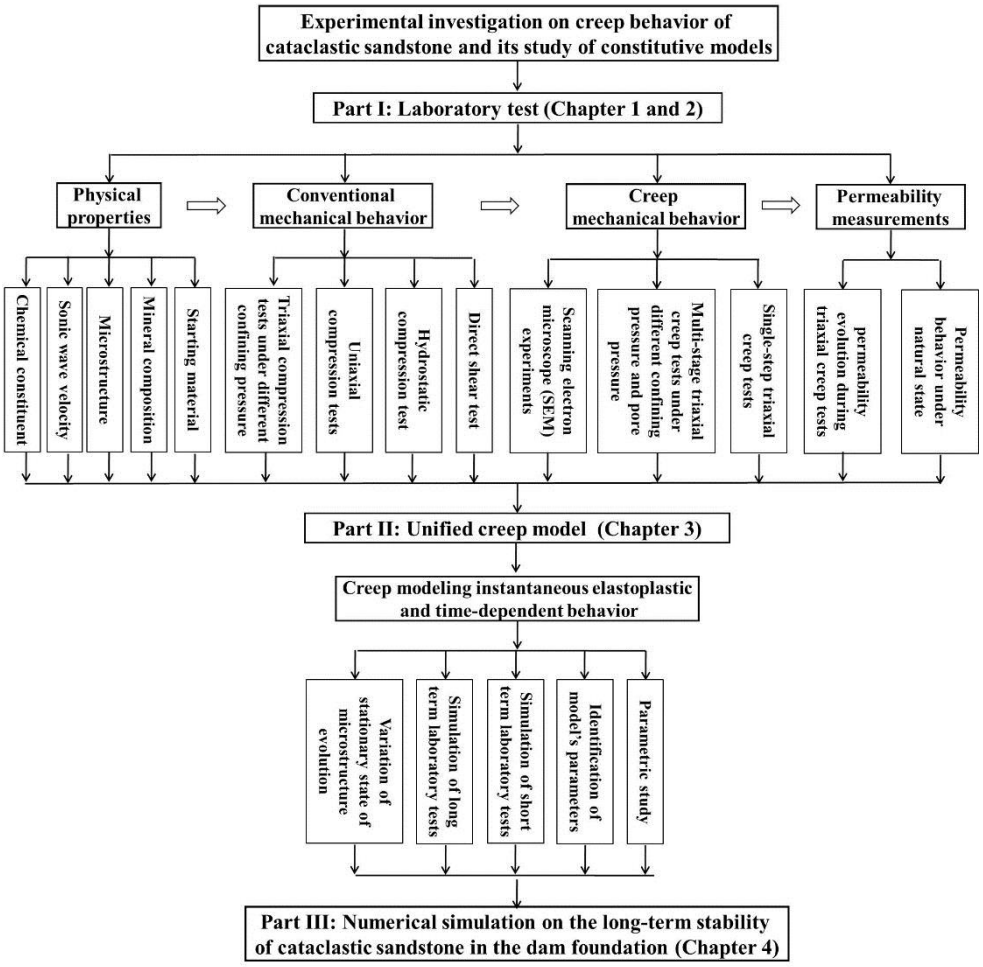

Figure 1 Diagram of technical route of the thesis

The first chapter focuses on the instantaneous behaviour of cataclastic sandstone. The mechanical properties of rock are generally related to their physical properties. Therefore, the physical properties of cataclastic sandstone such as water content, porosity, mineral composition and wave velocity are first examined in detail. Then a series of mechanical tests including hydrostatic, uniaxial, direct shear tests and triaxial compression tests under the various confining pressure are performed. The characterization of deformation and strength properties of cataclastic sandstones are obtained. The results will be used as basic data in the formulation of the constitutive model.

The second chapter consists to study the time-dependent behaviour of studied material. A series of multi-stage triaxial creep tests are performed. The creep behavior of axial strain, lateral strain and volumetric strain are analyzed in detail. In addition, an exponential relationship is

established for the evolution of creep strain rate. The long term strength can be defined as the critical point of expansion rate greater than the compression rate. Based on the SEM results obtained on the failure samples, the macro-micro creep failure mechanisms are also obtained. On the other hand, the permeability evolution of cataclastic sandstone during triaxial creep tests is measured. The experimental result revel the effects of time dependent deformation on the permeability behavior of the specimens.

Based on the experimental results obtained in previous two chapters, a unified creep model is proposed for the description mechanical behavior of cataclastic sandstone at different time scales. The time-dependent deformation can be described in terms of evolution of microstructure. This evolution is numerically simulated by a progressive degradation of elastic modulus and failure strength of studied material. Main features observed in experiments are taken into account, in particular irreversible deformations, pressure dependency, volumetric transitrion between compaction and dilatancy and creep. The performance of the model is examined by comparing numerical simulations of a series of triaxial compression tests and creep tests.

Finally, the proposed model is applied to study the stability of a dam foundation in which a cataclastic sandstone zone composed is presented. The numerical simulation is performed by using a fully coupled hydro-mechanical finite element code developed in Lille Mechanics Laboratory. Due to the presence of fault zone of cataclastic sandstone, an important displacement and damage is observed in cataclastic sandstone zone. Furthermore, a rapid equilibrium of liquid pressure is also obtained due to the great permeability of foundation materials. Finally, a series of parameter sensitivity are performed with different hydro-mechanical parameters for the fault zone in order to help engineers to complete their knowledge on the treatment of cataclastic sandstone zone.

Published in Rock Mechanics and Rock Engineering, DOI: 10.1007/s00603-014-0623-8

Chapter 1. Experimental investigations on strength and deformation behavior of cataclastic sandstone

Abstract: This chapter is devoted to the characterization of deformation and strength properties of cataclastic sandstones. The physical properties are first examined. These sandstones are characterized by a loose damaged microstructure and poorly cemented contacts. Then a series of mechanical tests including hydrostatic, uniaxial, direct shear tests and triaxial compression tests are performed to study the mechanical strength and deformation of sandstones. The results obtained show nonlinear stress- strain responses. The initial microcracks are closed at a hydrostatic stress of 2.6 MPa and the uniaxial compression strength is 0.98 MPa. Under triaxial compression, there is a clear transition from volumetric compressibility to dilatancy and a strong dependency on applied stress state. The results obtained in these tests will be used as basic data in the formulation of the constitutive model, which will be proposed in chapter 3.

Keywords: Soft rocks; cataclastic sandstone; physical properties triaxial compression test; strength and deformation

1.1. Introduction

Knowledge of the strength and deformability of rocks is an important issue for design, construction and stability evaluation of engineering structures (Chen et al. 2012). Furthermore, the mechanical properties of rock are not only influenced by its geometric characterization (such as constituent mineral composition, porosity and microstructure etc.) but also by the loading conditions (such as the climate change, the applied stress and the load duration etc.) (Meerea and Mulchrone 2003; Yang et al. 2008). In the laboratory, it can be identified by using a series of compression tests under different loading conditions.

The compression test can be divided into three categories, which include hydrostatic, uniaxial and triaxial tests. The triaxial compression test is by far the most common laboratory test that is used to measure the mechanical behavior (Yang et al. 2010). Generally, the material exhibits an evolution of the brittle behavior toward a ductile one as the confining pressure increases (Renner

and Rummel 1996; Hudson and Harrison 1997).

Over the years, a series of experimental studies, including microstructure analysis and mechanical behavior investigation of various soft rocks, have been performed (Homand and Shao 2000; Chen et al. 2003; De Gennaro et al. 2004). For instance, Li (2012) carried out a series triaxial compression tests for low porosity meta-sedimentary rocks, and investigated the influences of confining stress on strength, deformation and failure modes. The results show that strain hardening, softening and plastic behaviors depend on confining pressure and stress state. Furthermore, these works have shown that the mechanical behavior of soft rock is very complex, and characterized by various features: such as low material cohesion, strong pressure sensitivity, creep deformation, dependency on porosity and mineralogical compositions.

Under ordinary laboratory conditions, the presence of different mineralogical composition and the inherent complexity of their geometrical parameters and divers loading conditions make it difficult to measure directly the mechanical properties of rock (Fischer and Paterson 1989; Meerea and Mulchrone 2003; Yang et al. 2008). However, the effect of micro-structural parameters on the mechanisms of compaction and dilation have not yet been clearly identified (Homand and Shao 2000; Chen et al. 2003; De Gennaro et al. 2004; Li et al. 2012).In this view, a series of experimental study on the physical properties and mechanical behavior of cataclastic sandstone specimens are presented in this chapter. These results can provide a basis for the establishment of a constitutive model.

1.2. Physical properties of tested rock

As the mechanical properties of rock are generally related to their physical properties, this section is devoted to determine some physical properties of cataclastic sandstone such as water content, porosity, mineral composition, permeability and wave velocity.

1.2.1. Starting material

The cataclastic sandstone samples were cored from fresh intact blocks in the fractured zone of dam foundation, as shown in Fig. 1.1. The field and laboratory observations have revealed that the filling material of such quartz-based sandstones is mainly composed of sandy, feldspar and angular fragments. However, comprehensive and accurate mineralogical analyses of those rocks were

difficult due to the complex lithology and peculiar tectonics.

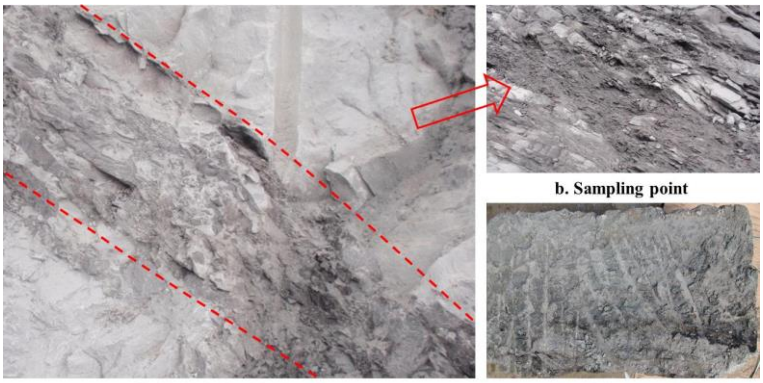

Fig. 1.1 Geological distribution of cataclastic sandstone

The physical properties have the characteristics of less specific gravity, loose damaged microstructure and poorly cemented contacts through qualitative analysis. Before the experimental study on mechanical behavior of the studied rock, the physical properties have been carefully examined. Basic physical properties of each specimen were measured quantitatively and the results showed that this rock had relative high heterogeneity (Fig. 1.2). Lu et al. (2005) considered that the sandstone could be classified according to different porosity, and in view of the porosity of this rock ranged from 13.1% to 22.0 % with an average value of about 17.9 %, it was small porosity sandstone.

1.2.2. Mineral composition and microstructure

Mineral composition determines not only the mechanical properties such as strength, capability of resistance deform but also the sensitivity of the rocks to environmental factors such as weathered, hydration and ground stress (Gudmundsson et al. 2010). On the other hand, the microstructure determines the physical parameters such as the porosity, water absorption. Based on the results of the optical microscope test, the mineral compositions as well as microstructure of cataclastic sandstone were analyzed. The experimental results exhibit that the main mineral compositions consist of quartz, chalcedony, feldspar, sericite, chlorite, a small amount of iron compounds and trace minerals (Fig. 1.3, detailed test results shown in **Appendix**, Table 1.4Table 1.4 Mineral compositions of cataclasic sandstone under X-Ray test). The principal trace minerals include tourmaline, zircon, phosphorites, zoisite, glauconite, etc.

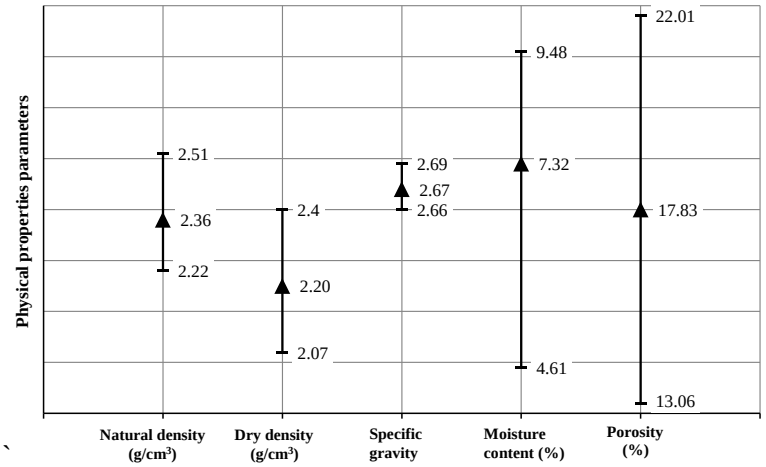

Fig. 1.2 Average physical parameters of cataclastic sandstone. The error bar spans from the minimum to maximum measured values

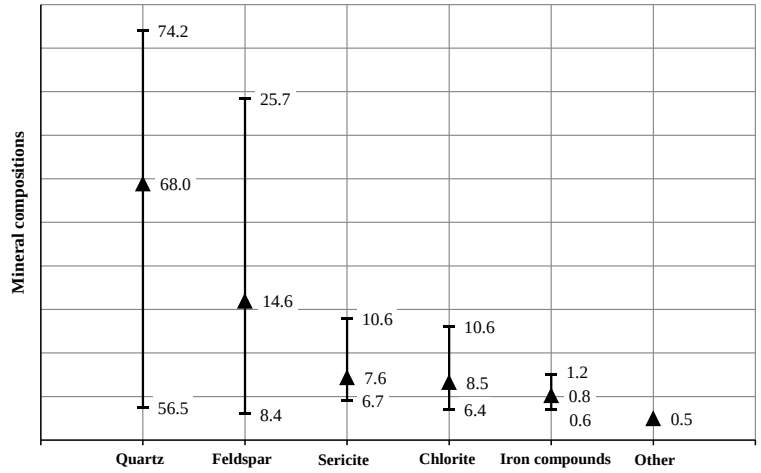

Fig. 1.3 Average mineral compositions of cataclasic sandstone under X-Ray test. The error bar spans from the minimum to maximum measured values

The results also indicated that this rock has still retained fine-grained texture and has an extremely complex microstructure (Fig. 1.4). In addition, the internal structure has been damaged seriously under impact of tectonic compression, weathered and groundwater. For the cementation type, the fragments distribution of quartz, debris and feldspar appear irregularly in different sizes. And fine-grained particles are disseminated in cement structure as sericite, chlorite, and so on. Mainly chemical constituent is composed of SiO_2, followed by Al_2O_3 and a small mixture of Fe_2O_3, CaO, MgO (Fig. 1.5, Detailed test results shown in **Appendix**,Table 1.5).

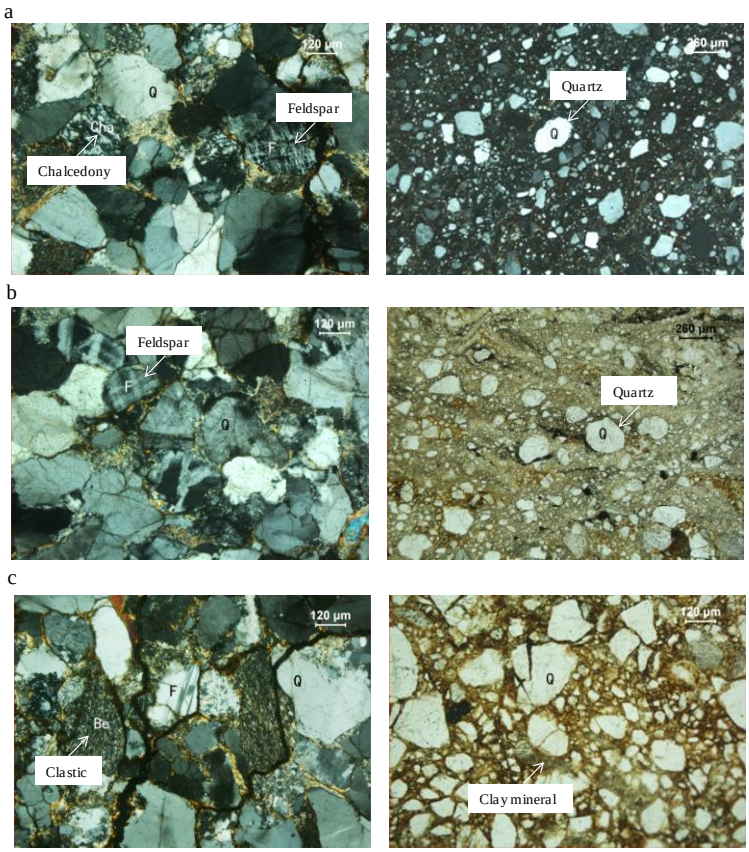

Fig. 1.4 Photomicrographs of various thin sections of cataclasic sandstone

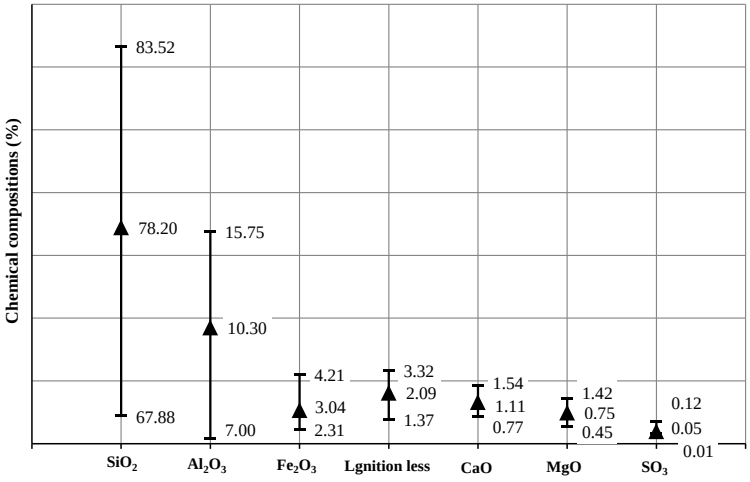

Fig. 1.5 Average chemical compositions of cataclasic sandstone. The error bar spans from the minimum to maximum measured values

1.2.3. Sonic wave velocity of specimen

Furthermore, sonic wave velocity of each rock specimen from various depths were measured, the wave velocity increased with increasing the test sample depth. The velocities vary from 2.0 to

2.5 km/s and 2.5 to 3.0 km/s across the depth of 0 to 1.6 m and 1.6 to 2.4 m. However, it is in a state of stability below the depth of 2.4 m in which value is 2.5 km/s. It is indicated that the specimen is more compact when the depth increases, and tends to be stable when the depth reaches 2.4m. Souley et al. (2001), Song et al. (2004) and Homand et al. (1993) obtained a closely relationship between the elastic modulus and wave velocity: the elastic modulus increases when the wave velocity is increased.

1.3. Testing procedures

1.3.1. Test equipment

In order to investigate the strength and deformation behavior of this material under the various confining pressures, direct shear tests, hydrostatic, uniaxial and triaxial tests were performed at room temperature (24±1.5 ℃) . The compression tests were conducted under drained condition using rock servo-controlled triaxial equipment which is developed by Laboratory of Mechanics in Lille (LML) (Fig. 1.6- Fig. 1.7) (Wang et al. 2013; Zhang et al. 2013). It includes a loading system, a constant-stability pressure equipment, a hydraulic pressure transfer system, a pressure chamber equipment, a water pressure system and an automatic data collection system. Its main accessory is self-equilibrium triaxial pressure system which is made up of three high-precision pumps controlling axial deviatoric pressure (P1), confining pressure (P2) and pore pressure (P3), respectively. The pressure is automatically regulated by the computer. Both the axial strain and lateral stain are properly recorded by the acquisition system according to the corresponding sensors. The computer robotized operations of this equipment are used to perform the controlled test safely, timely and precisely. The confining pressure and axial load are applied at a constant rate of 0.0125MPa/s.

1.3.2. Test procedures

Cylinder samples were used and carefully prepared from intact rock blocks extracted in the quarry of the fractured zone (see Fig. 1.1). The average sample size is 50 mm in diameter and 100 mm in height (see Fig. 1.16). Due to the very poor quality of some rock samples, extreme care was necessary in the handling of the specimens and some special preparations were required. For instance, the samples were stored by sealing technic. The preparation of samples for uniaxial

compression tests was even more difficult (no confinement) and several specimens were lost during the preparation.

The test procedure of triaxial compression tests is given as follows. The test begins with a hydrostatic compression phase, in which the axial stress and confining pressure increase simultaneously to the pre-established value. The confining pressure is loaded at a constant rate of 0.75 MPa/min. Afterwards, the confining pressure keeps constant and the axial stress continues to increase with a constant rate of 0.0125 MPa/s until the macroscopic failure of the sample.

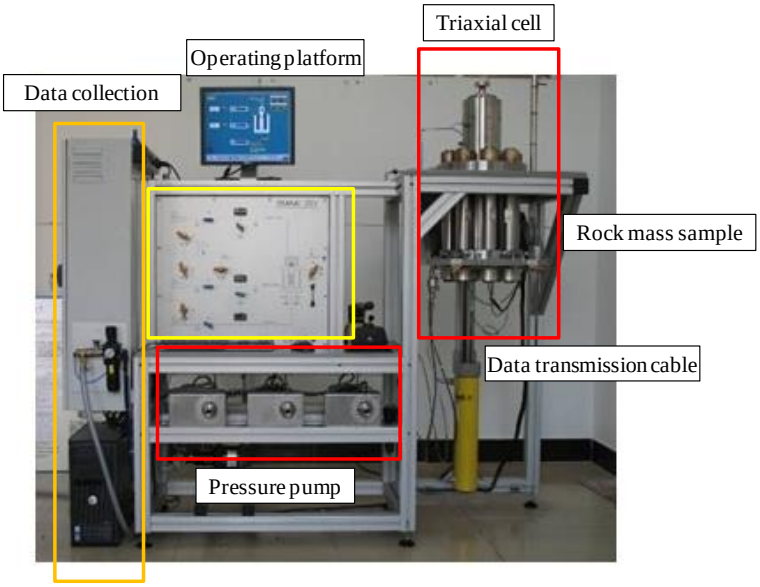

Fig. 1.6 Rock servo-controlled triaxial creep equipment

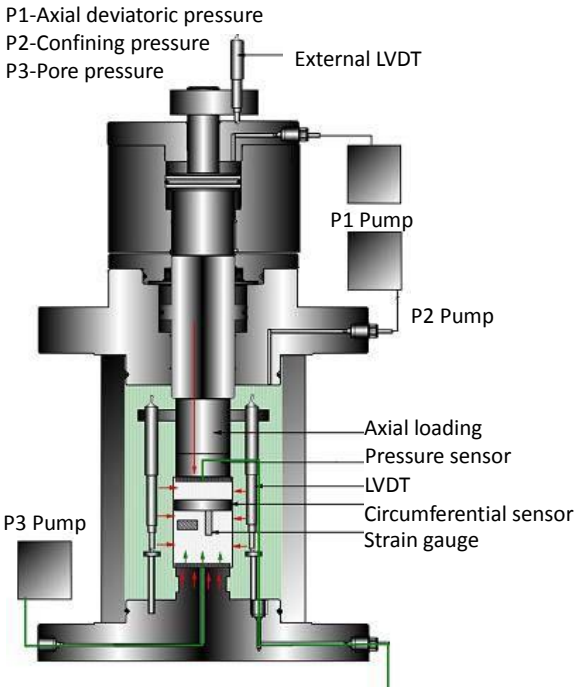

Fig. 1.7 Self-equilibrium triaxial pressure chamber system

1.4. Results for the short term test

The experimental results of different laboratory tests are presented in this section. We begins with the hydrostatic compression test.

1.4.1. Hydrostatic compression test

Drained hydrostatic compression tests were firstly performed. The axial strain versus hydrostatic stress curve is shown in Fig. 1.8. The applied confining pressure induces important volumetric strain in the sample. The volumetric strain-stress curve is strongly nonlinear. This phenomenon is mainly due to the compressibility of the pore system and closure of microcracks.

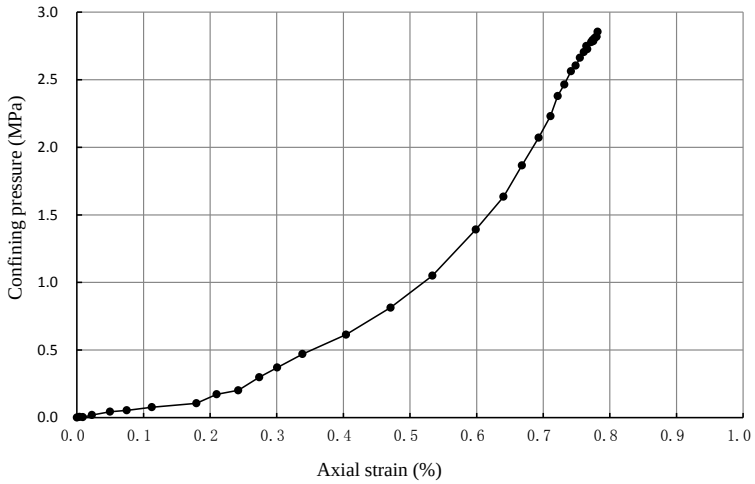

Fig. 1.8 Typical stress-strain curve for cataclasic sandstone in hydrostatic compression test

1.4.2. Uniaxial compression test

Uniaxial compression tests are carried out to study mechanical behavior of cataclastic sandstone subject to deviatoric stress. Typical stress- strain curves of unaxial compression tests are shown in Fig. 1.9 and six phases can be observed: (1) there is a slight inclination region (toe) due to closure of existing micro-cracks during the first stage of loading (OA). (2) A liner elastic deformation portion in which the matrix deforms and the material has an intact rock behavior, characterized by constant stiffness (AB). (3) When the applied stress is greater than the yield strength of studied material, an inelastic deformation is observed with significant increase of strain and micro-fracture begins to propagate in a stable manner (BC). Noted that the yield strength is the stress point at which stress-strain curves become non-linear. (4) After this, a plastic hardening stage in which the initiation and propagation of cracks result into strain increase in an unstable manner up to attaining peak stress and an asymptotic failure state is obtained (CD). (5) A post-peak softening phase is then observed. During this phase, the macro-crack coalesced and the rock is highly disrupted (DE), and (6) late post-failure stage, in which the samples are split in a series of block a (EF).

In general, the basic behavior of cataclasic sandstone is elastoplastic. To quantify the brittleness of the material based on the complete axial stress-strain curve, different brittle or ductile index can be used (Andreev 1995). In this study, the ratio of residual strength to the peak stress

($\lambda = \sigma_{tr} / \sigma_t$) is adopted as a measure for ductility of the sample. The material properties obtained from uniaxial tests are as follows: the uniaxial yield stress, peak stress and residual stress are 0.62 MPa (B), 0.89 MPa (D) and 0.74 MPa (F), respectively. And the Young's Modulus and ductile index are 79.2 MPa and 84 %.

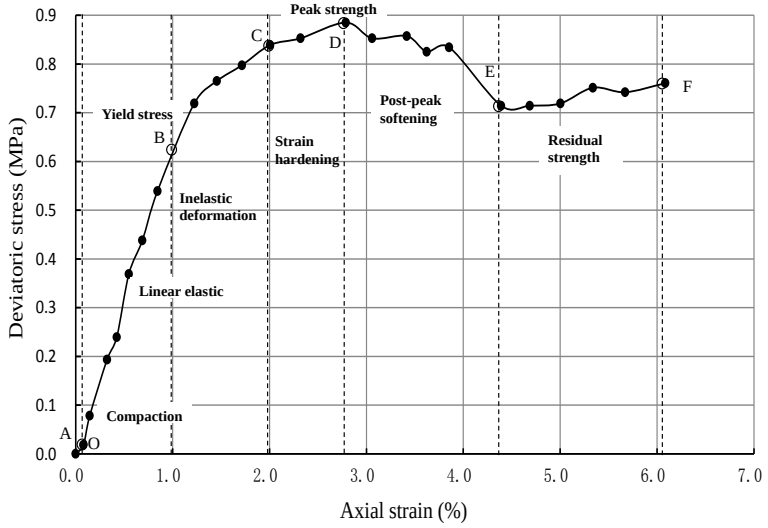

Fig. 1.9 Typical stress-strain curve for cataclasic sandstone in uniaxial compression test

1.4.3. Triaxial compression tests under various confining pressures

In order to reduce the influence of rock heterogeneity on the triaxial test results, repetitive triaxial compression tests were performed on the three specimens of each group with various confining pressures (Table 1.1). Typical stress-strain curves are presented in Fig. 1.10- Fig. 1.12 for different values of confining pressure, say 1.0, 1.5 and 2.0 MPa. Similar behaviors can be observed from all specimen series. Based on the experimental results, the basic mechanical properties of this rock can be summarized as follows:

(1) As most of the rock materials, the cataclastic sandstone exhibits a pressure dependent behavior. The strain increases when the stress increases. In a general way, the response can be decomposed into four phases for all tests. During the initial loading, a quasi-linear and reversible stress strain relation is obtained, this represents the elastic compressibility of rock skeleton and the elastic bulk modulus can be determined from the slope of the stress strain curve in this phase. When the stress reaches a limit value, called the yield stress, a nonlinear and plastic phase is observed with significant increase of strain, and the slope of curve decreases. With the increase of stress, a

generally strain hardening phase is produced due to an increase of contact surface between grains. Followed by a large axial and lateral strain, the phase of plastic failure is performed, where the cracks coalesce. This observation is similar to plastic consolidation in soil mechanics.

(2) Generally, significant low strength, no obvious peak stress and plastic failure is observed in the laboratory samples. The stress-strain curves show a plastic platform when the strain exceeds a limit value. On the other hand, in some laboratory tests, no post peak failure phase is observed. It is also worthwhile to point out that when the specimen failed, both axial and lateral strain achieve more than 3.5 %, which is much larger than that for hard rock.

(3) In addition, an important influence of confining pressure is observed. The peak stress increases with the increase of confining pressure (Table 1.1). This phenomenon has been observed in many rock materials (Renner and Rummel 1996; Hudson and Harrison 1997; Haimson 2006; Mogi 2007; Li et al. 2012).

(4) As the triaxial compression test begins with a hydrostatic phase, the rock is compacted and initial microcraks presented in the samples are closed. Therefore, the stiffness of rock increases with the increase of the confining pressure (Budiansky and O'Connell 1976). The values of Young's modulus and Poisson's ratio in different triaxial compression tests are given in Table 1.1.

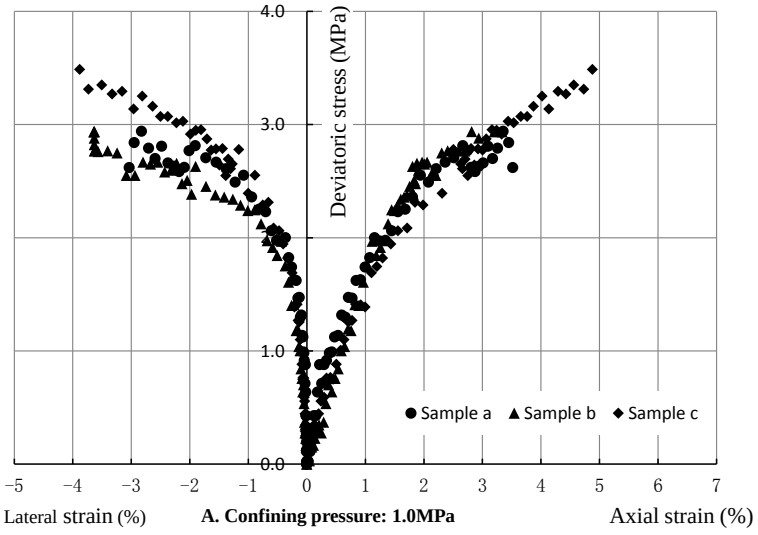

Fig. 1.10 Stress strain curves under confining pressure of 1.0MPa

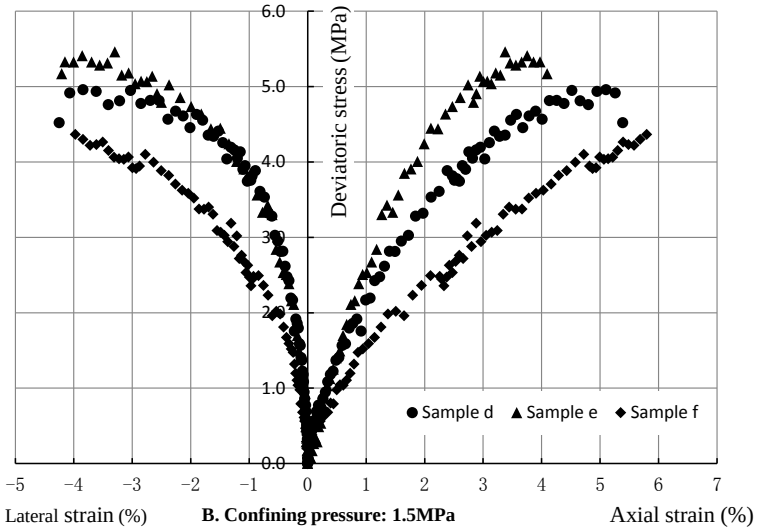

Fig. 1.11 Stress strain curves under confining pressure of 1.5MPa

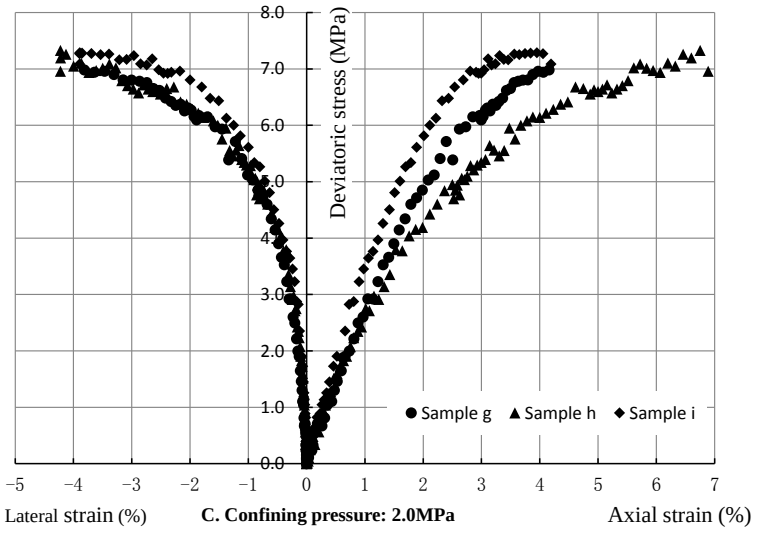

Fig. 1.12 Stress strain curves under confining pressure of 2.0MPa

Table 1.1 Mechanical parameters in triaxial compression tests

Sample	Confining pressure (MPa)	Peak stress (MPa)	Young's modulus (MPa)	Poisson's ratio
a	1.0	2.94	325	0.16
b	1.0	2.94	312	0.18
c	1.0	3.48	354	0.19
d	1.5	4.96	346	0.21
e	1.5	5.46	386	0.26

f	1.5	4.36	364	0.21
g	2.0	6.98	420	0.17
h	2.0	7.32	406	0.17
i	2.0	7.29	436	0.22

1.4.4. Direct shear strength

The laboratory large-scale direct shear tests were also carried out. In order to reduce the influence of rock heterogeneity on directs shear test results, repetitive directs shear tests were performed on the four groups with various vertical stresses (Table 1.2). Similar behaviors can be observed for all the samples. Typical shear stress-strain curves are plotted in Fig. 1.13 with different applied vertical stress. A linear elastic response is firstly observed at the beginning of the test. With the increasing shear stress (τ), the curve becomes nonlinear with an important increase in shears strain (ε). This phenomenon is due to the plastic yield of studied rock. Finally, the shear strain increases significantly and induces the failure of studied sample. Then a post-peak softening phase is observed after the peak shear stress. The shear strength decreases with the increase of the strain in this phase.

By comparing of the tests performed under different shear stress, it is observed that the level of vertical stresses have a significant impact on the form of shear stress-strain curve. In the early plastic yield, the curve shows the phenomenon of strain hardening. Moreover, the yield point increases as the vertical stress increases. And the increase in vertical stress (σ) induces an increase in the slope of curve and the peak value of shear stress. On the other hand, the softening characteristic is more important when the vertical stress is lower. Therefore, it is concluded that the softening behavior of the samples decreases with the increase of the vertical stress,. The relationship of residual and peak strength is given in Table 1.2.

Table 1.2 Shear strength indexes under different normal force

Types	Vertical stress（MPa)	Peak strength (MPa)	Residual strength (MPa)	Ratio
Group a	0.40	0.85	0.48	0.56

	0.80	1.21	0.84	0.70
	1.20	1.48	1.07	0.72
	2.00	1.87	1.58	0.84
Group b	0.40	1.44	1.30	0.90
	0.80	1.37	1.15	0.84
	1.20	2.19	2.04	0.93
	2.00	2.77	1.93	0.69
Group c	0.6	0.85	0.32	0.38
	0.9	1.20	0.62	0.52
	1.2	1.50	0.99	0.66
	1.5	1.64	1.23	0.75
Group d	0.3	0.51	0.30	0.59
	0.6	0.77	0.51	0.66
	0.9	0.83	0.63	0.76
	1.5	1.16	0.86	0.74

In a general way, the stress-strain curves are divided into four stages , i e., contact and compaction stage during the first stage of loading, linear elastic stage, nonlinear and plastic failure stage and post-peak softening stage. The residues and the peak strengths increased with increase of vertical stress. Moreover, the ratio between residues stress and the peak stress is gradually increased and tends to 1, indicating that the differences decrease gradually. However, some scatters are observed in the experimental results. This phenomenon is firstly due to the heterogeneous distribution of the muddy siltstone, siltstone and coal line in the samples which creates the heterogeneous deformation and local stress concentration. Furthermore, the permutations of studied rock related to the local smaller broken and dislocated induce also a stress drop. In addition, their cutting surfaces have more debris and contain a partial coal line.

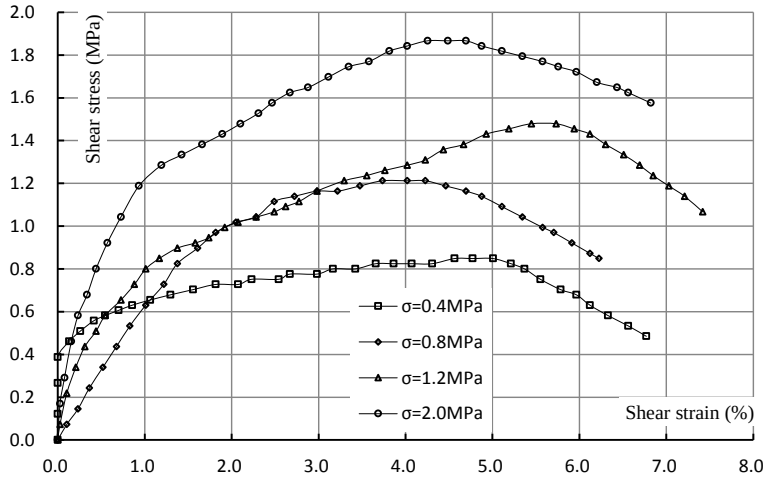

Group: a

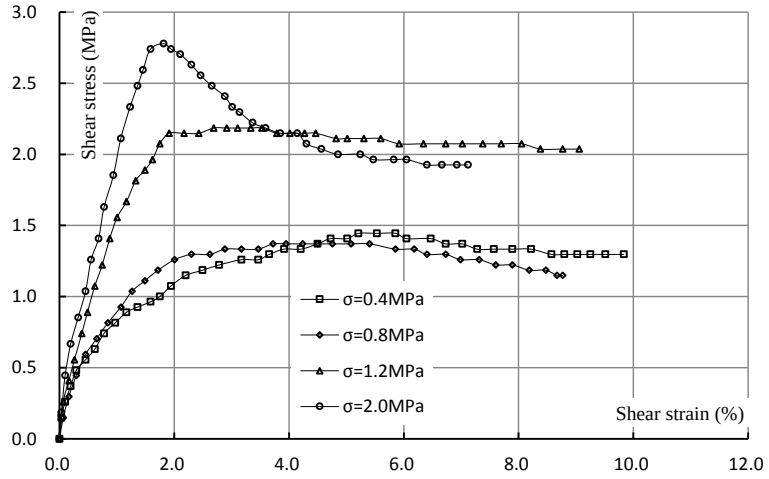

Group: b

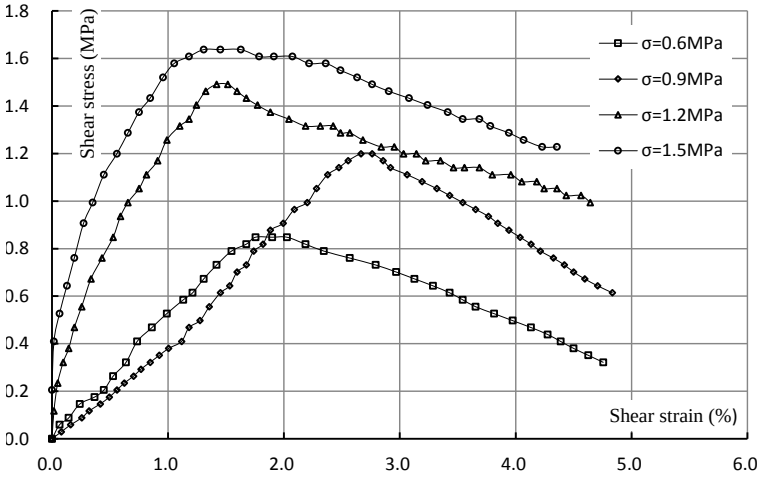

Group: c

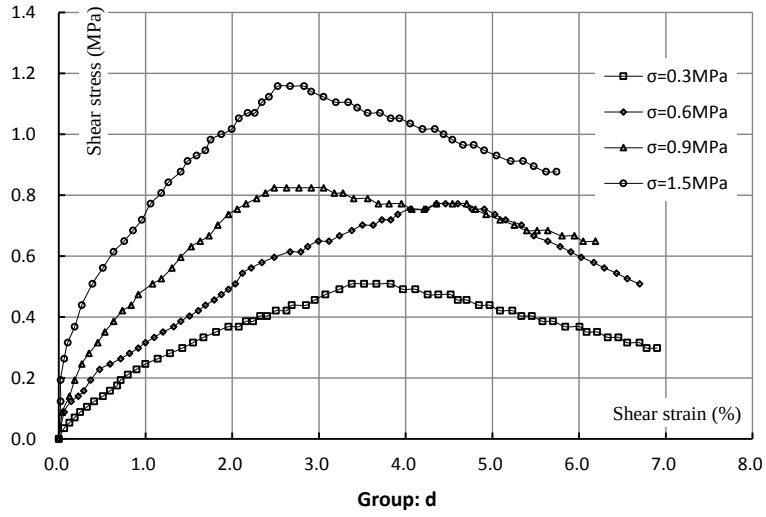

Fig. 1.13 Shear stress-strain behavior of cataclastic sandstones

1.5. Discussion of triaxial compression tests

1.5.1. Behavior of volumetric strain

Under the triaxial compression tests, large deformation and significant volumetric dilatancy are observed in cataclastic sandstone when the rock attains the rupture. It is shown that the specimens displayed obvious volumetric compressibility changes to dilatancy in the process of tests. Volumetric strain (ε_V) can be calculated according to

$$\varepsilon_V = -\Delta V / V_0 = \varepsilon_1 + 2\varepsilon_3 \tag{1.1}$$

where ε_1 and ε_3 represent the axial and lateral strain respectively. The measured volumetric strain versus stress is shown in Fig. 1.14. The volumetric strain can be divided into two stages. At the initial low stress, lateral strain is smaller and only the compressible strain is obtained continuously throughout elastic deformation, while the volumetric strain decreases with deviatoric stress. With the increase of deviatoric stress, the lateral expansion gradually becomes predominant resulting in volumetric dilatancy, and ductile behavior with distributed inelastic deformation. When it's failed, the volumetric strain increases rapidly, and trend to a perfect plastic.

The volumetric strain is closely related to the pressure. In the loading process, the volume change is mainly due to the propagation of micro-cracks. When the deviatoric stress is low, the primary micro-fissures are closed resulting in volume compression without generation of new

damage. With the increase of stress, the volume dilates as cracks propagation. Meanwhile, rock damage begins to develop. In the final stage, because of the coalescence of cracks, the rock volume dilates rapidly until large strain is observed in the sample. Typical complete stress-strain curve is shown in Fig. 1.15. The rock volume is compressed when the stress is less than 3.53 MPa. The volume reverses from compression to dilatation when the stress is more than 3.53 MPa. With further increase of stress, the volumetric strain rate increases rapidly and then keeps constant until failure.

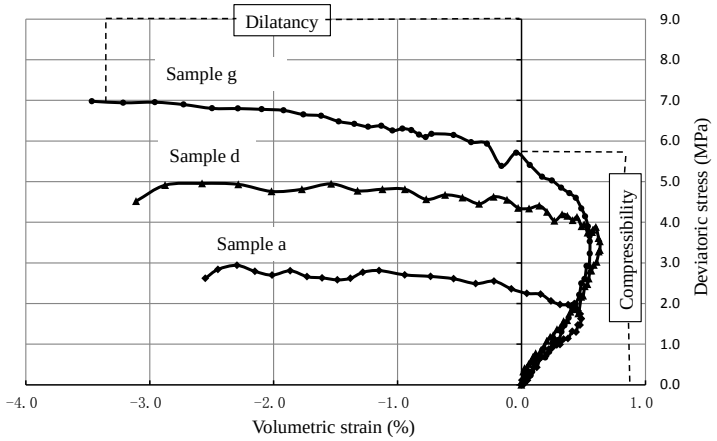

Fig. 1.14 Volumetric strain curves under different confining pressures

The points A and B in Fig. 1.15 represent the inflection of volumetric strain and the onset of dilation. The corresponding stress and strain values are shown in Table 1.3. The stress at point A increases with confining pressure. The point A also corresponds to the maximum of volume compressive strain. In general, when the confining pressure is higher, the maximum of compressive volumetric strain is larger. The confining pressure has also a significant effect on the volumetric transition point B where the volumetric strain changes from compressive to dilative. It is considered that confining pressure reinforces the strength of the rock.

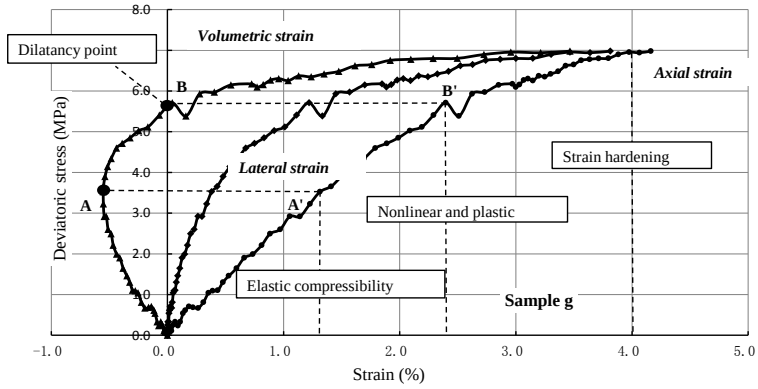

Fig. 1.15 Typical complete stress-strain curve in triaxial compression test

Table 1.3 Stress and volumetric strain at points A and B

Sample	Confining pressure (MPa)	Stress at point A (MPa)	Volumetric strain at point A (%)	Stress at point B (MPa)
a	1.0	1.63	0.48	2.33
b	1.0	1.18	0.39	1.97
c	1.0	1.82	0.64	2.54
d	1.5	3.53	0.63	4.35
e	1.5	2.10	0.26	3.42
f	1.5	1.96	0.44	3.37
g	2.0	3.53	0.55	5.70
h	2.0	4.70	0.91	6.60
i	2.0	3.45	0.50	5.33

1.5.2. Process of specimens failure

According the rock materials, four kinds of failure patterns are generalized in the previous study (Jaeger et al. 2007), which include brittle fracture, brittle shear, ductility and shear failure along weak planes. It can be remarked that the specimen failure is classically produced by the pore compression and cracks coalescence. It is a result of synthetic effect of the material defects and micro-cracks damage. The deformation of such rock shows diffusion of lattice dislocations, crack

expands and compatible deformation among grains. The rock has a different scale of initial micro-defects such as fissures, joints, dislocations etc. These microscopic behaviors control the macroscopic behavior of the rock. It is very easy for the micro-defects to slip and dislocate between grains and cleavages under loading, therefore, ductile deformation accompanied by moderate dilation or even compaction was shown in specimens without macroscopic fractures (Fig. 1.16).

The failure of a specimen may be due to the generation, growth and coalescence of micro-cracks. The process of failure was cracks originated from the initial defects firstly and the micro-movement is caused by the crystal displacement of mineral cleavages. And then the cracks begin to widen nonlinearly accompanied with the initiation and expansion of some new micro-cracks, which leads to the increase of strain. Meanwhile, the pore structure were changed and collapsed, which showed significant nonlinear plastic behavior. Followed by an increase of contact surface between grains would strengthen the mechanical properties. The volume deformation expands continuously and induces dilatancy. Finally the plastic deformation continued increasing and its rate also accelerated, which formed a yield platform. At this moment, the specimen was wholly yield which showed plastic flow and macro unstable ductile failure. Because the continuous damage of micro-fissures inside the specimens accumulated in the process of test, there are a number of small macro-cracks and ductile zones arising on the sample surface.

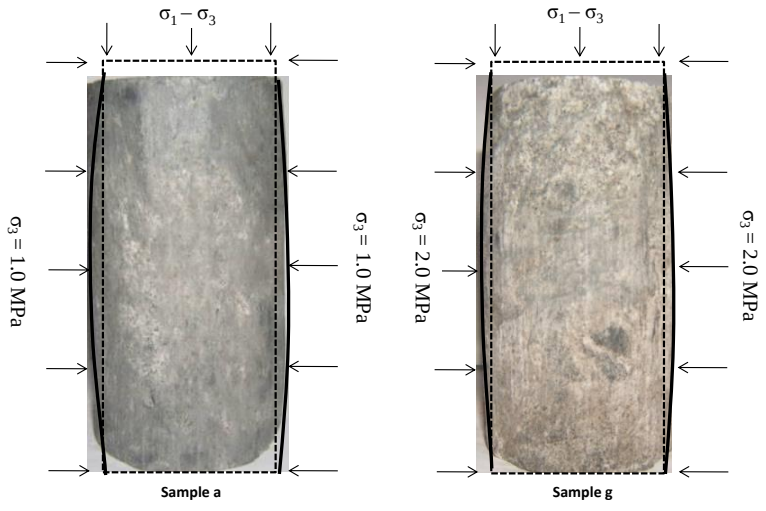

Fig. 1.16 Typical failure pattern of cataclastic sandstone

1.6. Conclusions

In order to systematically study the mechanical behavior of cataclastic sandstone, a series of tests were performed on specimens. It’s possible to formulate some main concluding remarks as follows:

- Based on the characteristics of loose damaged microstructure and poorly cemented contacts, the physical properties were examined first. It's considered that such rock which belongs to small porosity sandstone has an extremely complex microstructure. The main mineral compositions are quartz, feldspar, sericite and so on, main chemical constituent is SiO_2 and the chemical erosion is not significant.

- The hydrostatic, uniaxial and triaxial tests have been successfully conducted, including volumetric strain measurement. The results show that the internal micro-crack is fully compacted when hydrostatic pressure reaches 2.6 MPa. The uniaxial compression curve shows the characteristics of six distinct phases with a peak stress of 0.89 MPa.

- In triaxial compression tests, it is observed that the mechanical behavior of studied materials depends on the applied stress. Moreover, the strain-stress curves can be decomposed into four stages. The volumetric strain shows significant dilatancy and compression features. In addition, the maximum stress and transition point from compression to dilatancy generally increased with the increase of confining pressures. Therefore, the confining pressure can effectively enhance the strength of studied rock.

Appendix:

Table 1.4 Mineral compositions of cataclasic sandstone under X-Ray test

Sample	Quartz	Feldspar	Sericite	Chlorite	Iron compounds	Other
S1	68.7	12.1	7.5	10.2	1	0.5
S2	70.6	9.4	8.1	10.6	0.8	0.5
S3	69.3	12.8	7.2	9.4	0.8	0.5
S4	67	16.5	6.7	8.3	1	0.5
S5	64.9	17.3	7.4	9.1	0.8	0.5
S6	74.2	8.4	7.2	8.7	1	0.5
S7	73.5	11.3	7.2	6.8	0.7	0.5
S8	56.5	25.7	8	8.7	0.6	0.5
S9	61.5	24	6.8	6.5	0.7	0.5
S10	71.7	12.4	7.2	7.4	0.8	0.5
S11	63.7	13.8	10.6	10.2	1.2	0.5
S12	73.8	11.2	7.5	6.4	0.6	0.5

Table 1.5 Chemical compositions of cataclasic sandstone

Sample	Lgnition less	SiO_2	SO_3	Fe_2O_3	Al_2O_3	CaO	MgO
S1	1.39	83.19	0.00	2.31	8.04	1.19	0.50
S2	1.56	81.65	0.05	3.12	7.27	0.77	0.56
S3	1.50	80.75	0.00	2.92	8.54	0.91	0.55
S4	1.46	83.10	0.03	2.96	7.00	1.19	0.50
S5	2.10	82.40	0.01	2.47	9.05	1.05	0.45
S6	1.37	83.52	0.01	2.51	7.53	0.84	0.55

S7	3.01	71.38	0.12	4.21	13.38	1.34	1.42
S8	3.09	70.91	0.10	3.14	15.12	1.54	1.00
S9	2.75	73.89	0.01	3.13	13.27	1.32	0.90
S10	1.79	79.61	0.07	2.94	9.15	1.05	0.55
S11	1.78	79.66	0.09	3.39	9.55	1.05	0.70
S12	3.32	67.88	0.07	3.40	15.75	1.05	1.36

Chapter 2. Creep behaviors and permeability evolution of cataclastic sandstone in triaxial creep tests

Abstract: This chapter reports the results of triaxial creep tests of cataclastic sandstone. Meanwhile, the experimental data on the permeability is also presented in this chapter. The creep behaviors of studied rock and their effects on the permeability evolution have been analyzed in detail. The results show that the studied rock exhibits pronounced irreversible time-dependent deformations. The strain rate increases by exponential functions as the deviatoric stress increased and the confining pressure decreased. The long term strength can be defined as the critical point of expansion strain rate greater than the compression strain rate. In addition, important plastic deformation, obvious dilation and large strain rate are observed in the last stage of experimental tests. The permeability change shows some mutative correlation with the material porosity during the time-dependent deformation. But the trend of change is decreasing with the increases of deviatoric stress for all specimens. During the stage of steady creep, the permeability variation slowly decreases quasi-linearly. It indicates that the fluctuation has no significant effect on permeability evolution. These ensemble observations may provide a basis for the establishment of hydro-mechanical coupling creep model and the long term stability analysis of structures.

Keywords: Rock mechanics; cataclastic sandstone; triaxial creep test; permeability measurement; time-dependent deformation

2.1. Introduction

The creep behavior is an important mechanical property of geotechnical materials. As the basic mechanical properties of rock, creep characteristics directly relate to the long-term stability and security of the rock engineering. Not only soft rocks and clays, but for moderate strength rocks and hard rocks in high stress state also presents creep characters. And the creep properties of soft rock have bigger influence than hard rock. Furthermore, faults and fracture zones are often encountered for large hydropower projects, in which soft rock mass has adverse effects on the long-term stability of dam foundation. Therefore, it is important to study the time dependent deformation and failure characteristics of soft rock from fracture zone for the structural design, rock reinforcement and

long-term stability evaluation of engineering.

Due to the ubiquity of creep phenomena of rock, it's greatly important and urgent to study such mechanical properties and to produce a relational expression of constitutive model. Especially the soft rock under the fluid flow, its creep behavior are particularly significant, and have brought many uncertainty to the long-term stability of the projects, so studying on the creep and permeability mechanical properties, proposing an accurate constitutive model with the simulation and the prediction, are still difficulty and hotpots on research of rock creep theory. Therefore, it is crucial to understand the creep behavior by means of both laboratory tests and numerical methods. Experimental investigation on creep mechanics under the various confining pressure of rock is not only an important means of the research on creep mechanical properties, but also an important foundation for building constitutive model.

Based on the analysis in chapter 1, it is noted that the considered rock is a typical soft rock. Over the years, although different research programs have been performed on the studied rock, there are several phenomena have not been clearly identified:(1) the existence (or not) of a threshold for plastic creep deformations when a steady state creep strain rate (CSR) is observed under long term constant loading, (2) the influence of confining pressure (CP) on strain rate on the evolution of creep deformation, (3) the evolution of long term strength of studied rock , (4) divers physical mechanisms of creep deformation. Therefore, it is necessary to perform a series of laboratory tests to get a better understanding on these phenomena. As the impact of both confining pressure and applied stress on time-dependent behavior of studied rock can be incorporated simultaneously in a triaxial creep test, a series of triaxial creep tests are performed in this chapter. The obtained experimental results will be used to formulate a constitutive model which will be applied in study the long-term stability of a hydropower station.

In addition, faulty zones may act as barriers, conduits, or mixed conduits/barriers systems, which form important components of fluid flow regimes operating in the crust (Caine et al. 1996; Wibberley and Shimamoto 2003). Among the problems faced by rock engineers, the characterization of fluid flow through rocks in faulty zone is one of the greatest challenges, especially those in time-dependent deformation. Therefore, it is crucial discover how the permeability characteristics evolve within such rocks in time and space (Yasuhara et al. 2006),

which is significant to many engineering projects or scientific applications. In recent years, many studies have been focused on laboratory tests to estimate the permeability behavior of rock, and significant progress has been obtained in this domain (Barton et al. 1985; Zhu and Wong 1997; David et al. 2001; Ngwenya et al. 2003; Uehara and Shimamoto 2004; Wang and Xu 2013).

In general, the permeability changes are related to the closure and growth of micro-cracks (Hicks et al. 1996; Tang et al. 2002; Bojesen et al. 2009; Jiang et al. 2010; Wang et al. 2010). Moreover, numerous research results exhibits that the permeability behavior is more a 'process' than a 'material' property because it changes within one formation due to changed boundary conditions (e.g. stress, deformation) (Heiland 2003). On the other hand, the evolution of pore pressures controlled by the permeability has also an important impact on the mechanical behavior of porous media (e.g. stress, deformation). Therefore, the mechanical behavior and the evolution of permeability of porous media is a fully coupling problem (David et al. 1994; Souley et al. 2001; Gutierrez and Lewis 2002; Millard et al. 2005). Furthermore, the rock permeability depends strongly on both the geometry of the pore space within the rock and the prevailing stress environments (David et al. 2001, Souley et al. 2001). It is of fundamental importance in geophysics to indicate the interplays among mechanical deformation, microstructure evolution and fluid flow in rock material (Bai et al. 1999; Heiland and Raab 2001; Shao et al. 2005; Billiotte et al. 2008). However, the relationships between the permeability variation and the time-dependent deformation have not been goodly identified (Zhang et al. 2007).

Cataclastic sandstone is the main matrix of fault zone in the studied region. These rocks are characterized by a loose damaged microstructure and poorly cemented contacts. Consequently, coupled permeability variation during the time dependent deformation must be determined to fully understand the hydro-mechanical response. In view of this, in the present study, a series of triaxial creep tests accompanied with permeability measurements are presented on triaxial rheological conditions to quantify the creep behavior and their relationship with the permeability evolution. The effects of confining pressure (between 1.0 and 2.0 MPa) and deviatoric stress level (DSL) on creep behavior and permeability are analyzed quantitatively. The result provides an important reference for the analysis of long-term stability and safety of hydropower station.

2.2. Permeability behavior under natural state

The particles of cataclasitic sandstone are small and contain more clay mineral such as illite, montmorillonite, etc, which has a strong hydrophilic. It is indicated that the cohesive force of each cell within clay mineral is relative weak and the specimen shows quickly expanding, softening and disintegrating under the effect of water.

The permeability tests are performed on the samples under natural stress state. Firstly, the specimen was saturated by the method of promoting water head during 42 to 90 hours. Secondly, the permeability measurement was carried out by using two flows in the directions parallel and perpendicular to the bedding planes, respectively. Finally, the chemical analysis of supply and exit water was carried out.

The fluid flow behavior showed that the permeability coefficient varies from $0.14*10^{-5}$cm/s to $16.3*10^{-5}$cm/s under natural state and its values are almost the same in the direction parallel and perpendicular to the bedding plane with a mean value of (Table 2.1). In view of this, one can conclude that at the sample scale, the studied rock belonged to a mid-permeable rock with isotropic permeability. On the other hand, for a great part of laboratory tests, chemical composition between supply and exit water were the same (Table 2.2). However, only a very slight change in chemical composition of water is observed in a very small quantity of samples: a increase in K^++Na^+ and Cl^- accompanied with the decrease in Ca^{2+}、Mg^{2+}、HCO^{3-} . This observation is related to the ion exchange produced between water and rock matrix in which Silicate and aluminum silicate are main mineral component of the studied rock. Therefore, the chemical erosion is generally not significant during the laboratory tests.

In conclusion, the studied material is a mid-permeable rock and could be considered as a relatively isotropic porous media at the sample scale. Furthermore, the chemical erosion is not significant under long term fluid flow.

Table 2.1 Results of permeability characteristics

Sample	Flow direction	Saturation time	Natural density	Water level	Seepage path	Permeability coefficient	Failure mode
		h	g/cm^3	cm	cm	(10^{-5}) cm/s	
S1	Parallel	66	2.3	4300	51.3	0.3	Piping

S2	Vertical	66	2.2	1220	48.2	0.2	Flowing
S3	Vertical	42	2.1	2020	47.3	0.4	Piping
S4	Parallel	90	2.3	1650	52.5	0.2	Flowing
S5	Vertical	90	2.4	2400	49.7	0.3	Piping
S6	Vertical	42	2.4	2820	52.4	0.3	Flowing
S7	Vertical	66	2.5	6500	47.8	16.3	Piping
S8	Parallel	66	2.6	5800	49.2	2.5	Piping

Table 2.2 Chemical analysis of the experiment water

Water sample	PH	K^++Na^+	Ca^{2+}	Mg^{2+}	Cl^-	SO_4^{2-}	HCO_3^-		CO_3^{2-}	CO2	alkalinity	hardness	Erosion
		mg/L	mg/L	mg/L	mg/L	mg/L	mg/L	mmol/L	mg/L	mg/L	mg/L	mg/L	
Supply	8	24.1	72.2	23.9	29.4	119.2	177.7	2.9	6.8	69.1	157.1	274.4	no
Exit(S1)	8.2	25.8	69.7	23.1	31.2	121.0	169.6	2.8	6.8	66.1	150.4	268.9	no
Exit(S2)	8	42.0	56.4	17.6	56.4	119.6	103.8	1.7	4.6	40.8	92.8	213.1	no

2.3. Experimental procedures

Before the creep tests, the short-term tests at the same confining pressure were performed in the chapter 1. The short term strength was used as reference for setting applied stress in multi-stepped creep tests. The prior works have shown that the mechanical behavior of this material is very complex, and can be characterized by various features: such as low material cohesion, strong pressure sensitivity, plastic pore collapse and strong dependency on porosity.

Creep tests had been performed at ambient temperature (20±1.5 ℃), and the permeability measurements in the process of multiple-step triaxial creep tests were also conducted. The same confining pressure (CP) conditions was set in order to compare short term behavior during the tests. Meanwhile, simultaneous water pressure (WP) (0MPa, 0.25MPa and 0.35MP) was also applied to

measure the permeability evolution. As the steady state method is very precise and acceptable for permeability larger than $10^{-19}m^2$ (Yang et al. 2010), this method has been employed for determination of the permeability of cataclastic sandstones.

All the tests were conducted by using rock servo-controlled triaxial equipment (Zhang et al. 2013) under drained condition. Moreover, the test system includes a triaxial cell and a water injection pump, and the procedure of conducting the coupled mechanical/flow tests is similar to that of a normal triaxial compression test. The difference of water pressure, on the lower and upper sides of sample, is applied by an injection pump and maintains a constant value throughout the creep tests. Before the test, all samples are fully saturated with water in vacuum. It is important to note that there is a permeable panel at the top and bottom ends of the specimens. The permeable panel is a steel plate with many evenly distributed small holes, and its function is guarantee a uniform distribution of liquid pressure on the extremities of the whole specimens. The plastic insulation tape and the thermal shrinkage plastic top wrap are used to seal the rock specimens. The used cylinder samples are carefully prepared from intact blocks taken in the quarry. Moreover, due to the poor quality of some rock samples, extreme care and careful preparation are required in the handling of the specimens. For instance, the specimens were stored by sealing technique after taken from in situ rock mass. The average sample size is 50 mm in diameter and 100 mm in height.

The triaxial creep tests can be divided into two groups: one-step creep tests and mutli-step creep tests. By using the one step loading procedure, six creep tests were performed with at different level of applied axial stress under the same confining pressure. On the other hand, night mutli-steps creep tests were also performed by under different confining pressure. In the triaxial creep test, the confining pressure is firstly in a hydrostatic phase. Once the confining pressure attains the desired value and then keeps constant, the axial stress increases with a step rate of 0.75MPa/step until the failure of laboratory samples. At each load level, deviatoric stress was kept constant for a time interval of more than 172800 seconds during which axial and lateral strains were continuously recorded. For every triaxial creep test, four to seven levels of deveiatoric stress are used. The detailed test scheme is shown in Table 2.3- Table 2.4.

Table 2.3 Test schemes for triaxial creep test under one-step loading procedure

Specimens	Confining pressure(MPa)	Creep duration(s)	Failure stress (MPa)
S1	1.5	259200	1.00
S2		259200	1.75
S3		259200	2.50
S4		259200	3.25
S5		259200	4.00
S6		259200	4.75

Table 2.4 Test schemes for triaxial creep test under multi-step loading procedure

Specimens	water pressure(MPa)	Confining pressure(MPa)	Stress level	Creep duration(s)	Failure stress (MPa)
L1	0	1.0	4	777600	3.25
L2	0	1.5	5	950400	6.00
L3	0	2.0	5	950400	5.50
R1	0.25	1.0	6	1123200	4.75
R2	0.25	1.5	6	1166400	6.50
R3	0.25	2.0	4	540000	5.00
R4	0.35	1.0	5	781200	4.00
R5	0.35	1.5	6	957600	4.75
R6	0.35	2.0	7	950400	5.50

2.4. Creep deformation behavior under one-step loading procedure

The result of triaxial creep test under one-step loading procedure is shown in Fig. 2.1. The creep curve is smooth without fluctuation, which indicates that the deformation has a good continuity with time. The experimental results exhibits that important creep deformation is

developed in cataclastic sandstone. According to the evolution of creep rate, the creep curve can be divided into transient and steady stages. In the transient stage, an important evolution of creep rate is observed while a stable creep rate is obtained in the steady stage. Moreover, the increase of deviatoric stress induces an important evolution of creep deformation and accelerates the creep rate.

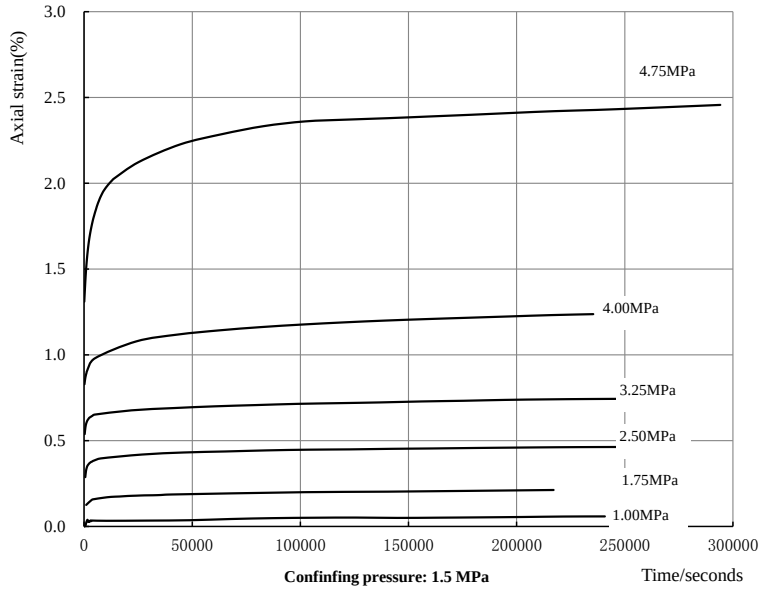

Fig. 2.1 Triaxial creep test results under one-step loading procedure

2.5. Creep deformation behavior under multi-step loading procedure

2.5.1. Behavior of axial strain

The results of triaxial creep test under multi-step loading procedure are shown in Fig. 2.2- Fig. 2.4. In the experimental results, the strain is positive for compaction and negative for dilantacy.

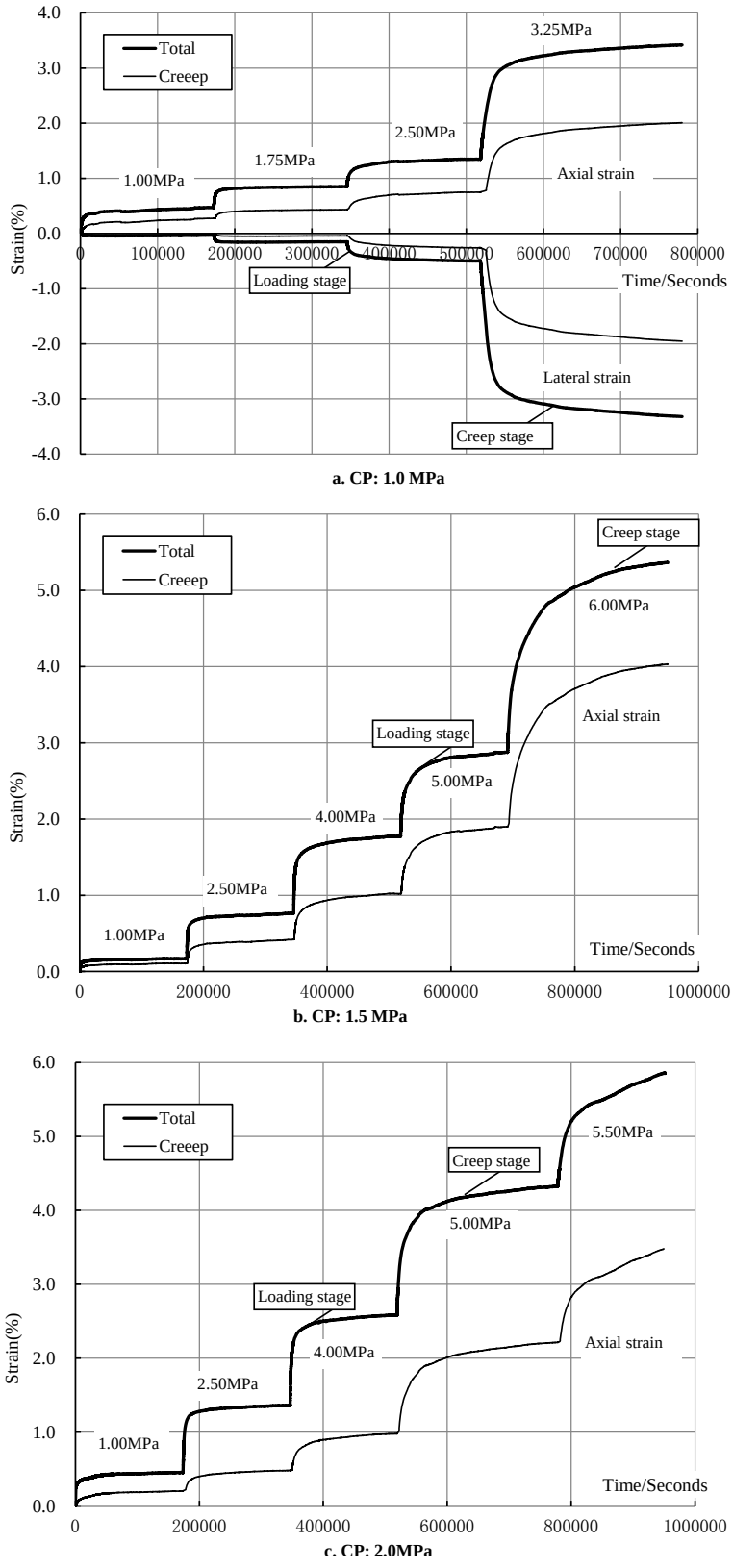

Fig. 2.2 Triaxial creep test results under natural state

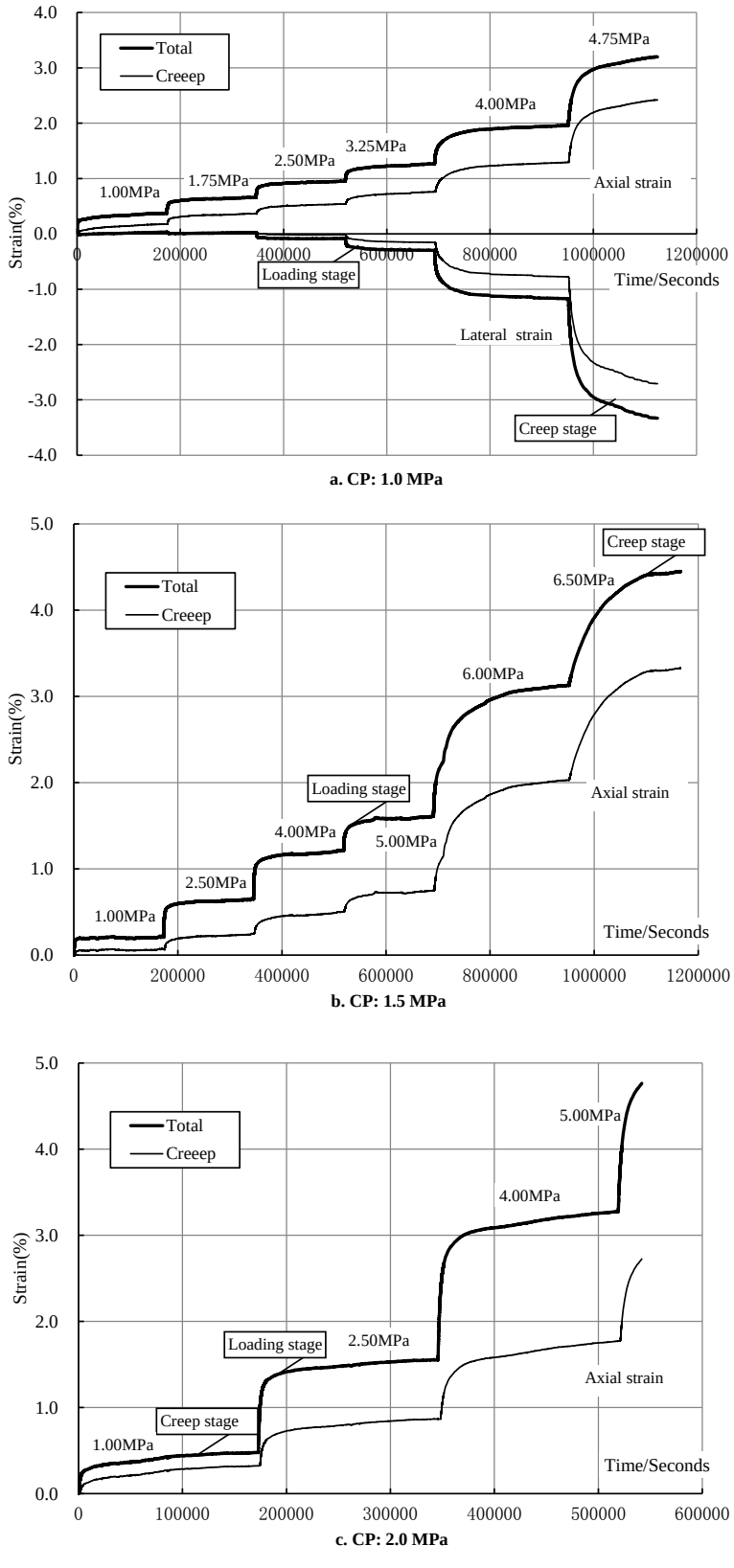

Fig. 2.3 Triaxial creep test results under 0.25 simultaneous water pressure

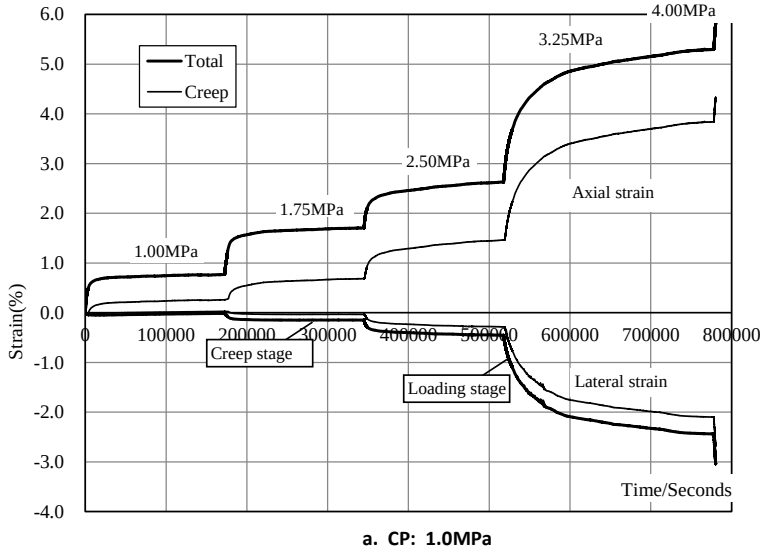

a. CP: 1.0MPa

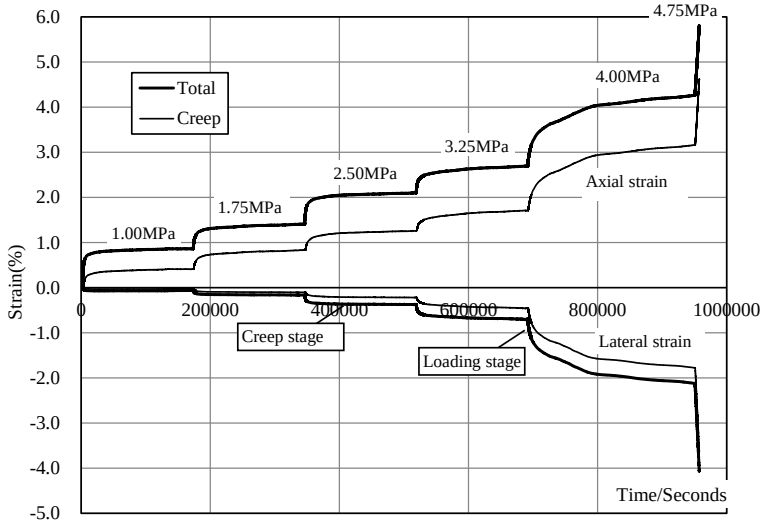

b. CP: 1.5MPa

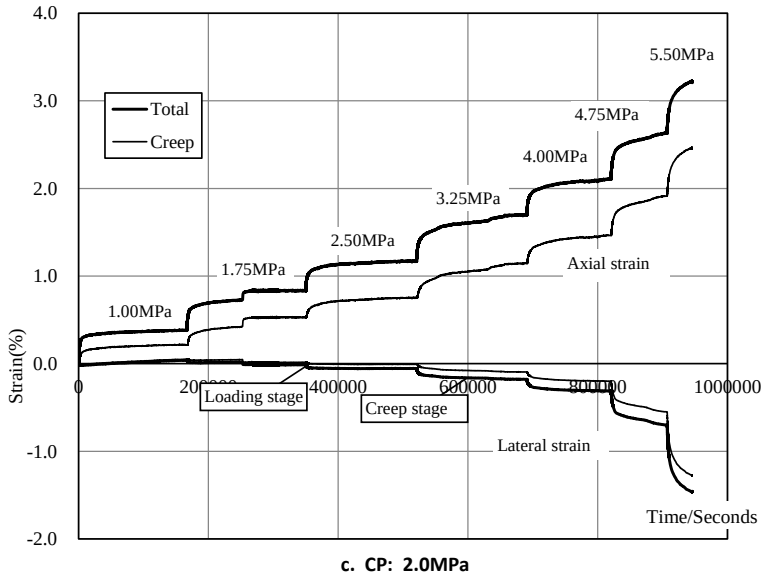

c. CP: 2.0MPa

Fig. 2.4 Triaxial creep test results under 0.35 simultaneous water pressure

In general, creep curves exhibit three distinct phases: primary creep deformation which is characterized by a rapid deformation rate that decreases slowly to a constant value, steady-state creep deformation which is characterized by a relative constant /low-deformations rate, and the third stage creep deformation which is called creep rupture (Li and Xia 2000; Fujii et al. 1999). The same evolution tendency is clearly observed in the cataclastic sandstone creep curves. The first-stage and second-stage creep deformations are generally observed in the creep curves. Furthermore, the creep failure is observed in the last-step loading. By comparing the different curves obtained at different levels of applied stress, it is noted that the creep stain increases with the applied deviatoric stress. Furthermore, the applied deviatoric stress plays a more important role on the duration of second-stage creep deformation (Yin and Graham 1994; Yang et al. 1999): the smaller of applied deviatoric stress is, the less time is taken for the studied rock to get a steady-state creep. Finally, the rock failure is obtained when the stress reach a critical value. Such rock material undergoes micro-structural adjustment such as microscopic fracturing and pore closure at low stress. The main feature associated with failure is large axial plastic deformation, highly volumetric ductility dilation and large steady strain rate due to a long term accumulation action of creep effect (Table 2.5- Table 2.7). Therefore, no clear brittle damage is observed in the samples.

Table 2.5 Creep strain values under natural state (mm)

Strain	CP/MPa	Deviatoric stress level/MPa								Creep strain
		1.00	1.75	2.50	3.25	4.00	5.00	5.50	6.00	
Axial	1.0	0.27/172800s	0.17/172800s	0.30/172800s	1.23/259200s					1.97/777600s
	1.5	0.11/172800s		0.31/172800s		0.60/172800s	0.88/172800s		2.09/259200s	3.99/950400s
	2.0	0.21/172800s		0.26/172800s		0.50/172800s	1.20/259200s	1.25/172800s		3.42/950400s
Lateral	1.0	0.0088/172800s	0.035/172800s	0.21/172800s	1.65/259200s					1.91/777600s

Table 2.6 Creep strain values under 0.25MPa simultaneous water pressure (mm)

Strain	CP/MPa	Deviatoric stress level/MPa									Creep strain
		1.00	1.75	2.50	3.25	4.00	4.75	5.00	6.00	6.50	
Axial	1.0	0.18/172800s	0.19/172800s	0.18/172800s	0.22/172800s	0.54/172800s	1.12/172800s				2.42/1123200s
	1.5	0.067/172800s		0.19/172800s		0.25/172800s		0.25/172800s	1.28/259200s	1.30/216000s	3.33/1166400s
	2.0	0.32/172800s		0.54/172800s		0.91/172800s		0.96/21600s			2.73/540000s
Lateral	1.0	-0.038/172800s	0.001/172800s	0.056/172800s	0.14/172800s	0.63/259200s	1.93/172800s				2.72/1123200s

Table 2.7 Creep strain values under 0.35MPa simultaneous water pressure (mm)

Strain	CP/MPa	Deviatoric stress level/MPa							Creep strain
		1.00	1.75	2.50	3.25	4.00	4.75	5.50	
Axial	1.0	0.26/172800s	0.43/172800s	0.77/172800s	2.37/259200s	0.48/3600s			4.32/781200s
	1.5	0.41/172800s	0.42/172800s	0.43/172800s	0.44/172800s	1.45/259200s	1.47/7200s		4.63/957600s
	2.0	0.21/46h	0.32/50h	0.22/172800s	0.39/172800s	0.32/136800s	0.45/82800s	0.54/39600s	2.45/950400s
Lateral	1.0	0.028/172800s	0.062/172800s	0.25/172800s	1.81/259200s	0.57/3600s			2.67/781200s
	1.5	0.023/172800s	0.077/172800s	0.12/172800s	0.24/172800s	1.32/259200s	1.84/7200s		3.62/957600s
	2.0	0.054/46h	0.039/50h	0.023/172800s	0.087/172800s	0.11/136800s	0.35/82800s	0.72/39600s	1.28/950400s

On the other hand, the confining pressure has a great impact on the creep deformation (Fig. 2.5): the higher the confining pressure is, the smaller the creep strain is observed. For instance: the creep strain obtained under the confining pressure of 1.0 MPa is larger than that obtained with 2.0 MPa. Moreover, the creep failure is delayed by the increase in the confining pressure. The

accelerated creep appears shortly right after the application of instantaneous loading under confining pressure of 1.0 MPa and 1.5 MPa while three creep phases is clearly developed in the sample under the confining pressure of 2.0 MPa.

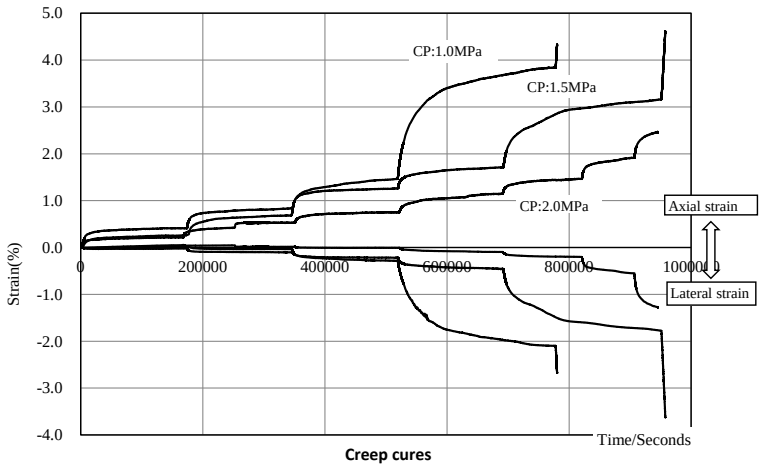

Fig. 2.5 Axial and lateral creep curves under 0.35 simultaneous water pressure

2.5.2. Behavior of lateral strain

In general, three creep phases are also observed in the lateral strain curves. Moreover, the influence of confining pressure on lateral strain is similar to that on the axial strain. However, the kinetic of lateral stain and axial strain is not the same. At the beginning of creep test, the lateral strain is lower than axial strain and the samples are then generally under compaction. Afterwards, with the increase of applied deviatoric stress, the lateral stain increases more significantly than the axial one and becomes to the dominant strain. Therefore, an important volumetric dilatancy is observed in the creep failure phase.

By comparing the total strain with the creep strain, one observes that the influence of instantaneous loading on the lateral strain is less than that of axial strain. The axial creep strain is only 75% of total strain, while the lateral creep strain takes a more important part of total strain (about 90%). Moreover, in the light of reported faster lateral strain rate than axial strain rate, it is sees reasonable that the corresponding deviatoric stress is close to the long term strength of the specimen. Therefore, the lateral strain can be a good indicator of rock damage and provide a different viewpoint to determine the long term strength. These observations is coherent with the research resulted obtained by Fujii (1999).

In accordance with the creep strain values under different applied stress (Table 2.5- Table 2.7), a threshold of applied deviatoric stress is observed in the evolution of lateral creep deformations. It is important noted that this threshold is not clear observed in the axial strain. Once the deviatoric stress reaches the threshold limit value, the lateral strain begins to increase rapidly. Its values for the creep tests under different confining pressures are given in the Table 2.8. Based on the obtained values for the ratio between the threshold stress/peak stress, one can conclude that the threshold stress seems to be greater than the 50 % of the peak stress (Ma 2004).

Table 2.8 Threshold values for the creep tests under 0.35MPa simultaneous water pressure

Confining pressure (MPa)	1.0	1.5	2.0
Threshold value (MPa)	2.5	3.25	4.00
Ratio of threshold stress /peak stress	62.5%	68.4%	72.7%

2.5.3. Behavior of volumetric strain

The volumetric deformation of cataclastic sandstone is studied in this section (Fig. 2.6 - Fig. 2.8). Generally, two distinct phases can be identified in the volumetric deformation curves: a volumetric compaction phase followed by a dilantacy phase.

When the applied deviatoric stress reaches the mentioned threshold stress (point A, B and C), the studied material begins to dilate. Finally, when the peak stress (point A', B' and C') is attained, the dilatancy strain increases sharply. Therefore, we can considered that the points "A" and "A'" in Fig. 2.6 - Fig. 2.8 represent the inflection of volumetric strain and the onset of dilation (Table 2.9-Table 2.11).

On the other hand, the point "A" also corresponds to the maximum compressive strain, which should depends strongly on the confining pressure and the porosity. In general, according to the same material, the volumetric compressive stain observed in the sample should increase with the applied confining pressure. However, in the case of the studied rock, the impact of confining pressure on the volumetric compressive deformation is very limited due to its very low compressibility and a small change in applied confining pressures. As shown in Table 2.10, corresponding to the various confining pressure, the maximum compressive strain are 0.90, 0.83 and 1.07 respectively. Thus we can consider that the variation is small.

The "A'" corresponds the transition point from a positive volumetric strain to a negative one. Its values increase with the confining pressure through the Fig. 2.8. Therefore, confining pressure can effectively strengthen the compressibility of the rock. Moreover, it is also noted that the strain rate in compaction phase is smaller than that in the dilatancy phase. This fact is due to the development of microcraks and the failure of studied material. And noted that only in the last step creep test, the maximum dilation strain is very important due to the duration of creep test is longer (Fig. 2.8) .

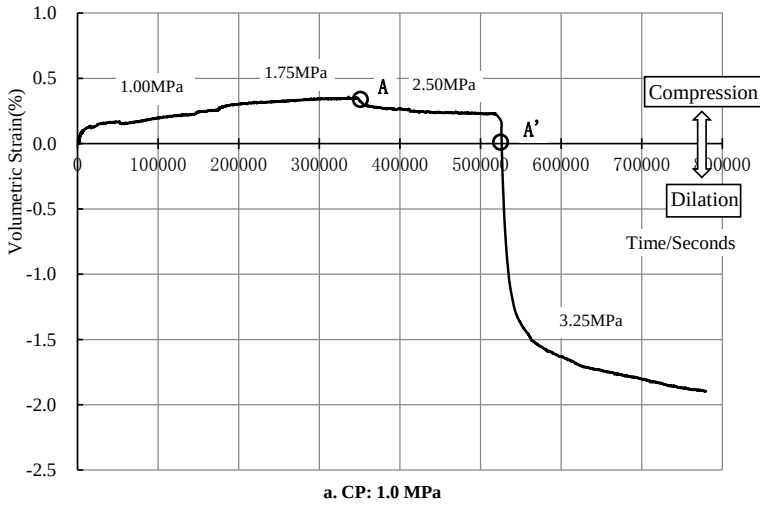

Fig. 2.6 Volumetric creep curves under natural state

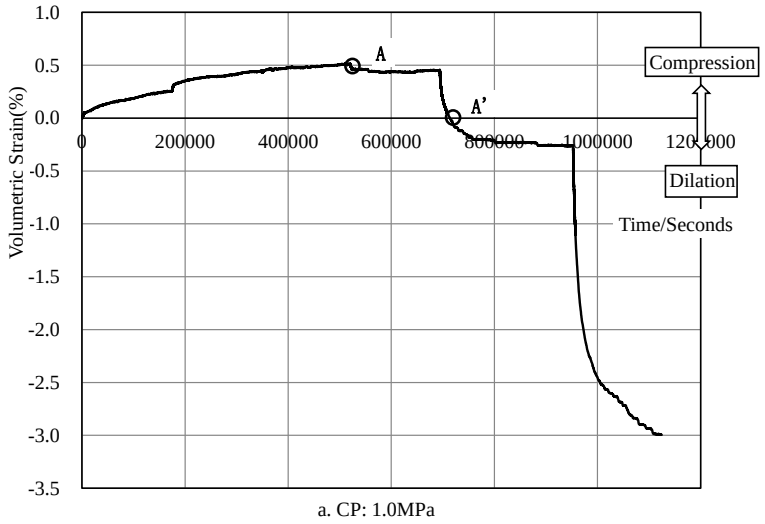

Fig. 2.7 Volumetric creep curves under 0.25MPa simultaneous water pressure

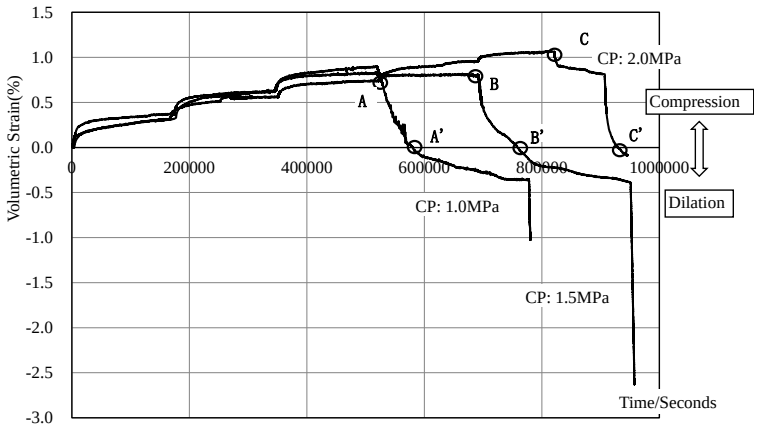

Fig. 2.8 Volumetric creep curves under 0.35MPa simultaneous water pressure

Table 2.9 Volumetric creep strain values under natural state (mm)

CP/MPa	Deviatoric stress level/MPa				Compression		Dilation	
	1.00	1.75	2.50	3.25	Strain value	Duration	Strain value	Duration
1.0	0.26	0.096	-0.12	-2.07	0.36	345600s	-1.90	432000s

Table 2.10 Volumetric creep strain values under 0.25MPa simultaneous water pressure (mm)

CP/MPa	Deviatoric stress level/MPa						Compression		Dilation	
	1.00	1.75	2.50	3.25	4.00	4.75	Strain value	Duration	Strain value	Duration
1.0	0.25	0.19	0.064	-0.065	-0.72	-2.74	0.51	518400s	-3.0	604800s

Table 2.11 Volumetric creep strain values under 0.35MPa simultaneous water pressure (mm)

CP/MPa	Deviatoric stress level/MPa							Compression		Dilation	
	1.00	1.75	2.50	3.25	4.00	4.75	5.50	Strain value	Duration	Strain value	Duration
1.0	0.32	0.29	0.27	-1.25	-0.66			0.90	518400s	-1.03	262800s
1.5	0.36	0.27	0.19	-0.032	-1.18	-2.32		0.83	691200s	-2.72	268200s
2.0	0.32	0.24	0.18	0.22	0.11	-0.25	-0.90	1.07	835200s	-0.087	126000s

2.6. Permeability variations during time dependent deformation

2.6.1. Permeability change with the time dependent deformation

In this section, the permeability changes during time-dependent deformation of cataclastic sandstone are studied (Fig. 2.9-Fig. 2.11). This rock presents obvious creep characteristics during the multi-level loading tests.

The experimental results exhibit that the permeability behavior of studied material depends strongly on the time-dependent deformation. The same tendency of permeability evolution is observed in all cases. Generally, the permeability decreases progressively with the increase of the stress and attains finally a constant value once the applied stress reaches a certain level. It is observed that the permeability variation dependent strongly on the strain evolution : (1) at the beginning of test, due to the closure of the primary micro-cracks existed in the samples, the permeability decreases rapidly; (2) afterwards, the kinetic of the decrease in permeability is decelerated due to the fact that the material has been strongly compacted during the previous phase (3) A steady-stage is observed in the evolution of permeability. During this period, an important irreversible deformation is observed in the sample due to the growth and coalescence of micro-cracks. However, as the sample has a high porosity, the volumetric compaction of material plays a more important role on the evolution of permeability than the closure and growth of micro-crack. Therefore, the permeability change in this phase is very limited and the similar observations have been also observed by many other investigators (Kiyama et al. 1996; David 2001).

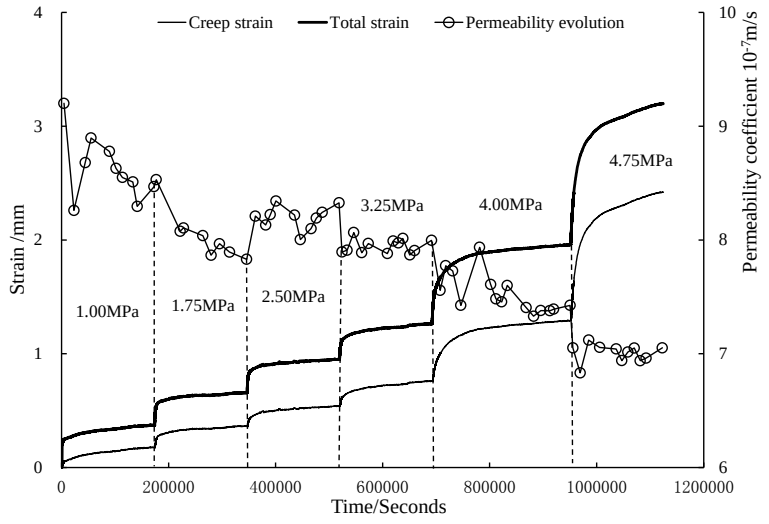

(a) R1; CP：1.0MPa; WP：0.25MPa

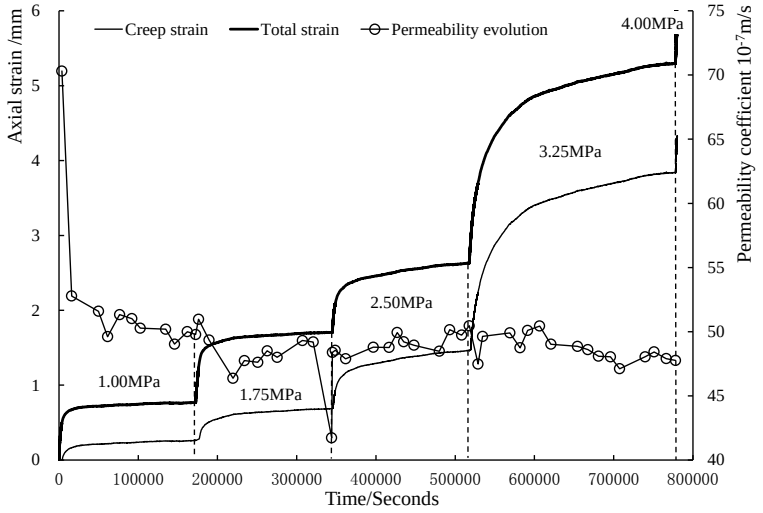

(d) R4; CP：1.0MPa; WP：0.35MPa

Fig. 2.9 Axial strain and permeability evolution cures under CP of 1.0MPa

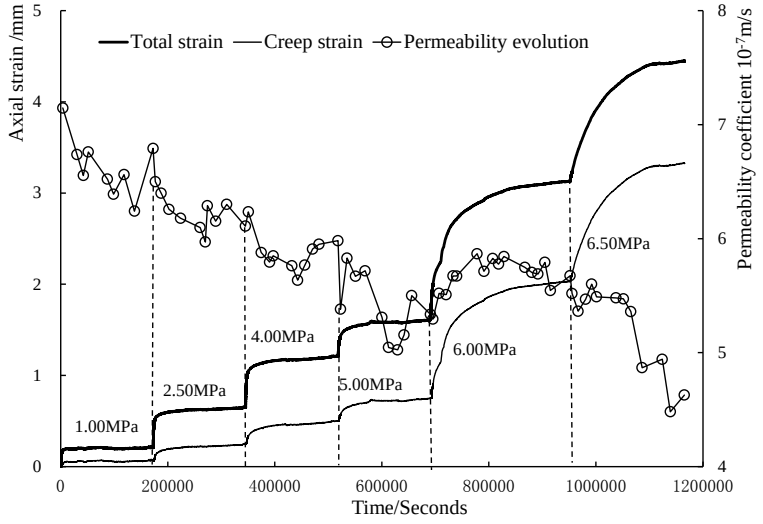

(b) R2; CP：1.5MPa; WP：0.25MPa

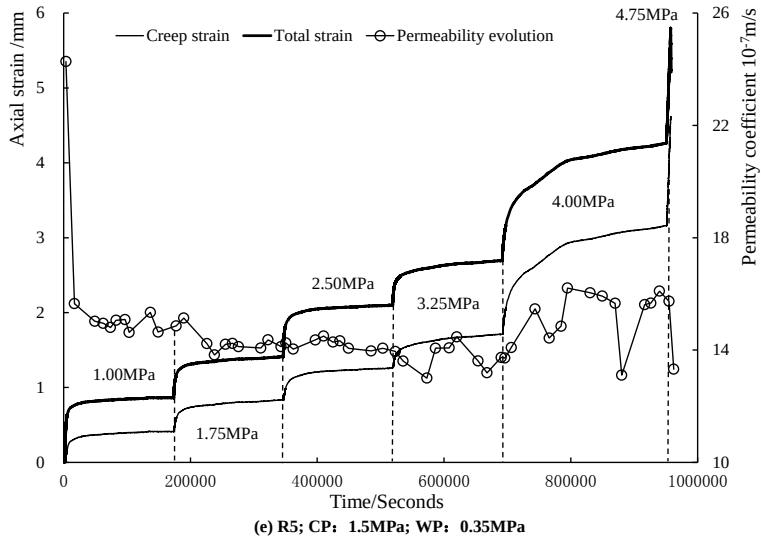

(e) R5; CP：1.5MPa; WP：0.35MPa

Fig. 2.10 Axial strain and permeability evolution cures under CP of 1.5MPa

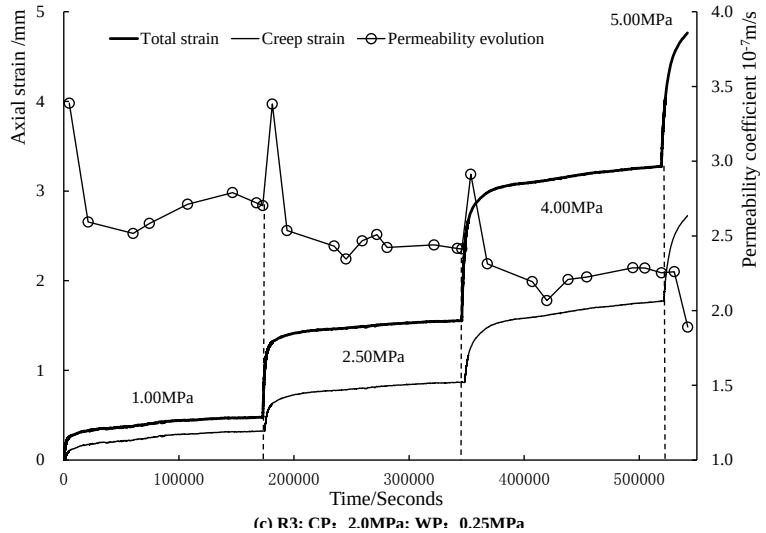

Fig. 2.11 Axial strain and permeability evolution cures under CP of 2.0MPa

Fluctuations were observed in the variation of permeability at the instantaneous part. The reason may be that those specimens have a definite difference in the porosity and inner structure. On the one hand, the fluctuation can conceptually be divided into three types at the initial stage with a high compressibility. If a specimen has big porosity and moisture content, the permeability abruptly rises as soon as the applying of stress. These features can be explained by means of the closure of the effective porosity and extrusion of pore water. Such characterization can be well observed for specimen R3. In addition, the specimen has a medium porosity and thus the reduction of fluid flow is basically the same as the extrusion of pore water. The permeability coefficient keeps

constant when the applying of stress, e.g. the R5 specimen. Otherwise, the permeability drops abruptly. For the R4 specimen, the permeability decreases from $49.20e^{-7}$m/s to $41.72e^{-7}$m/s when applying stress of 2.50MPa. On the other hand, in the first loading stress (1.00MPa) and high applied stress, the permeability variation is consistent among three types of specimens. We think that the permeability drop rapidly due to micro-crack closure and porosity decreases under the effect of stress.

Let us focus on the other region. We can see that the permeability evolution decreases slowly and quasi-linearly during steady stage. This feature is observed in many sandstones and other granular materials (David 2001; Kiyama et al. 1996). However, the reduction in permeability is much smaller than that during initial loading. The reduction can be explained in terms of evolution of microstructure. It is because that the micro-cracks and pores are closed when stress is applied. But the long term constant loading can cause the accumulations of damage; meanwhile, some factors, such as the fluid flow, may result in the growth of micro-fissure and the coalescence of pore. Thus the trend of permeability turns to be stable. Furthermore, the micro-cracks and pores become smaller and smaller during the creep course, which may cause the permeability to reduce gradually. It is also indicated that the fluctuation has non-significant effect on permeability evolution in course of creep tests.

2.6.2. Permeability evolution with the confining pressure and fluid flow pressure

Furthermore, the confining pressure has also an important impact on the permeability behavior. The permeability decreases rapidly when the confining pressure increases from 1 MPa to 2 MPa (Fig. 2.12). This observation is related to the diminution of porosity and the closure of some micro-fissures in the sample. Moreover, the permeability decreases sharply under the high confining pressure while a very limit decrease of permeability is observed under low confining pressure. On the other hand, by comparing the permeability measurement obtained under different confining pressure, one observes that the permeability behaviour of studied rock is also influenced by the fluid flow pressure (Nur and Yilmaz 2006). The permeability increases with the increase of water flow pressure. The permeability obtained with high fluid flow pressures is greater than that obtained with small liquid pressure. Therefore, the stress redistribution and the variation of the hydraulic conditions can create the time dependent deformation and change the permeability of the rock.

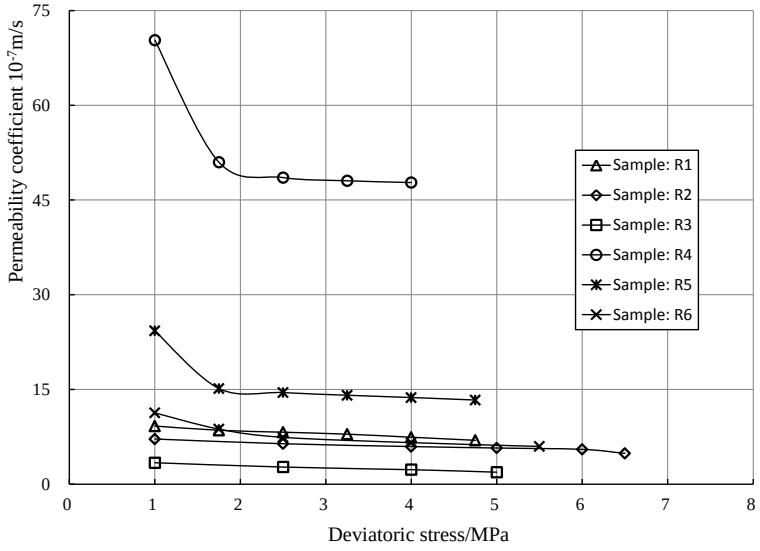

Fig. 2.12 Relationship between permeability evolutions and stress

2.7. Stress-strain curves during creep tests

The Stress-strain curves of triaxial creep tests are analyzed in detail. During the laboratory test, the studied material exhibits important the instantaneous deformation (Fig. 2.13). Moreover, the sandstone samples exhibits small creep deformation at low stress levels while important creep deformations are observed at high stress levels. In general, the total axial strain curves can be divided into three stages:

(1) Crack closure and elastic deformation (OA): Strain-stress curves of studied samples have a concave shape. This phenomenon is due to the closure of existing micro-cracks when the compression stress is applied. With the increase in applied deviatoric stress, a linear elastic phase is observed. At a given stress level, the curve still progresses along with primary stress path when reloading rock sample after carrying out the creep experiment. This observation is similar to the cyclic loading tests of rock at low applied stress (Yang and Jiang 2010). The experimental results exhibits that the studied rock has no new microscopic damage and can attains rapidly in stable creep state. Therefore, the performance of creep tests has almost no effect on the stress-strain curves of sandstone.

(2) Crack initiation and stable crack growth (AB): micro-fissures in the sample begin to propagate accompanied the creation of microcracks. In this phase, the strain-stress curve becomes

non-linear. The studied material hardens gradually and plastic deformation increases as a long-term accumulation action of creep effect. The curve could not continue along the primary path after the creep test in which important irreversible non-linear deformation is created. Moreover, we can notice that the yield stress of point A is about 50 % of peak stress which marks the start of micro-fracturing, and indicated that the deformation of studied rock begins to increase continuously with time.

(3) Crack damage and unstable crack growth (BC): micro-cracks in the rock continue to develop, propagate and then coalesce under the combinative effects of applied stress and creep. Therefore, some macrocraks are created in the sample and induces the failure of studied sample. During this phase, the strain increase more significantly than that observed in two previous phases. The creep failure of studied sample is characterized by important expansion and development of macro-cracks. The stress of point B is about 75 % of ultimate strength which marks the onset of specimen failure (Ma 2004). And the values are almost same with the threshold stress.

Corresponding to the axial strain, the volumetric strain-stress curves also can be divided into three phases: a volumetric compaction phase (OA') in which the primary micro-fissures are closed ; a constant volume phase ($A'B'$) and a volumetric dilatation phase($B'C'$). Furthermore, we can conclude that the initial nonlinear portions and elastic strain is much smaller than the axial one. And the lateral strain rate is relatively faster, thus it is earlier and faster to deviate from the linear elastic state than the axial strain. We can consider that the lateral strain is more sensitive than the axial strain to reflect the change of permeability of the rock specimens.

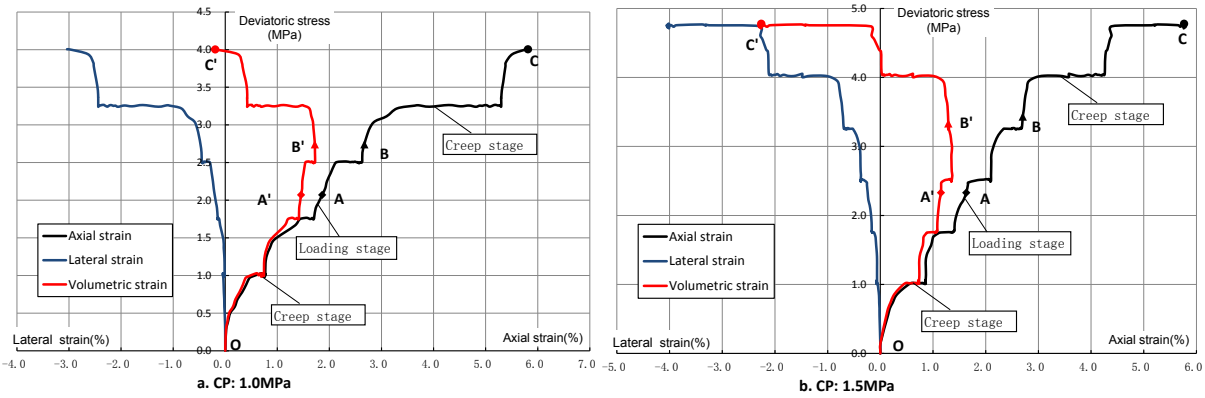

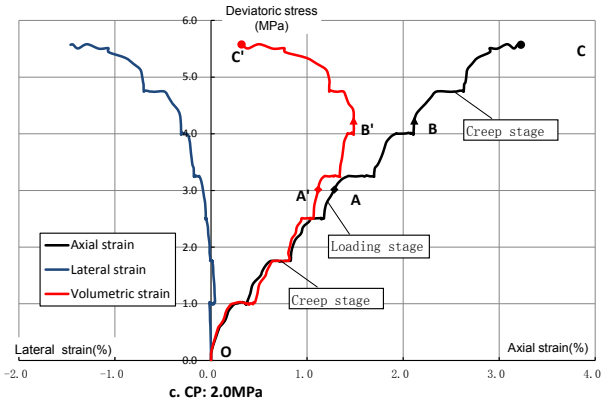

Fig. 2.13 Creep stress-strain curve under 0.35MPa simultaneous water pressure

2.8. Strain rate analysis and long term strength

2.8.1. creep strain rate analysis

The creep strain rate is discussed in this section. It is observed that the magnitude order of strain rate reaches 10^{-3} mm/h (Fig. 2.14). In general, the evolution of strain rate exhibits two stages: decelerating transient stage and steady stage (Jaeger et al. 2007). The development and duration of each stage depends strongly on the behavior of the studied material and the applied load level. At high stress level, the strain rate decreases sharply and it takes more time for the creep deformation to attain its steady-state. In particular, when the applied stress is greater than the threshold limit one, for instance at the last-step of creep test performed under the confining pressure of 1.5 MPa and 2.0 MPa, the strain rate increases sharply and much greater than that observed at the previous loading levels, which can be considered as the sign of rock failure. Therefore, an average time of 68400 seconds is defined as a limit between transient and steady creep for cataclastic sandstone. This observation is coherent with experimental results obtained by Tsai (2008).

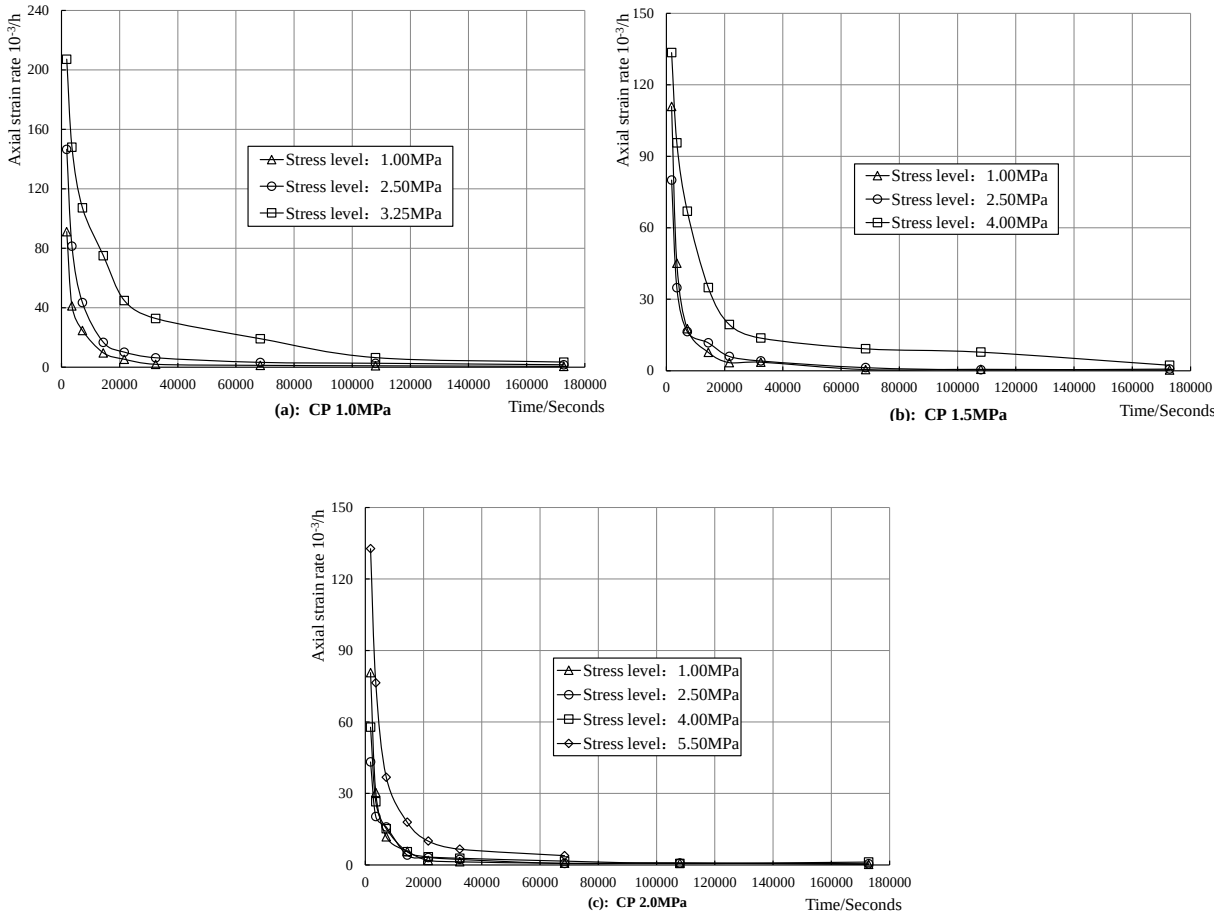

Fig. 2.14 Relationship between axial strain rates and time under 0.35MPa simultaneous water pressure

To get a good understanding on the kinetic of the creep strain of studied rock, two different strain rate are calculated: (1) the transient strain rate, which is the mean value of stain rate during a period of 19 hours period after the start of the creep test; (2) the steady strain rate, which is the mean value obtained between the 19 hours and the end of the steady step. The obtained values are given in Fig. 2.15. It is observed that the strain rate can be expression as an exponential function of applied stress and confining pressure. Generally, those steady strain rates are quasi-independent of the loading history and depend only on the current stress state (Yang et al. 1999; Yin and Graham 1994). As the specimen failure is not observed in the transient phase in which the strain rate decreases with time, the evolution of creep deformation in steady creep stage should be taken into account in order to long term stability of engineering structure (Chan 1997; Ma 2004; Brantut et al. 2013).

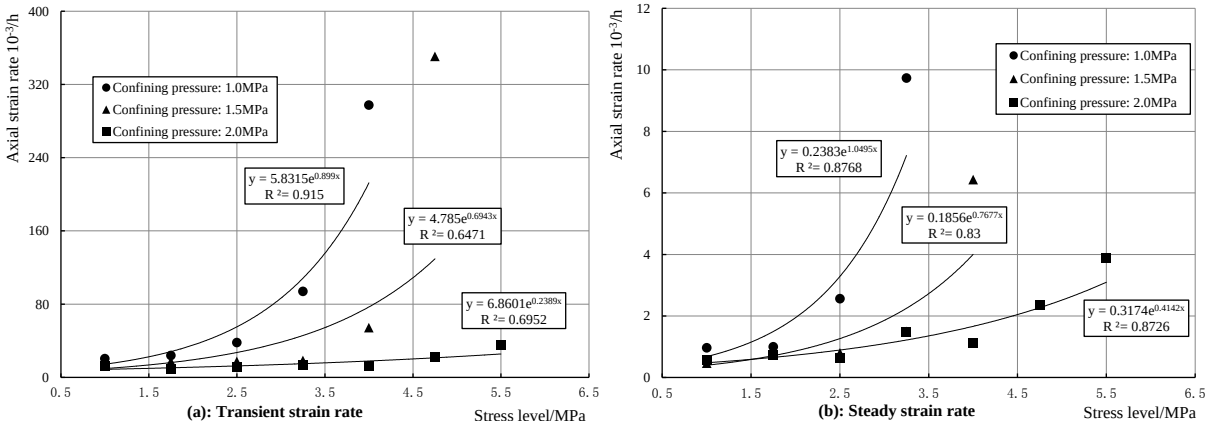

Fig. 2.15 Relationship between axial creep rates and deviatoric stress level under 0.35MPa simultaneous water pressure

On the other hand, the confining pressure seems to prevent the development of creep deformation in the samples. Both the duration of transient creep and the strain rate decrease with the increase in confining pressure (Fig. 2.16). The relationship between steady strain rate and confining pressure also can be approximated by an exponential function. The impact of confining pressure on the strain rate decreases with the increase of confining pressure and deviatoric stress. Therefore, we can conclude that the reinforcement can improve the long term stability of such hydropower engineering.

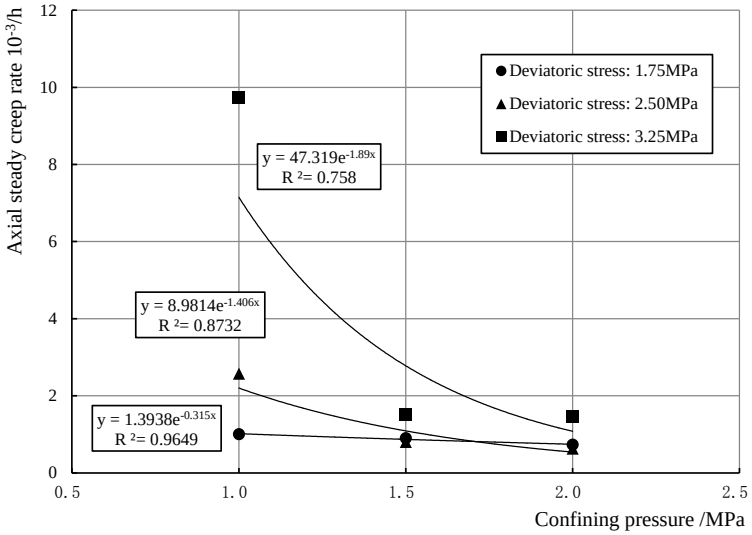

Fig. 2.16 Relationship between steady-state creep rate and confining pressure under 0.35MPa simultaneous water pressure

In conclusion, the strain rate increases with the deviatoric stress which it decreases with the confining pressure. Therefore, the strain rate can be expressed as a function of confining pressure and of applied stress: $\dot{\varepsilon} = h(\sigma_{cp}) \times f(\sigma_{ds})$, where $h(\sigma_{cp})$ and $f(\sigma_{ds})$ are the functions representing, respectively, the effects of confining pressure and applied stress. Based on the experimental investigations and inspired by the research works of Carter (1993), explicit exponential functions will be used in the present study.

2.8.2. Long term strength

In the previous studies, the long-term strength may be just a fraction of that measured in the relatively short-term experiments of the laboratory. The long term strength seems to decrease rather than increase with time (Damjanac B. 2010). It is observed that the long-term strength of rock in situ can be as low as 50% of the unconfined strength (Read 2004). However, rather than applying an arbitrary strength reduction for stability analyses, there is a need for a definitive failure criterion that can be derived from laboratory test data. Chandler (2013) defines that the long-term rock strength is the stress at volume strain reversal. At stresses higher than the long-term strength, damage in the rock increased unabated and failure of the specimen ultimately resulted. Moreover, Marti and Chandler (1993, 1994) proposed that the long-term strength of the rock corresponds to the stress at the onset of this micro-crack induced dilation.

In this section, an important volumetric dilatancy and a steady creep phase are observed before the failure of studied rock. Therefore, it may be interesting to study the relationship between the long-term strength and the strain state of studied material. The kinetics of axial, lateral and volumetric strain are compared in Fig. 2.17. The experimental results exhibit that the axial strain rate is larger than that of lateral and volumetric one at low level of stress. It is noted that the strain rate in lateral direction becomes greater than that in axial direction when the stress reached a limit value. Moreover, the volumetric strain is a function of axial strain and lateral strain. The long term strength can be defined as the critical point of expansion strain rate greater than the compression strain rate. An intersection point exists for the curves of axial, traverse and volumetric steady strain rate (Fig. 2.17). At this interaction point, the sample is in a state of static deformation equilibrium in which the strain rates of lateral and axial strain are the same. Following the fast creep failure is observed when the stree more than this point. In view of this, the stress corresponding to

intersection point is defined as the long term strength of studied material. The long-term strength of sandstone under different confining pressure is given in Table 2.12 and it is noticed that the value of long-term strength is very close to that of stress threshold for the volumetric transition from compaction to dilatancy. Therefore, the identification of long-term strength is reasonable and feasible to be applied in the long-term stability analysis of engineering structures.

The long-term strength of sandstone is closed to its short-term strength under the confining pressure of 1.0MPa (Table 2.12). However, the difference between the long-term and short-term strength increases gradually with the confining pressure. Under the confining pressure of 1.5MPa and 2.0MPa, the ratio between long-term strength and short-term strength are 79.3% and 64.8%, which identifies that the reduce rate of long term strength increases with the increased of confining pressure. This phenomenon is due to the accumulation of material damage during the creep tests. Therefore, the researched hydropower station would deform continuously and strength decreases significantly with time.

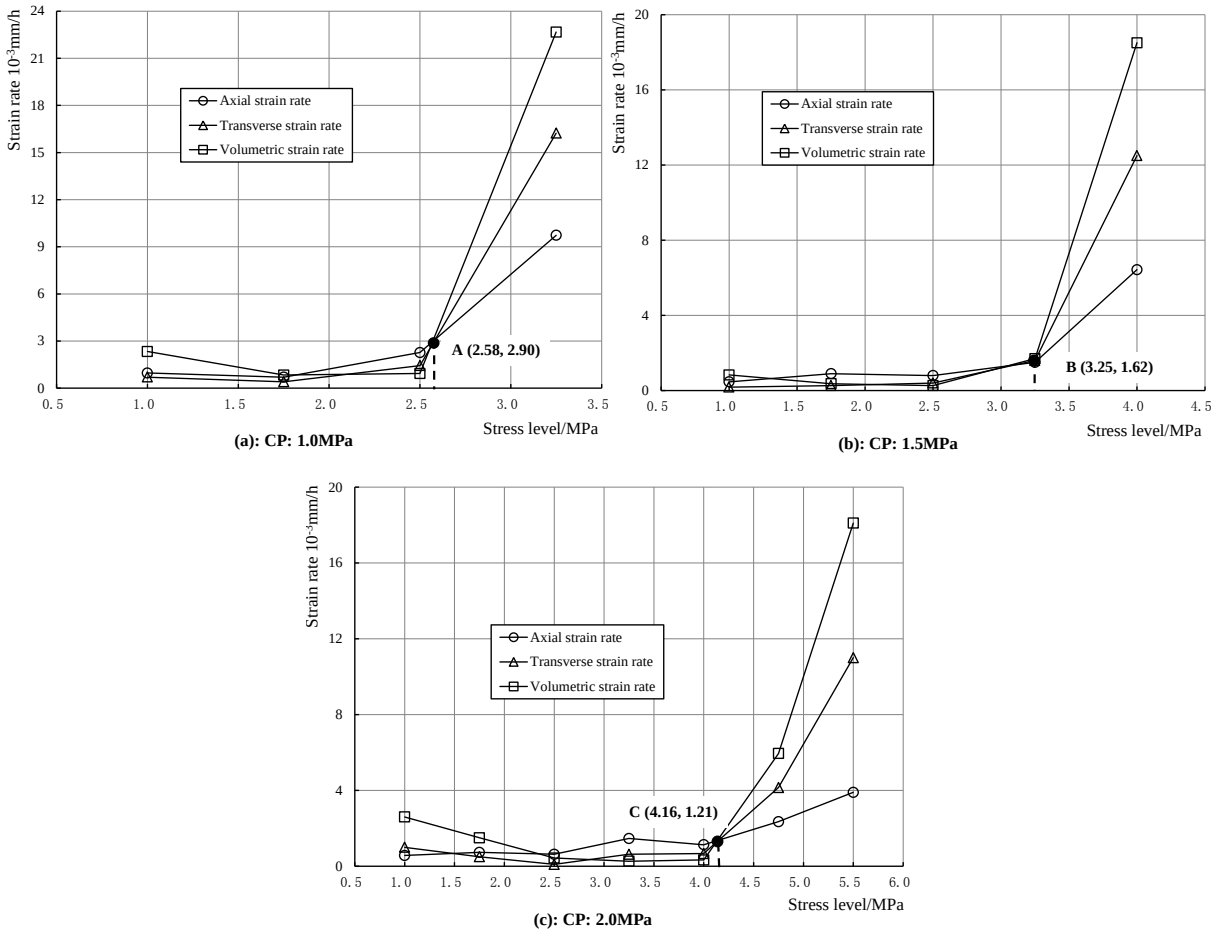

Fig. 2.17 Relationship between steady creep rates and level stress under 0.35MPa simultaneous water

pressure

Table 2.12 Long term strength for the creep tests under 0.35MPa simultaneous water pressure

Confining pressure (MPa)	1.0	1.5	2.0
Threshold value (MPa)	2.5	3.25	4.00
Long term strength (MPa)	2.58	3.25	4.16
Short term strength (MPa)	2.84	4.10	6.42

2.9. SEM experiments and creep failure mode

Cataclastic sandstone is a kind of heterogeneous material, in which there are many initial microdefects such as fissures, joints, dislocations, etc. It can be remarked that the creep failure is actually a synthetical result of flaw and heterogeneity of material structure, and a continuous damage of micro-fissures inside the specimen accumulate during the creep test (Chen and Azzam 2007). There are a number of small macro-cracks and ductile zones arising on the sample surface.

The scanning electron microscope (SEM) experiments were performed for the rock specimens to study the macro-micro creep failure mechanism (Fig. 2.18- Fig. 2.19). Microscopically, the nonlinear deformation characteristics are possibly related to the opening and closing of the void space and the micro-cracks during the creep processes. The microscope failure patterns are slightly different at various confining pressure. There are more growing cracks in the micro-fracture surface, and this surface is coarse with less micro grains at low confining pressure. With the increase of the confining pressure, the surface is clean with more micro grains, and the porosity is decreased. It is the same as macroscopic failure of specimen.

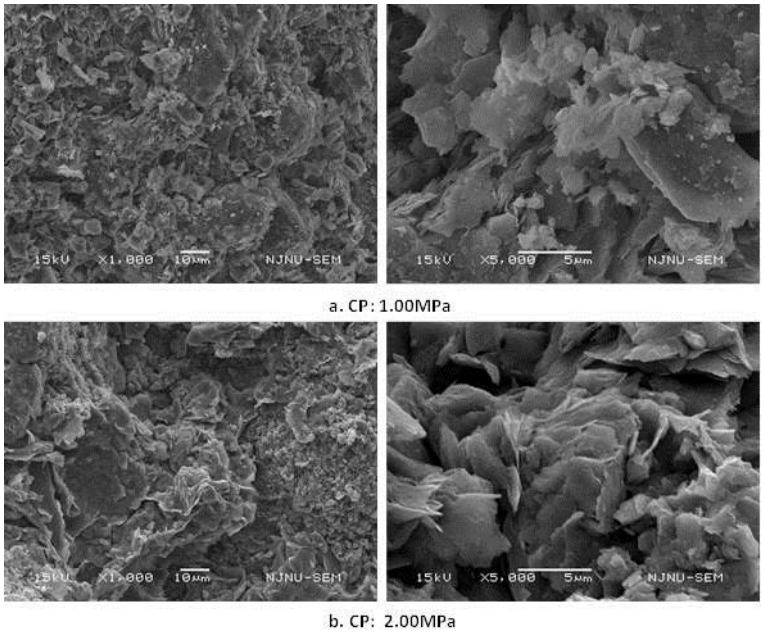

Fig. 2.18 SEM observations for specimen after creep failure under no simultaneous water pressure

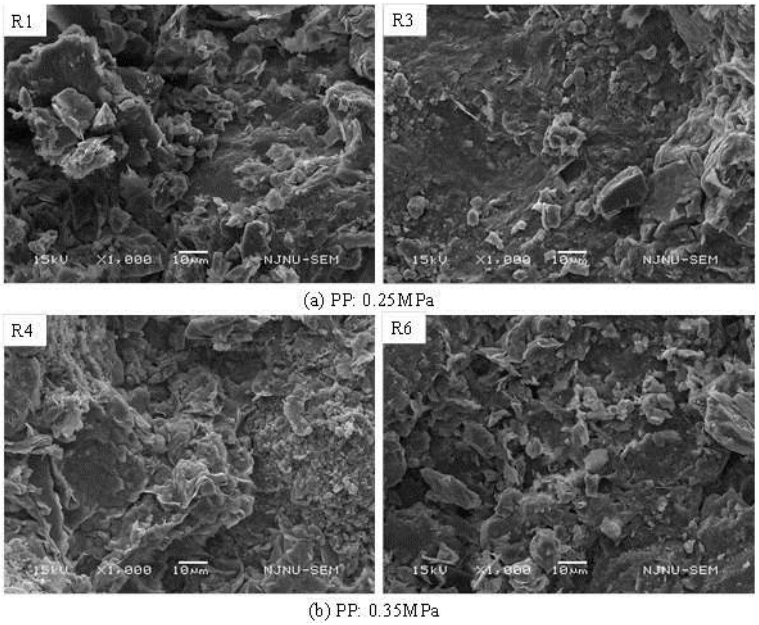

Fig. 2.19 SEM observations for specimen after creep failure under 0.35MPa simultaneous water pressure

2.10. Conclusions

Based on a series of creep tests and permeability measurements on cataclastic sandstone, the creep behaviors and their effect on the permeability evolution are analyzed in detail. It's possible to formulate some main concluding remarks as follows:

- The cataclastic sandstone presents obvious creep characteristics and the magnitude order of creep strain attains 2%. The complete creep curve generally experiences transient creep, steady creep and accelerated creep at the last applied stress. It is clear that the strain has an increasing tendency with the increase of applied stress. This means that the lower the creep load is, the less time is taken for such rock to enter creep stability. However, the creep strain obviously decreases with increasing confining pressure.

- The main feature associated with failure presents large axial plastic deformation, highly volumetric ductility dilation and large steady strain rate. At the initial stress, lateral creep strain is significantly lower than axial creep strain and the specimens mainly show obvious compression. When stress increased, the lateral strain gradually begins to be dominant and the volumetric seems reasonable in the light of reported dilatancy. There is a threshold stress exists in the process of transition from compression to dilatation. Therefore, the lateral strain can be a good indicator of rock damage and can offer a different viewpoint to determine the long term strength.

- There is an intersection point existed among the curves of axial, traverse and volumetric steady strain rate. We can define that the stress corresponding to intersection point as the long term strength of cataclastic sandstone. The dilation rate are greater than the compression rate when the stress more than this point and the fast creep failiure of sample is observed. Take 0.35MPa fluid flow pressure as an example, it can be seen that the long term strength under 1.0 MPa, 1.5 MPa and 2.0 MPa are 2.58 MPa, 3.25 MPa and 4.16 MPa, respectively, which is basically the same as the stress threshold of expansion.

- The permeability variation dependent strongly on the applied stress and deformation state. At first, the permeability of rock decrease with the increase of applied stress and tends to a constant value one the applied stress reaches up to a certain level. This phenomena is due to the the transition from compaction to dilatancy. Moreover, because the specimen has a high porosity, the porosity compaction is predominant compared to the micro-crack closure and growth.

- The permeability change shows some mutative correlation with the porosity of material during creep test. But the overall trend of change is decreasing slowly and quasi-linearly at different applied stress owing to continued compaction, which indicates that the fluctuation has no significant effect on permeability evolution. In addition, the curve of permeability variation is composed of an

instantaneous part due to applied stresses and a steady fluid flow part induced during creep process. The reduction in permeability during steady stage is much smaller than that during initial loading.

Chapter 3. Numerical modeling of mechanical behaviour of cataclastic sandstone

Abstract: In this chapter, a unified constitutive model is proposed for the description of mechanical behavior of cataclastic sandstone at different scales. The short term behavior of studied material is characterized by the Drucker-Prager elastoplastic model while the time-dependent deformation is described in terms of evolution of miscrostructure. The proposed model is used to simulate the conventional triaxial compression tests and multi-step creep tests, presented in the previous chapter. Generally, a good concordance is obtained between numerical simulations and experimental data. The proposed model is capable to describe the main features observed in cataclastic sandstone, such as plastic deformations, volumetric dilation, pressure sensitivity and creep.

Key words: Rock; Constitutive model; Creep; Damage; Plasticity; Microstructure

3.1. Introduction

The previous laboratory investigation exhibits that both instantaneous and time-dependent irreversible deformations have been observed in cataclastic sandstone. In the framework of the long-term stability analysis of hydropower station, it is necessary to take into account the time-dependent responses of studied rock (Zhou 2003). In classic modes, two separate constitutive models are used for the description of short-term (instantaneous) plastic responses due to applied stress variation and long-term (creep) plastic deformation due to material viscosity effect (Dusseault and Fordham 1993; Bodas Freitas et al. 2011; Yin and Tong 2011). Generally, a mathematical description of creep is provided by these models. However, the physical mechanisms of creep have not been taken into account. In studied sandstone, the experimental results obtained in the previous chapters show that the development of creep deformation in studied sandstone is mainly associated with progressive evolution of microstructure, such as the sub-critical propagation of micro-cracks. Moreover, numerous consistent experimental results have been obtained in the literature (Bazant and Xi 1994; Xie and Shao 2006; Bonini et al. 2009; Barla et al.2012). In view of this, some constitutive models have been proposed to describe the time dependent behavior of rocks

(Bourgeois et al. 2002; Haupt and Kersten 2003; Voyiadjis et al. 2004 Saleeb and Arnold 2004; Zhou et al. 2011; Yang et al. 2014; Zhou et al. 2013; Xie and Shao 2014). In these models, the time-dependent inelastic behavior is generally described by using visco-plastic theory and a large number of models' parameters need be determined. Recently, Pietruszczak et al. (2002) have proposed a general methodology for the description of creep in terms of microstructural evolution. Shao (2003) have used this methodology to propose a unified model for the description of short-term and long-term responses of an argillaceous rock.

Based on the previous research works of Pietruszczak et al. (2004) and Shao et al. (2006), a unified constitutive model is proposed to describe the short term and long term behavior of studied sandstone. The constitutive model for long term behavior is logically formulated from the extension of the model for short term behavior. The time dependent deformation is considered as a macroscopic consequence of progressive degradation of material structure. The evolution of microstructure is quantified by an internal variable, which is a function of plastic deformation and in return evolves in time. using a series of triaxial compression testes and a creep test, all the parameters of proposed model are determined. Parametric sensitivity studies are also presented to capture influences of some main parameters involved in mechanical behaviour of studied sandstone at different scales. The proposed model is applied to simulate short term triaxial compression tests and creep tests. Comparisons between simulations and experimental data are provided. In general, a good concordance is obtained between experimental data and experimental results. The investigation and discussion of numerical results can give us some advices on the treatment of cataclastic sandstone zone located in a dam foundation.

3.2. General framework

It is assumed that the sandstone exhibits irreversible deformation in different time scale: time independent instantaneous plastic strain $\varepsilon_{ij}^{\sigma p}$ due to stress evolution and time-dependent creep strain ε_{ij}^{vp} due to microstructural evolution. Therefore, the total strain is given as follows:

$$\varepsilon_{ij} = \varepsilon_{ij}^{e} + \varepsilon_{ij}^{p}; \varepsilon_{ij}^{p} = \varepsilon_{ij}^{\sigma p} + \varepsilon_{ij}^{vp} \tag{3.1}$$

The general form of stress-strain relation is written as follows:

$$\sigma_{ij} = C^0_{ijkl}\left(\varepsilon_{kl} - \varepsilon^p_{kl}\right) \tag{3.2}$$

where C^0_{ijkl} is the component of initial elastic stiffness tensor.

As the emphasis of this chapter is put on the description of long term behavior of sandstone, it is assumed that the instantaneous damage is neglected. On the other hand, in order to give a quantitative description of evolution of microstructure, an internal variable ζ is introduced. It is expressed as a scalar valued function of plastic deformation and in turn evolves with time (Pietruszczak et al. 2002; Pietruszczak et al. 2004). And it is assumed that for $t \to \infty$ there is $\zeta \to \bar{\zeta}$. Therefore, $\bar{\zeta}$ represents a stationary state associated with microstructure equilibrium at the grain contact level, which depends on the confining pressure and deviatoric stress. It is postulated that the kinetics of microstructure evolution can be described in terms of the deviation from the equilibrium state, measured by $(\bar{\zeta} - \zeta)$. For the sake of simplicity, the evolution law may be expressed in a simple linear form:

$$\frac{\partial \zeta(t)}{\partial t} = \gamma(V_k)\left(\bar{\zeta} - \zeta\right) \tag{3.3}$$

where $\gamma(V_k)$ is a material constant. $\bar{\zeta} \in [0,1]$ while $\zeta \in \left[0, \bar{\zeta}\right]$.The function $\zeta(t)$ can be formally defined by using the Laplace transforms and convolution theorems. Taking $\zeta(0) = 0$, we obtain:

$$\zeta(t) = \int_0^t \gamma \bar{\zeta}(\tau) e^{-\gamma(t-\tau)} d\tau \tag{3.4}$$

Thus, the degradation parameter ζ depends on the history of the time derivative of $\bar{\zeta}$, whereas the exponential term represents the memory effect. As the parameter ζ represents the relative change in the cemented contact area of grains in a representative volume of material (Xie et al. 2006), the elastoplastic behavior of studied material should be affected by ζ.

Inspired by the research work of Shao et al. (2003), we assume the time dependent degradation affects the elastic modulus as follows:

$$E = (1 - \alpha\zeta) E_0 \tag{3.5}$$

E_0 is the initial elastic modulus of studied sandstone . The parameter α controls the influence of material degradation on the elastic modulus of studied material.

According to the plasticity mechanism, following the framework developed by Pietruszczak et al. (2002 and 2004) and taking into account the time dependent degradation effects, the plastic yield criterion and plastic potential can be respectively expressed as in the general form:

$$f\left(\sigma_{ij},\alpha_p,\zeta\right)\le 0 \tag{3.6}$$

$$g\left(\sigma_{ij},\alpha_p,\zeta\right)\le 0 \tag{3.7}$$

In these equations, σ_{ij} represents the Cauchy stress tensor. α_p is plastic hardening function and can be deduced by standard derivative of the thermodynamic potential.

By introducing the degradation of elastic modules into the constitutive equation (3.2), we have:

$$\sigma_{ij}=\left(1-\alpha\zeta\right)C^0_{ijkl}\left(\varepsilon_{kl}-\varepsilon^p_{kl}\right) \tag{3.8}$$

The incremental form of constitutive equation is written as follows:

$$d\sigma_{ij}=\left(1-\alpha\zeta\right)C^0_{ijkl}\left(d\varepsilon_{kl}-d\varepsilon^p_{kl}\right)-\alpha C^0_{ijkl}\left(\varepsilon_{kl}-\varepsilon^p_{kl}\right)d\zeta \tag{3.9}$$

According to the plastic deformation, it can be defined by using the plastic flow rule:

$$d\varepsilon^p=d\lambda_p\frac{\partial g\left(\sigma_{ij},\alpha_p,\zeta\right)}{\partial\sigma_{ij}} \tag{3.10}$$

The plastic multiplier $d\lambda_p$ is determined by introducing the equation (3.9) into the plastic consistency condition:

$$df=\frac{\partial f}{\partial\sigma_{ij}}d\sigma_{ij}+\frac{\partial f}{\partial\alpha_p}d\alpha_p+\frac{\partial f}{\partial\zeta}d\zeta \tag{3.11}$$

We have:

$$d\lambda_p=\frac{\left(1-\alpha\zeta\right)\dfrac{\partial f}{\partial\sigma_{ij}}C^0_{ijkl}d\varepsilon_{kl}-\left(\alpha\dfrac{\partial f}{\partial\sigma_{ij}}C^0_{ijkl}\varepsilon^e_{kl}+\dfrac{\partial f}{\partial\zeta}\right)d\zeta}{\left(1-\alpha\zeta\right)\dfrac{\partial f}{\partial\sigma_{pq}}C^0_{pqmn}\dfrac{\partial g}{\partial\sigma_{mn}}-\dfrac{\partial f}{\partial\alpha_p}\dfrac{\partial\alpha_p}{\partial\varepsilon^p_{ij}}\dfrac{\partial g}{\partial\sigma_{ij}}} \tag{3.12}$$

We can notice that the plastic flow can be decomposed into two parts: the instantaneous plastic deformation due to the strain variation $d\varepsilon_{kl}$ created by applied stress and the plastic creep

deformation due to material degradation $d\zeta$. In the absence of material degradation ($\zeta = 0$ and $d\zeta = 0$), one observes that the short term plastic behaviour is characterized by the basic plastic model.

Introduction the equations (3.12) and (3.10) into the constitutive equation (3.9), the increment of stresses for a prescribed increment of strains is obtained:

$$d\sigma_{ij} = C^{epd}_{ijkl} d\varepsilon_{kl} + \psi^{\zeta}_{ij} \dot{\zeta} dt \tag{3.13}$$

with

$$C^{epd}_{ijkl} = (1-\alpha\zeta)\left(C^{0}_{ijkl} - \frac{(1-\alpha\zeta) C^{0}_{ijpq} \frac{\partial g}{\partial \sigma_{pq}} \frac{\partial f}{\partial \sigma_{mn}} C^{0}_{mnkl}}{(1-\alpha\zeta) \frac{\partial f}{\partial \sigma_{pq}} C^{0}_{pqmn} \frac{\partial g}{\partial \sigma_{mn}} - \frac{\partial f}{\partial \alpha_p} \frac{\partial \alpha_p}{\partial \varepsilon^{p}_{ij}} \frac{\partial g}{\partial \sigma_{ij}}} \right)$$

$$\psi^{\zeta}_{ij} = (1-\alpha\zeta) \frac{\left(\alpha C^{0}_{ijpq} \frac{\partial g}{\partial \sigma_{pq}} \frac{\partial f}{\partial \sigma_{mn}} C^{0}_{mnkl} \varepsilon^{e}_{kl} + \frac{\partial f}{\partial \zeta} C^{0}_{ijkl} \frac{\partial g}{\partial \sigma_{kl}} \right)}{(1-\alpha\zeta) \frac{\partial f}{\partial \sigma_{pq}} C^{0}_{pqmn} \frac{\partial g}{\partial \sigma_{mn}} - \frac{\partial f}{\partial \alpha_p} \frac{\partial \alpha_p}{\partial \varepsilon^{p}_{ij}} \frac{\partial g}{\partial \sigma_{ij}}} - \alpha C^{0}_{ijkl} \varepsilon^{e}_{kl} \tag{3.14}$$

Where C^{epd}_{ijkl} is the tangent elastopalstic stiffness tensor of damaged material and corresponds to the instantaneous variation of stresses due to applied stress variation . ψ^{ζ}_{ij} is a second order tensor defining the variation of stress during relation process induced by material degradation. In the absence of material degradation ($\zeta = 0$ and $d\zeta = 0$), C^{epd}_{ijkl} is the fourth order tangent elastoplastic tensor. The equation (3.13) can be easily implemented in a computer code with finite element method (Bodas Freitas et al. 2011; Simo and Hughes 1998), with the displacements of nodes as principal unknowns.

In the case of creep test, the material is subjected to a given stress level. Therefore, it is necessary to determine the variation of strains as function of time. The general formulation for the creep path is provided in the following paragraphs. The stress-strain relation is first obtained by investing the equation (3.8):

$$\varepsilon_{ij} = \frac{1}{1-\alpha\zeta} D^{0}_{ijkl} \sigma_{kl} + \varepsilon^{p}_{ij}, \qquad D^{0} = \left(C^{0} \right)^{-1} \tag{3.15}$$

where D^0 is the initial elastic compliance tensor of intact material in drained condition. By

using the differentiation of the previous equation, the increment form of strain-stress relation can be obtained:

$$d\varepsilon_{ij} = \frac{1}{1-\alpha\zeta} D^0_{ijkl} d\sigma_{kl} + \frac{\alpha}{(1-\alpha\zeta)^2} D^0_{ijkl}\sigma_{kl} d\zeta - \frac{\dfrac{\partial f}{\partial \sigma_{mn}} d\sigma_{mn} \dfrac{\partial g}{\partial \sigma_{ij}} - \dfrac{\partial f}{\partial \zeta}\dfrac{\partial g}{\partial \sigma_{ij}} d\zeta}{\dfrac{\partial f}{\partial \alpha_p}\dfrac{\partial \alpha_p}{\partial \varepsilon^p_{ij}}\dfrac{\partial g}{\partial \sigma_{ij}}} \tag{3.16}$$

We can rewrite the strain–stress relation (3.16) in the following form:

$$d\varepsilon_{ij} = D^{epd}_{ijkl} d\sigma_{kl} + \psi^{\sigma}_{ij}\dot{\zeta} dt \tag{3.17}$$

With

$$D^{epd}_{ijkl} = \frac{1}{1-\alpha\zeta} D^0_{ijkl} - \frac{\dfrac{\partial g}{\partial \sigma_{ij}}\dfrac{\partial f}{\partial \sigma_{kl}}}{\dfrac{\partial f}{\partial \alpha_p}\dfrac{\partial \alpha_p}{\partial \varepsilon^p_{ij}}\dfrac{\partial g}{\partial \sigma_{ij}}}; \psi^{\sigma}_{ij} = \frac{\alpha}{(1-\alpha\zeta)^2} D^0_{ijkl}\sigma_{kl} - \frac{\dfrac{\partial f}{\partial \zeta}\dfrac{\partial g}{\partial \sigma_{ij}}}{\dfrac{\partial f}{\partial \alpha_p}\dfrac{\partial \alpha_p}{\partial \varepsilon^p_{ij}}\dfrac{\partial g}{\partial \sigma_{ij}}} \tag{3.18}$$

where D^{epd}_{ijkl} is the tangent elastic compliance tensor of damaged material and ψ^{σ}_{ij} a second order tensor defining creep deformation. Therefore, the creep strain can be evaluated as a function of material degradation. Moreover, we notice that the total increment of strains $d\varepsilon_{ij}$ can be decomposed into two parts: an instantaneous elastoplastic deformation due to applied load ($d\sigma_{kl}$) and a time dependent plastic part during creep process induced by material degradation ($d\zeta$). As a constant stress is applied on the laboratory sample during the creep test, we have $d\sigma_{kl} = 0$. On the other hand, in the absence of material degradation ($d\zeta = 0, \zeta = 0$), the elastoplastic plastic behavior described by the basic elastoplastic model is recovered.

3.3. Specific model for studied sandstone

By using the general framework defined in the previous section, specific functions for studied sandstone are now proposed. Typical stress-strain curves from triaxial compression tests have shown that large residual strains are observed in the axial and lateral directions after unloading of deviaotric stress. Moreover, the material strength, plastic flow and creep evolution depend strongly on the mean stress. Based on the experimental investigation, a Drucker-Prager type linear function

is used to describe plastic yielding and failure surface (Fig. 3.1):

$$f = q + A\alpha_p \left(p - C_0 \right) = 0 \tag{3.19}$$

$$p = \frac{1}{3}\sigma_{kk}, \quad q = \sqrt{3J_2}, J_2 = \frac{1}{2}S_{ij}S_{ij}, \quad S_{ij} = \sigma_{ij} - \frac{1}{3}\sigma_{kk}\delta_{ij} \tag{3.20}$$

where p is the mean stress, q deviatoric stress. The parameter C_0 represents the material cohesion, while A is the frictional angle of failure surface. The experimental investigation exhibits that the evolution of microstructure induces a degradation of material strength and has also an impact on the plastic behaviour of studied sandstone . Similary to the linear function proposed for the evolution of elastic module (3.5), the time-dependent degration effects on the evolution of failure surface parameter A is described by the following function:

$$A = \left(1 - \beta\zeta\right) A_0 \tag{3.21}$$

Where A_0 is the value of the frictional angle of failure surface for intact material. β controls the influence of material degradation on the evolution of failure surface. In a conventional triaxial compression test, $\zeta = 0$ and $d\zeta = 0$. The influence of two parameters C_0, A_0 on the failure surface are shown in Fig. 3.2-Fig. 3.3.

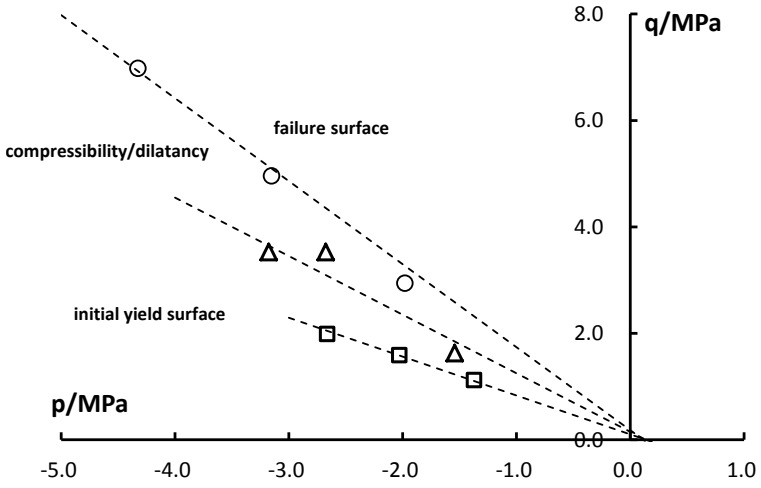

Fig. 3.1. Illustrationof plastic yielding surface, failure surface and compaction/dilatation boundary in $p-q$ plan for studied sandstone

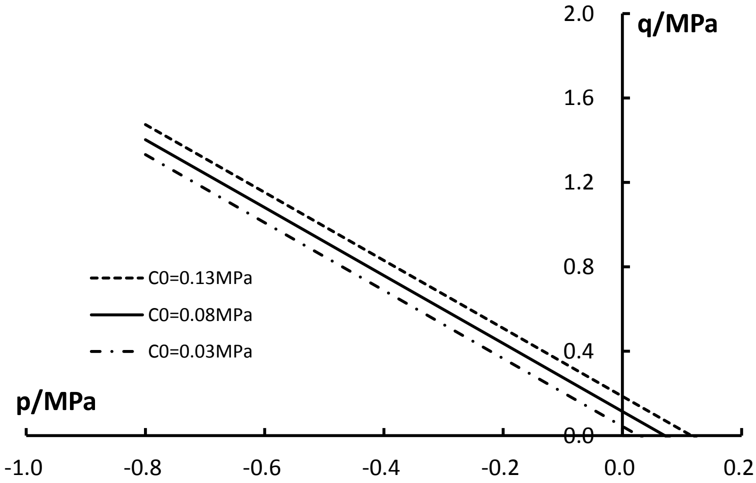

Fig. 3.2. Influence of cohesion parameter C_0 on the failure surface

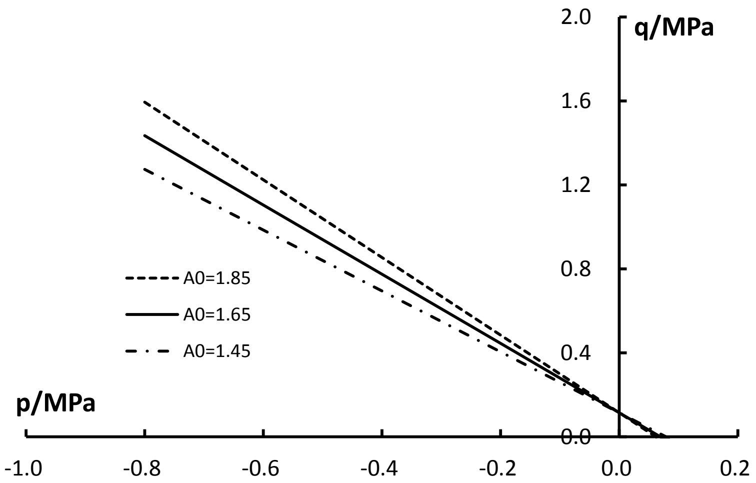

Fig. 3.3. Influence of frictional coefficient A_0 on the failure surface

The plastic hardening is described by the increasing function α_p of the generalized plastic shear strain γ_p. Base on the experimental data obtained on the studied sandstone, the following exponential function is proposed for the plastic hardening law:

$$\alpha_p = 1.0 - \left(1.0 - \alpha_p^0\right) e^{-b\gamma_p} \tag{3.22}$$

$$\gamma_p = \int \sqrt{\frac{2}{3} de_{ij}^p de_{ij}^p} \Big/ \chi_p, \quad e_{ij}^p = \varepsilon_{ij}^p - \frac{1}{3}\varepsilon_{kk}^p \delta_{ij}, \quad \chi_p = \left(\langle -p/3 \rangle + p_r\right)/p_r \tag{3.23}$$

The initial value of yield function α_p^0, defines the initial plastic yield threshold and can be

deduced by drawing the locus of stresses at onset of inelastic strains (Fig. 3.1). The ultimate value of the hardening function is $\alpha_p = 1$, corresponding to the material failure. The parameter b controls the hardening law rate. The evolution of yield surface with plastic hardening process is illustrated in Fig. 3.4.

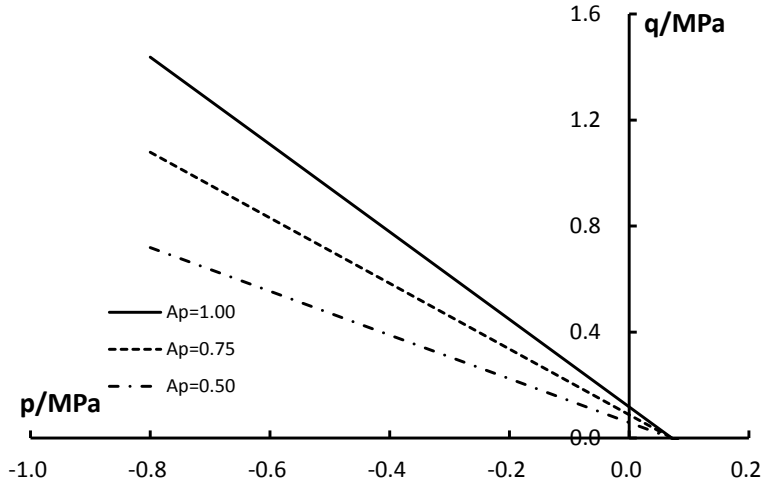

Fig. 3.4. Evolution of yield surface with plastic hardening function

Furthermore, the volumetric deformation of studied sandstone exhibits a dramatic transition from compaction to dilantacy in the conventional triaxial compression tests. In view of this, it is necessary to propose a non-associated plastic flow rule. Based on experimental inverstigation and inspired by the elastoplastic model proposed by Pietruszczak et al. (1988), the following function is used :

$$g = q + A\eta\left(p - C_0\right)\ln\left(\frac{p - C_0}{I_0}\right) = 0 \tag{3.24}$$

The variable I_0 represents the stress state at the intersection between the plastic potential surface and the mean stress axis $p - C_0$ and its value is negative $\left(I_0 < 0\right)$.By using this potential, the stress space is divided into two zones, respectively corresponding to plastic compressibility and dilation. The boundary between these two zones is defined by the condition $\partial g_\sigma / \partial p = 0$. In this model, we assume that this boundary can be given by a linear function:

$$f_s = q - A\eta\left(p - C_0\right) = 0 \tag{3.25}$$

The parameter η defins the boundary line between compressibility to dilation zones. In Fig. 3.1, take the sample **a**, sample **d** and sample **g** as example, the initial yield surface, failure surface and compaction/dilatation transition line are compared with the experimental data from studied sandstone.

3.4. Identification of model's parameters

The proposed model contains ten parameters: two elastic constants for the intact material (E_0, ν_0), five parameters $(A_0, C_0, \alpha_p^0, b, \eta)$ for the description of instantaneous plastic deformation and three parameters (α, β, γ) for the time-dependent deformation.

The initial elastic constants (E_0, ν_0) can be observed from the linear part of stress-strain curves from triaxial compression tests. As only very slight variation of elastic parameters is observed with the confining pressure, the mean values obtained in various triaxial compression tests are used in the numerical simulation.

According to four parameters $(A_0, C_0, \alpha_p^0, b, \eta)$ controlling the evolution of instantaneous plastic deformation, they can be identified by using a series of triaxial compression tests performed under different confining pressure. The parameters included in the failure criterion (A_0, C_0), characterizing the failure surface, can be deduced by drawing the locus of peak stresses in $p-q$ plane. The parameter for the initial yield surface α_p^0 is captured from the locus of stresses at onset of inelastic strains. The plastic hardening parameter B can be obtained by drawing the function of α_p versus plastic deviatoric strain γ_p (Fig. 3.5, take the sample **a**, sample **d** and sample **g** as example). By identifying the stress point where the volumetric strain rate is close to zero on stress-strain curves, the parameter η can be identified. The corresponding failure surface, initial yield surface and compressibility/dilatancy line are illustrated in Fig. 3.1.

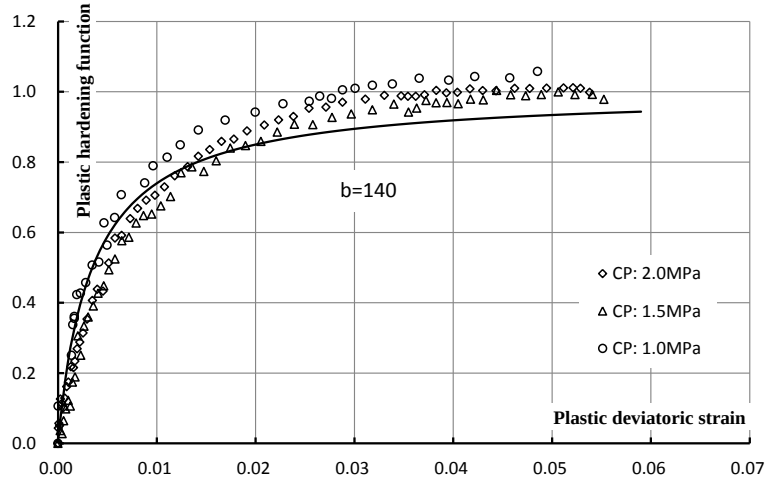

Fig. 3.5. Evolution of Plastic hardening function α_p versus plastic deviatoric strain γ_p

According the parameters related to the time dependent responses, their value can be determined by simulating a creep test. Therefore, using a ceep test and a series of triaxial compression tests performed under different confining pressures, all the parameters of the proposed model can be identified and their values are summarized in Table 3.1.

Table 3.1. Typical values of model's parameters for studied sandstone

Parameter	Elastic	Short term	Long-term
Value	$E = 430\ MPa$ $\upsilon = 0.2$	$A = 1.58$ $C_0 = 0.12\ MPa$ $\alpha_p^0 = 0.25$ $\eta = 1.0$ $B = 140$	$\gamma = 0.00005$ $\alpha = 1.0$ $\beta = 1.0$

3.5. Parametric study

Aforementioned, the parameters of proposed model can be identified from relevant experimental data. In order to get a good knowledge on the performance of proposed model, the influence of model's parameters on short term and long term behaviour of studied material are studied in this section. The values given in Table 3.1 are taken as the reference ones. When the influence of one parameter is studied, we change only the value of this parameter but leave the

others alone. In this section, two tests are simulated with different series of paremters, which include:

- A triaxial compression tests performed under the confining pressure CP=2.0 MPa
- A creep test conducted with the confining pressure 2.0 MPa and the diatoric stress 5.00 MPa.

3.5.1. Influences of drained Young's modulus E_0

The influence of the Young's modulus E_0 is firstly studied (Fig. 3.6-Fig. 3.7). The comparison of numerical results shows that deformations increase significantly when Young's modulus decrease. This phenomenon is due to the fact that the deformability of the rock increases when the drained Young's modulus decreases. However, the peak stress has not been disturbed by the variation of Young's modulus. The same tendency is observed in the numerical simulation of creep test. The creep deformations increase significantly with the decrease of elastic modulus E_0.

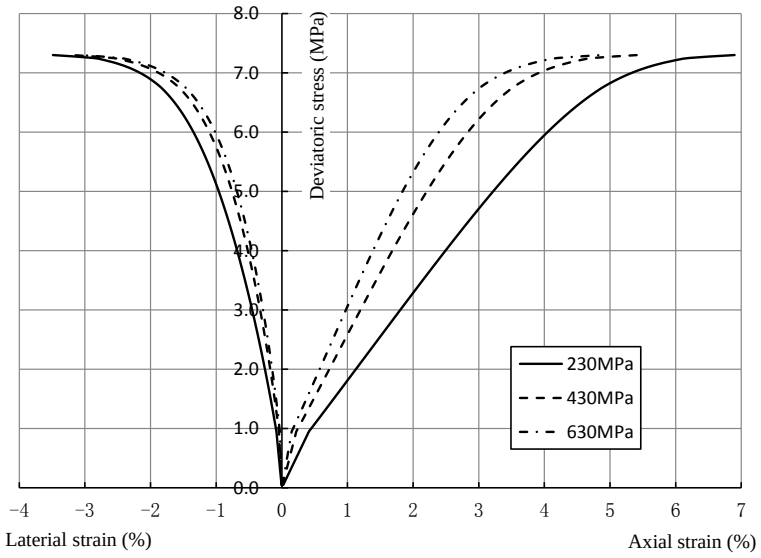

Fig. 3.6. Influence of elastic parameters E_0 on the strain-stress curves of triaxial compression test with the confining pressure 2MPa

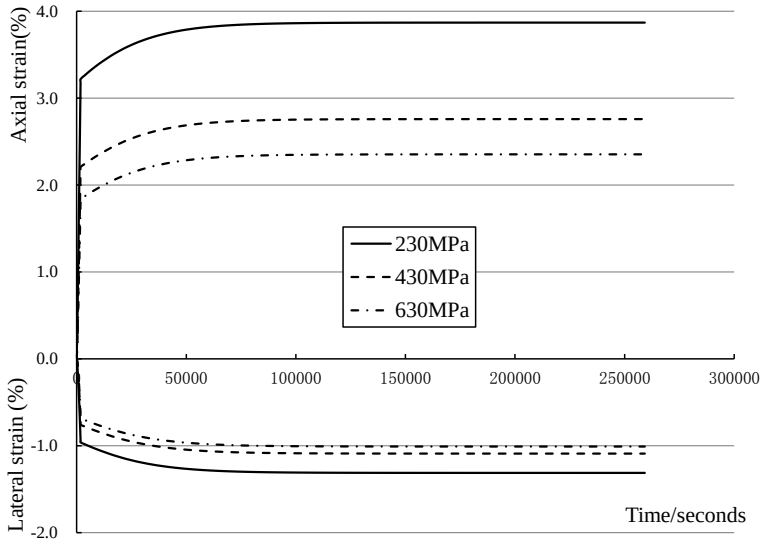

Fig. 3.7. Influence of elastic parameters E_0 on creep deformation with the confining pressure 2MPa

3.5.2. Influences of initial yield surface paramter α_p^0

In this section, different calculations with three values of α_p^0 are compared. The influence of intitial yield surface parameter α_p^0 is firstly presented in the Fig. 3.8. In the case where a small value of α_p^0 is used, large deformations are observed. this observation is due to the fact that with a small value of α_p^0, the plastic deformation starts to develop in the studied material at very low level of stress. However, the peak stress is always the same for three cases .

On the other hand, the numerical simulations of creep test with different values of α_p^0 are given in Fig. 3.9. Large creep deformation is observe in the case where a small value of α_p^0 is used. By comparing different creep curves, we observe that the creep deformation increases when the value of α_p^0 decreases. Therefore, the parameter α_p^0 has an impact on the deformation field evolution of rock and but cannot disturb the mechanical strength of rock.

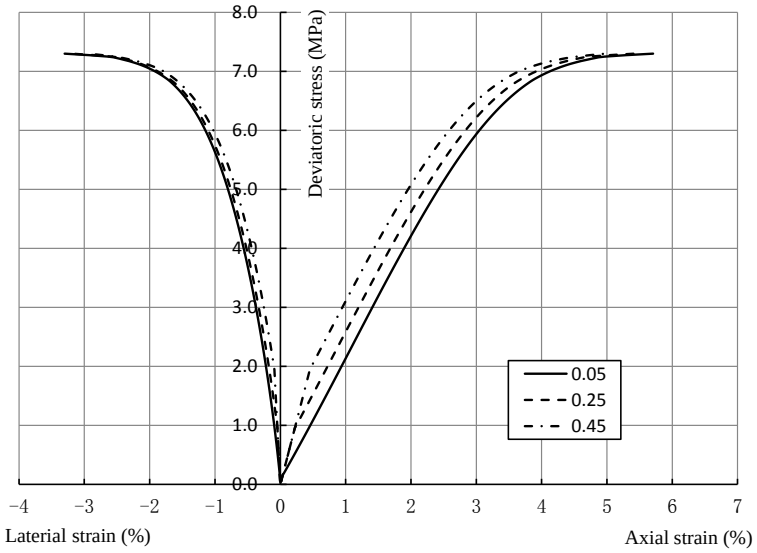

Fig. 3.8. Influence of α_p^0 on the strain-stress curves of triaxial compression test with the confining pressure 2MPa

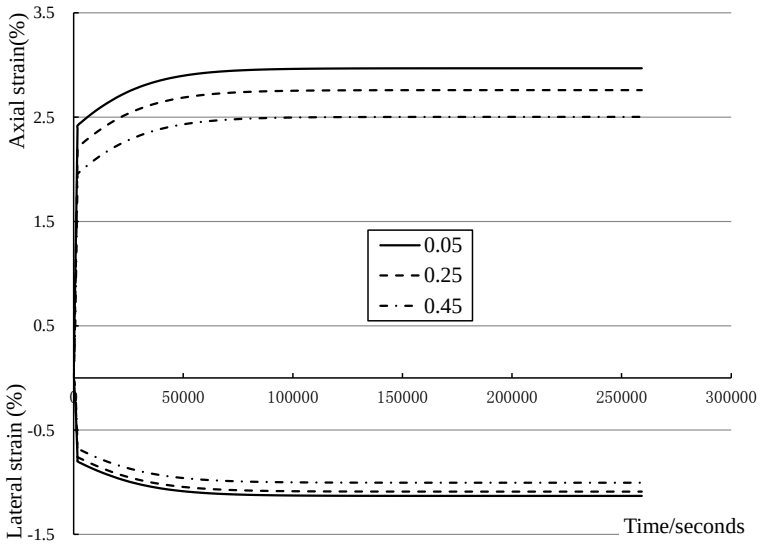

Fig. 3.9. Influence of α_p^0 on creep deformation with the confining pressure 2MPa

3.5.3. Influences of failure surface parameter A_0

According to Eqs. (3.19) and (3.24), the parameter A_0 has an important impact on the plasticity mechanism. The influence of parameter A_0 on the instantaneous mechanical behavior of studied material is presented in Fig. 3.10-Fig. 3.11. With a smaller value of A_0, the rock has

smaller yield stress. As a result, at a given stress level, large plastic strain are obtained a in the case where $A_0 = 1.35$ is used (Fig. 3.10). On the other hand, the same tendency is observed in the creep tests

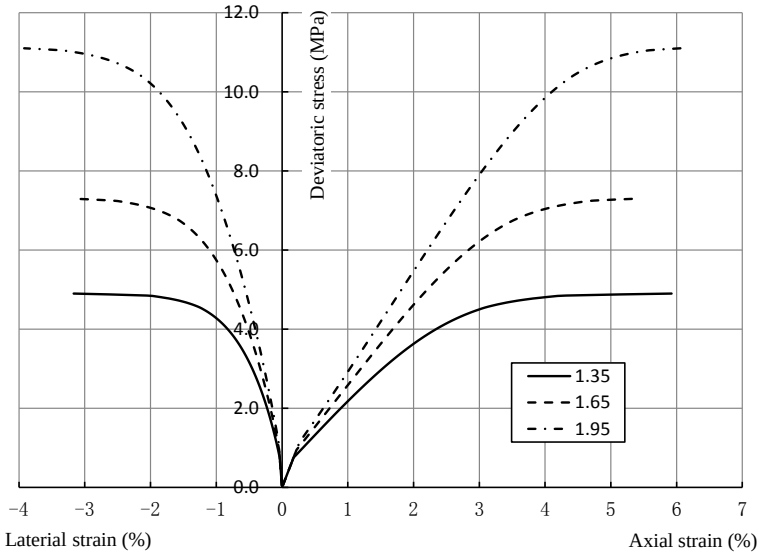

Fig. 3.10. Influence of A_0 on the strain-stress curves of triaxial compression test with the confining pressure 2MPa

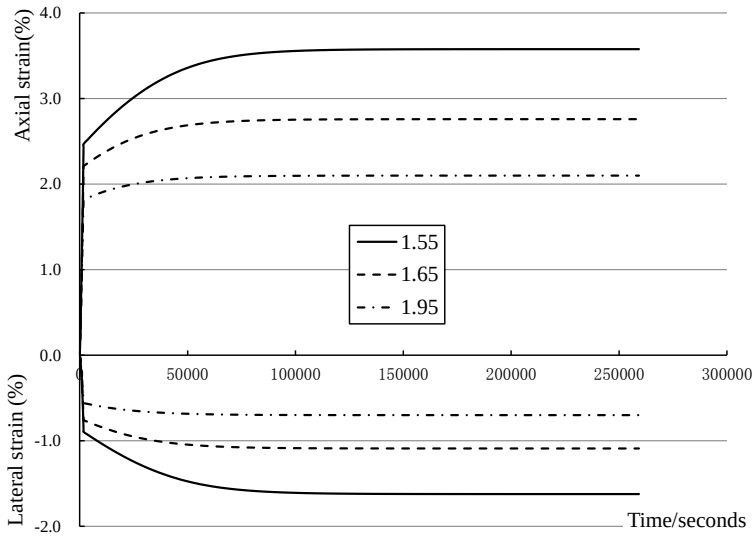

Fig. 3.11. Influence of A_0 on creep deformation with the confining pressure 2MPa

3.5.4. Influences of parameter η

According to the equation (3.24), the parameter η controls the volumetric transition

between compaction and dilatancy. The influence of the parameter η on the short term behaviour of studied material is firstly given in Fig. 3.12-Fig. 3.13. In the case where a lower value of η is used $(\eta = 0.5)$, an important volumetric dilatancy is observed at the end of test. On the other hand, the rock is always in compaction when $\eta = 1.5$. On the other hand, the time dependent behaviour of studied material is strongly disturbed by the variation of the parameter η.

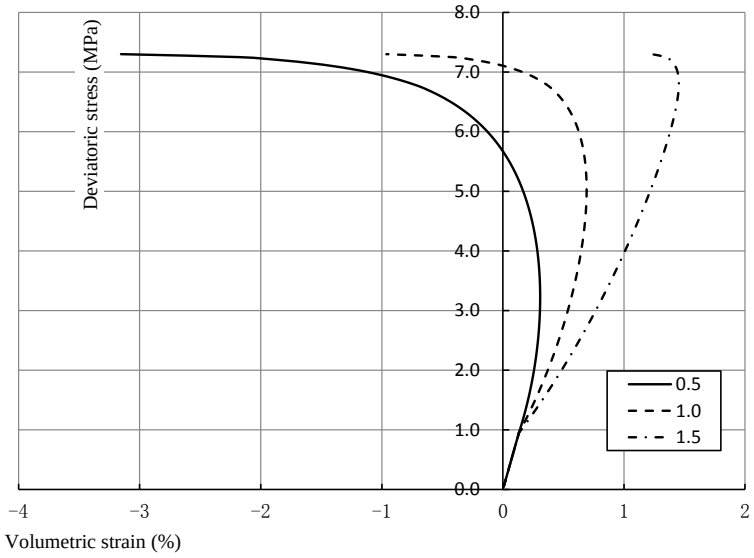

Fig. 3.12. Influence of η on the volumetric deformation of triaxial compression test with the confining pressure 2MPa

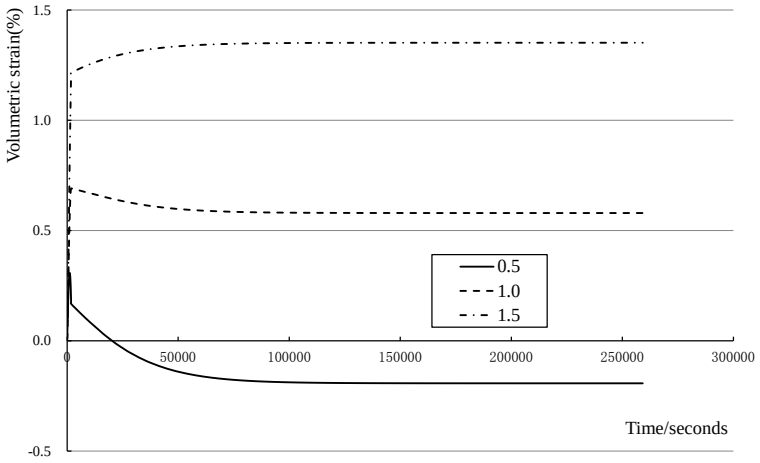

Fig. 3.13. Influence of η on creep deformation with the confining pressure 2MPa

3.5.5. Influences of parameter B

In the proposed model, the kinetic of hardening law is controlled by the parameter B. According to the equation (3.22), α_p increases significantly when the value of B is great(Fig. 3.14-Fig. 3.15).The yield surface of studied material attains rapidly the failure surface. For a given level of stress, a small strain is then observed in the case where $B=190$ while important deformation develops in the material when $B=90$.

By using the equation (3.23), the influence of confining pressure on the kinetic of hardening law is taken into account by using the function χ_p.Therefore, the proposed model is capable to describe the dramatic transition from brittle to ductile behavior observed in the triaxial compression tests . On the other hand, the same tendency is observed in the creep tests.

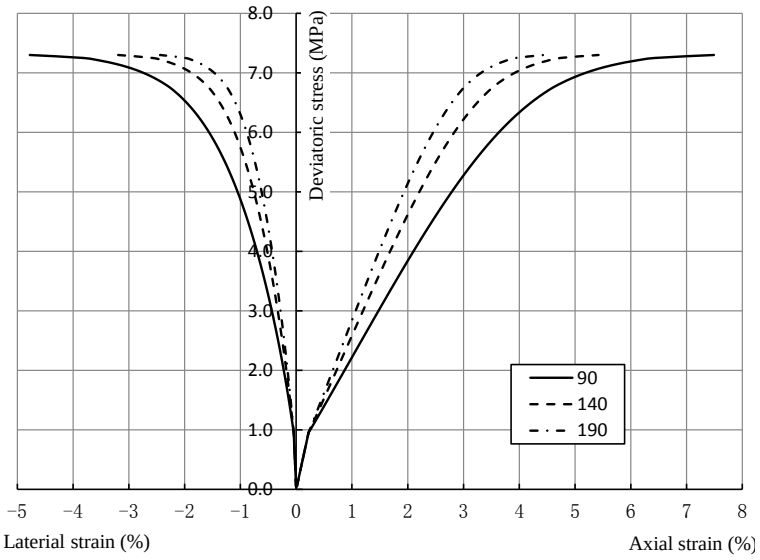

Fig. 3.14. Influences of B on the strain-stress curves with the confining pressure 2MPa

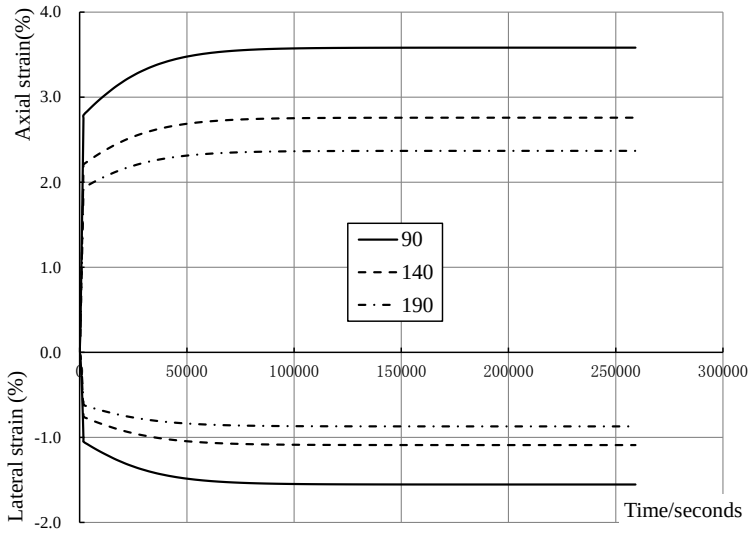

Fig. 3.15. Influences of B on creep deformation with the confining pressure 2MPa

3.5.6. Influences of creep parameter γ

As the creep parameter γ controls the evolution of time-dependent deformations, only the creep test is simulated in this section. We observe that the increase of γ accelerate the evolution of creep deformation. In the case where $\gamma = 0.0001$ is used , the creep deformation increases sharply (Fig. 3.16). However, the maximum value of creep deformation is always the same in three cases performed with different values of γ. In conclusion, the creep parameter γ controls the kinetic of creep deformations in creep test and has no influence on the maximum value of creep deformation.

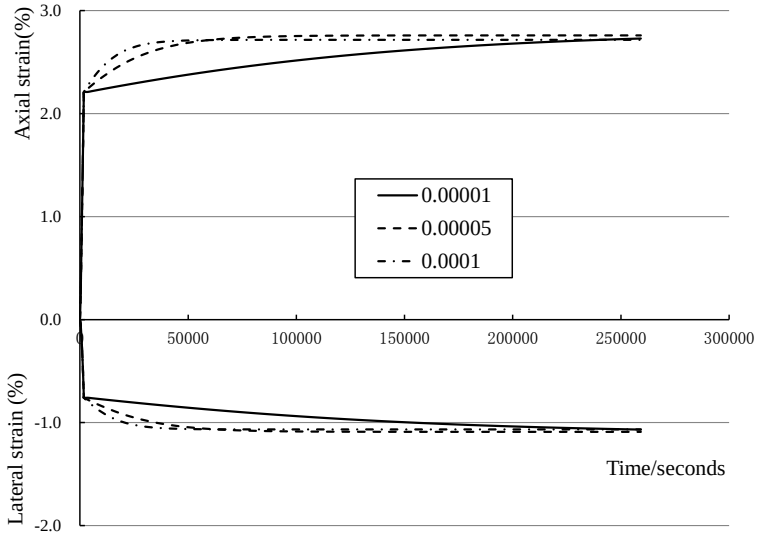

Fig. 3.16 Influences of γ on creep deformation with the confining pressure 2MPa

3.6. Simulation of short term laboratory tests

The simulations of triaxial compression test are presented in this section. The stress-strain curves of laboratory tests performed in the samples **a, d** and **g** are firstly presented in Fig. 3.17. Generally, a good agreement is obtained between simulation results and experimental data. Moreover, the dependence of mechanical behavior of studied material on the confining pressure is well simulated. As these tests have been used for the determination of the model's parameters, these comparisons represent firstly a verification of the consistency of parameters. In conclusion, the proposed model is able to reproduce the short term behaviour of studied sandstone under triaxial loading conditions. In next section, the proposed model will be used to estimate the creep deformation evolution of cataclastic sandstone.

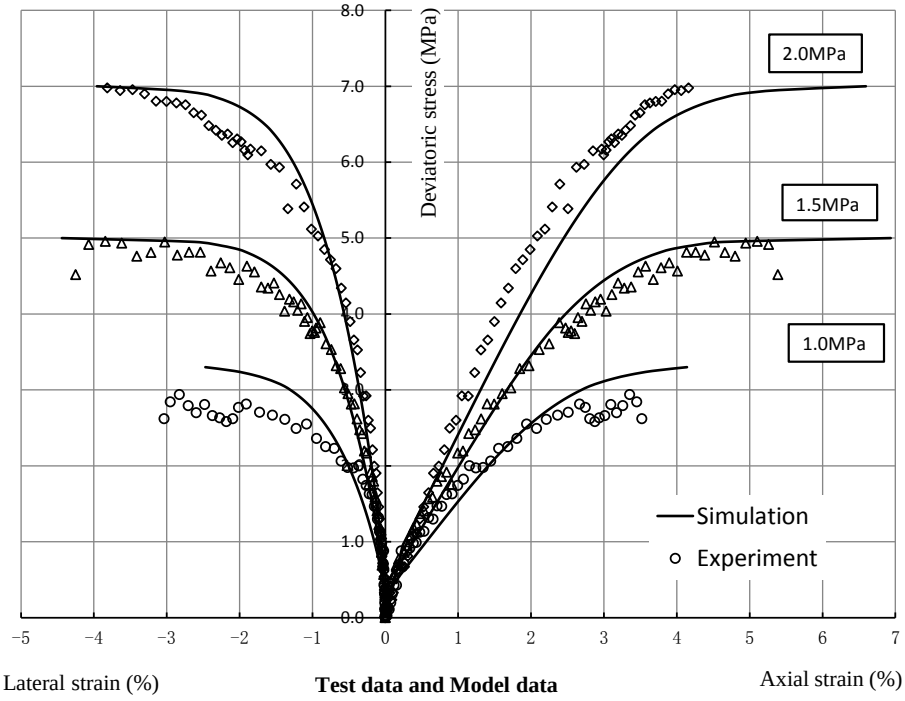

Fig. 3.17. Simulation of triaxial tests under different confining pressures.

3.7. Simulation of long term laboratory tests

The proposed model is now applied to simulate creep tests performed on the cataclastic sandstone. In Fig. 3.18-Fig. 3.20, the simulation of several traixail creep tests with different loading conditions are simulated. The applied confining pressures are respectively, 1.0MPa, 1.5MPa and

2.0MPa. During the tests, the axial stress is applied with several loading steps utile macroscropic failure of samples. The proposed model provides a good numerical prediction of creep stain during different steps and correctly reproduces the material failure by accelerated creep deformation due to unstable degradation process. Generally, a good agreement is obtained between experimental data and numerical simulation. In conclusion, the proposed model can correctly describe the creep behavior of cataclastic sandstone.

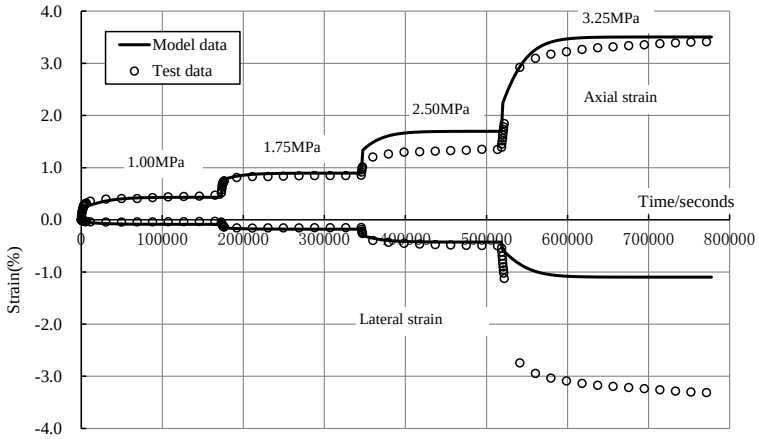

(a): PC=1.0MPa

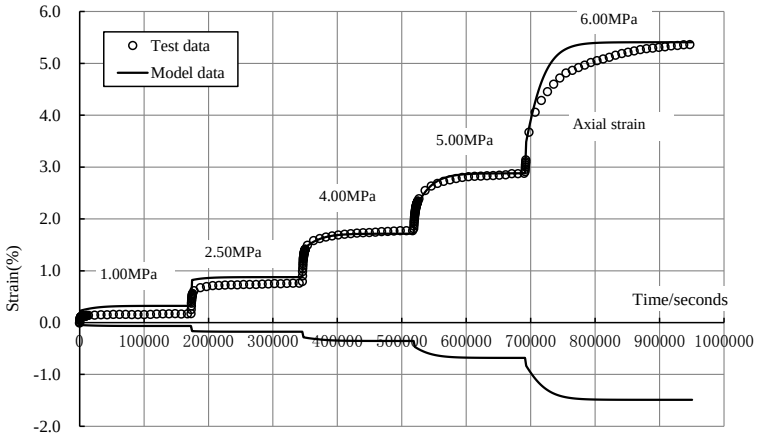

(b): PC=1.5MPa

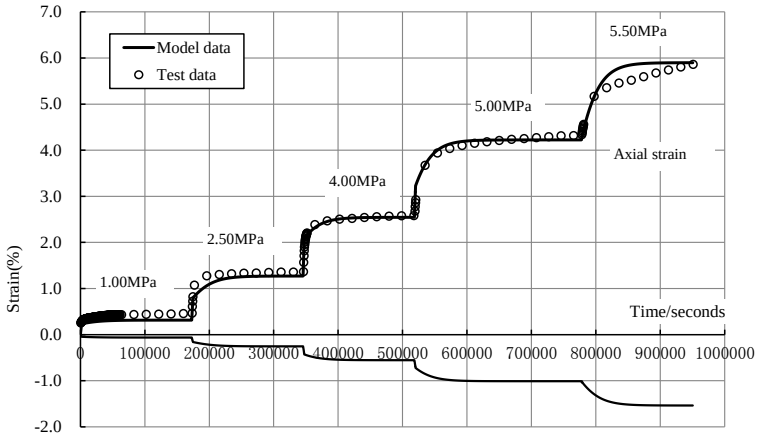

(c): PC=2.0MPa

Fig. 3.18 Simulation of creep tests performed on natural samples

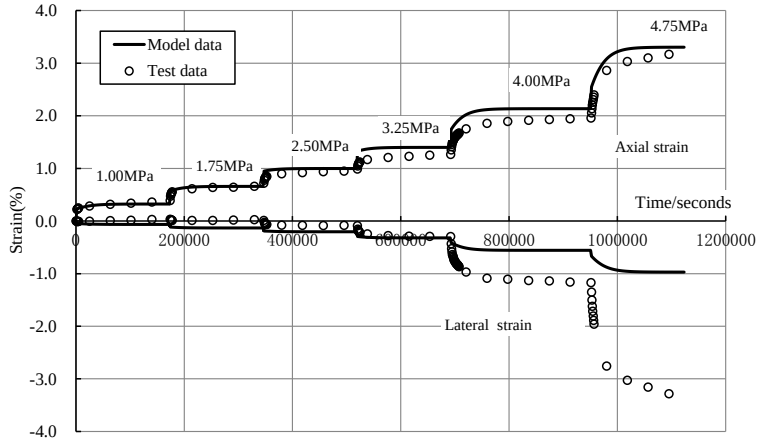

(a): PC=1.0MPa

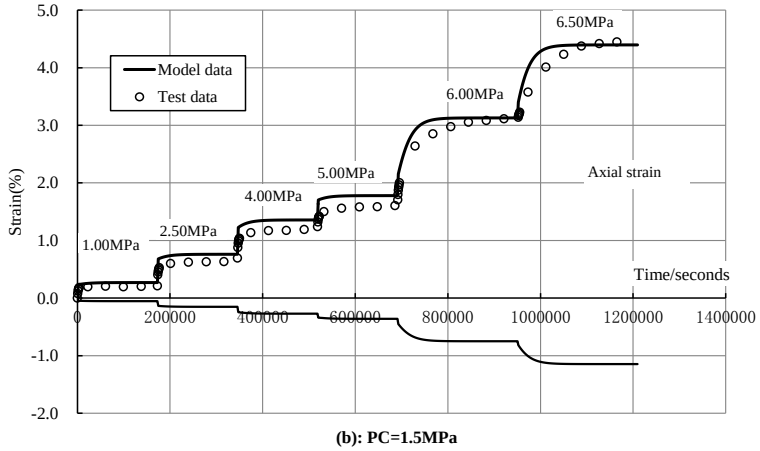

(b): PC=1.5MPa

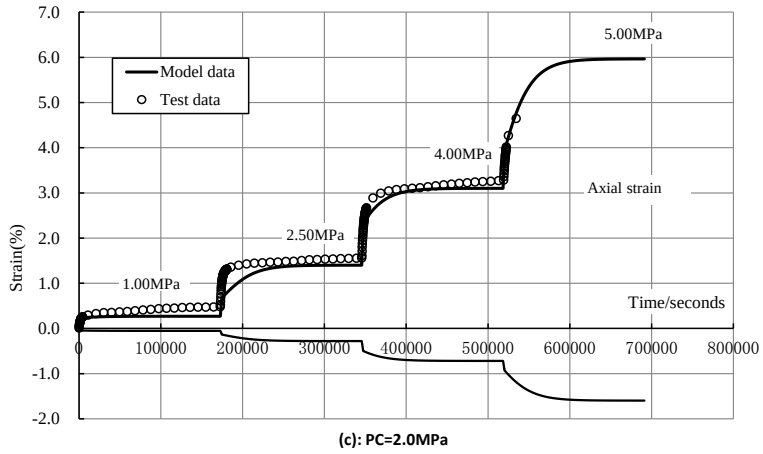

(c): PC=2.0MPa

Fig. 3.19 Simulation of creep tests under the water pressure 0.25MPa

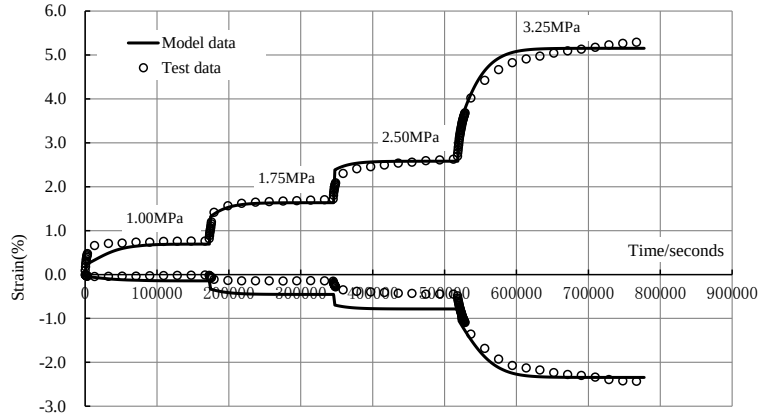

(a): PC=1.0MPa

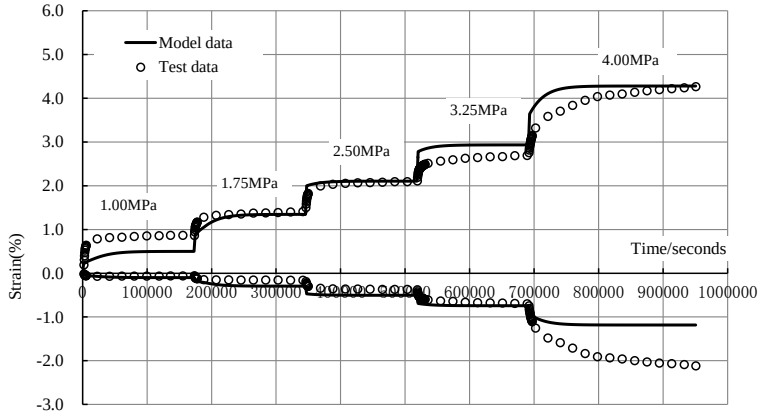

(b): PC=1.5MPa

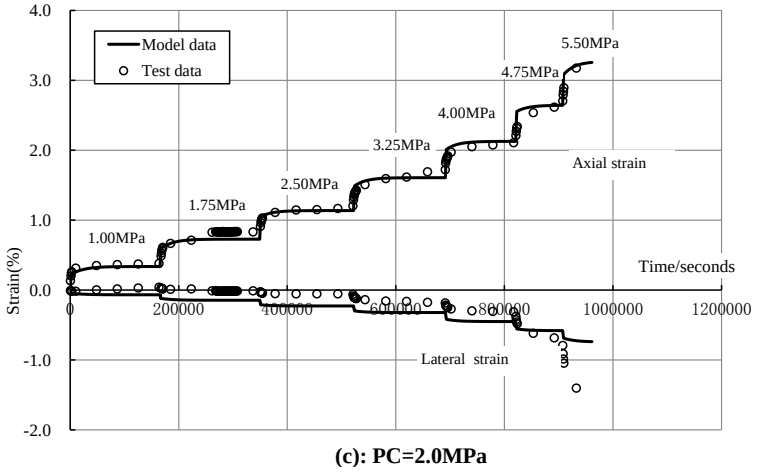

(c): PC=2.0MPa

Fig. 3.20 Simulation of creep tests under the water pressure 0.35MPa

3.8. Discussion

Furthermore, with the proposed model, we can predict the diminution of elastic modulus with time, as a macroscopic consequence of microstructural evolution (Fig. 3.21). In general, the elastic modulus is decreased progressively as time goes by. By comparing the evolutions of Young's modulus obtained under different confining pressures, we observe that the degration of elastic modulus is decelerated by the confining pressure. The curves obtained at the confining pressure of 1.0MPa are smaller than 2.0MPa.

The evolution of stationary state of microstructure $\bar{\zeta}$ is presented in Fig. 3.22 for creep tests performed under different confining pressures. Generally, the value of $\bar{\zeta}$ increases by a logarithmic function with the growth of deviatoric stress. By comparing the curves obtained with different confining pressures, it is observed that the confining pressure prevents the development of microstructure degradation. In the case where the confining pressure is 2.0MPa, the smallest $\bar{\zeta}$ is obtained. Therefore, the variation of $\bar{\zeta}$ depends strongly on the applied stress load.

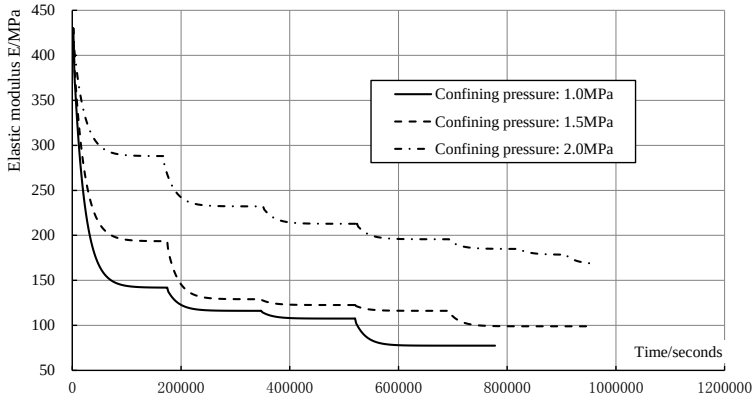

Fig. 3.21. Diminution of elastic modulus with time under water pressure 0.35MPa

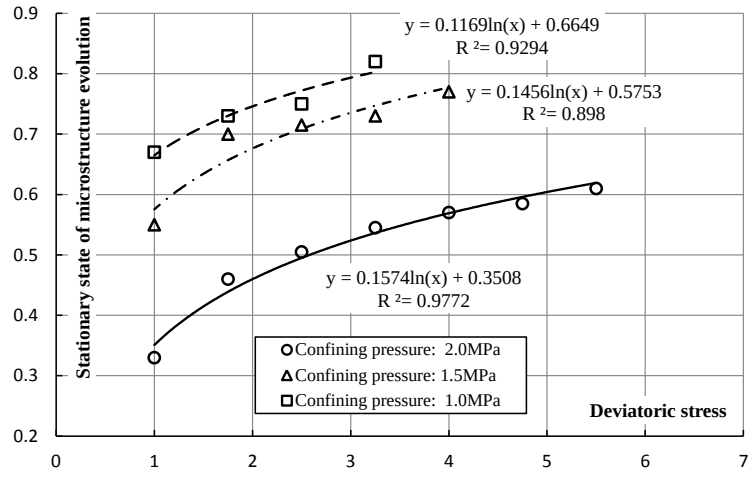

Fig. 3.22. Variation of stationary state of microstructure evolution under various water pressures

3.9. Conclusions

The mechanical behavior of cataclastic sandstone is studied in this chapter. A unified constitutive model is proposed for the description of instantaneous and time-dependent behavior of cataclastic sandstone. Starting from an elastoplastic model for the description of instantaneous behavior, a creep model for time dependent behavior is logically formulated from the extension of elastoplastic model. The creep behavior is described numerically by the progressive degradations of elastoplastic properties and failure coefficient of microstructure with time. The proposed model contains a small number of parameters which can be determined from standard triaxial compression tests and a creep test. Comparisons between numerical simulations and test data have been presented for various triaxial compression tests and creep tests. The proposed model is able to

describe the main features of the mechanical behavior of the cataclastic sandstone, such as plastic deformation, pressure sensitivity, plastic compressibility–dilation transition, degradation of elastic properties and failure coefficient. A series of parametric sensitivity studies have been performed in order to capture influences of some main parameters involved in mechanical behaviour of studied sandstone at different scales. Finally, even if only the triaxial compression tests and the creep tests are simulated in the present study, the proposed model can be used for the description of other time dependent behavior, such as relaxation test, unloading creep test and constant strain rate test. In the next chapter, we will use the proposed model to study the long term stability of a hydropower station.

Chapter 4. Study on the long-term stability of the bedrock of a hydro-power station

Abstract: Numerical modeling of the bedrock of a hydropower station in southwestern China is presented in this chapter. The in-situ investigation exhibits an important deflection cataclastic sandstone zone crossing the bedrock. The numerical simulation is performed by using a fully coupled finite element computer code. The numerical results show that an important displacement and plastic zone is observed in cataclastic sandstone zone as well as a rapid dissipation of liquid pressure due to the great permeability of foundation materials. In order to guarantee the long-term stability and performance of hydropower station, a series of sensitivity studied are performed with different hydro-mechanical parameters for cataclastic sandstone. The investigation and discussion of numerical results helps the engineers to complete their knowledge on the treatment of cataclastic sandstone zone.

Keywords: Hydropower Station; cataclastic sandstone; numerical simulations; long-term stability; two-dimensional finite element modeling

4.1. Introduction

The bedrock of a hydropower station in southwestern china is studied in this chapter. Southwestern China is a mountainous and high-rainfall area, where there are many existing large-scale hydropower engineering projects, such as the Jinping First or Second Hydropower Project on the Yalong River, the Xiangjiaba Hydropower Project on the Jinsha River, and the Xiaowan Hydropower Project on the Lanchang River, as well as some other hydropower projects under construction and will be completed in the coming decade, which bring severe challenge for experiment, theoretical and numerical researches on creep failure behavior of rock and long-term stability of rock engineering.

A key problem in hydropower station design is providing enough stability to prevent slide, and the difficulty increases if there are several weak structural planes in the dam foundation. According to the hydropower station, its foundation and abutments may be deformed during several decades due to the viscoplasticity of construction materials. Therefore, the stability loss and failure of dam

taken place eventually after several decades of its construction (Rudnicki and Rice 1975; Briffaut et al. 2012; Xiong et al. 2012). In order to guarantee the long term stability of engineering structure, it is necessary to study the long term behavior of foundation with the consideration of creep properties of bedrock .

In this chapter, the studied hydropower station project is firstly presented. Based on the laboratory data, the parameters of proposed model presented in previous chapter are determined respectively for two bedrocks and some reprehensive laboratory tests are simulated. By using a fully coupled finite element code, the bedrock is simulated. Important displacement and damage is observed in the fault zone, composed of catalclastic sandstone. Parametric sensitivity studies are also presented to capture influences of some main parameters involved to enrich the knowledge of engineers on the treatment of cataclastic sandstone zone.

4.2. General situation of the project

The hydropower Station is a dam and hydroelectric power plant currently being constructed on Jin-sha River in China, located on the border of Yi-bin in Sichuan Province (left bank) and Shui-fu in Yunnan Province (right bank) of China (Fig. 4.1). This project, which started at the end of 2006 and will be finished in 2015, is the fourth largest hydropower station of China. The station has a total installed power production capacity of 6000 megawatts (MW) and an average annual power production of 30 billion kilowatt-hours (KW•h). It is designed for power provision, farmland irrigation and flood control, as well as improved navigation downstream. The dam will be a concrete gravity dam with height of 161m and length of 909m. The altitude of the top of gravity dam is 384m.

The Limeiwan fractured zone, composed essentially the cataclastic sandston, crosses the dam foundation of the hydropower Station (Fig. 4.2). Its width and thickness range from 40m to 70m and from 10m to 60m, respectively. The in-situ engineering geological investigations exhibit that the main factors influencing the stability of the bedrock is fracture zone. The main media of fracture zone is cataclastic sandstone. Therefore, the long-term stability of bedrock should be investigated with the consideration of time dependent behavior of bedrock.

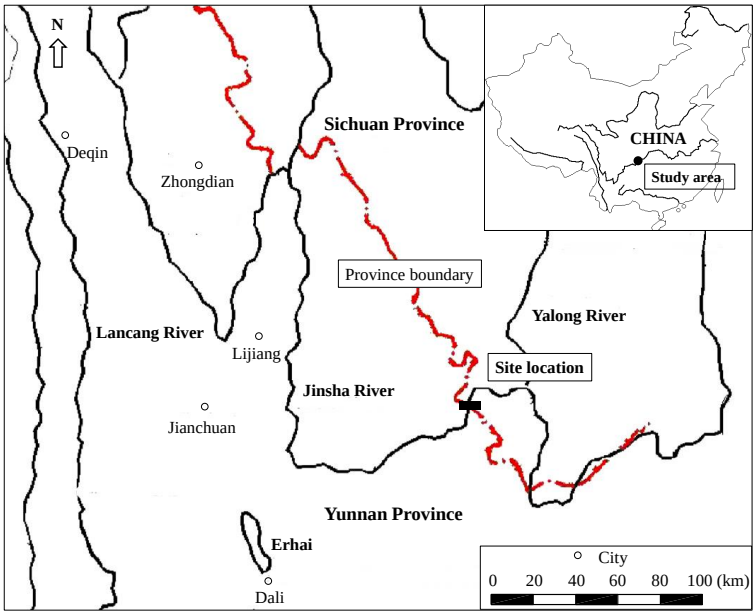

Fig. 4.1 Location of Hydropower Station in southwestern China

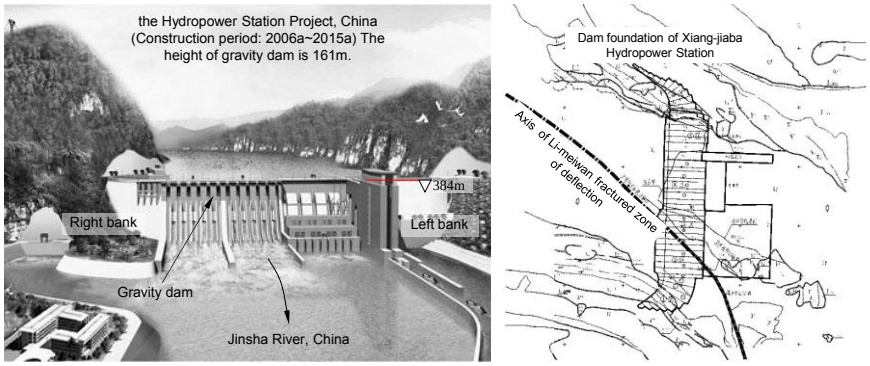

a. Concrete gravity dam model sketch of Hydropower Project **b.** Geological distribution of deflection fractured zone

Fig. 4.2 Geological distribution of deflection fractured zone

4.3. Governing equations for poroelastic coupling in saturated media

After the impounding of hydropower station, the intensifying interactions between water and rock will change the balance between the stored water and geologic environment. Consequently, the stress distribution in the rock may be significantly modified. Due to the different permeability of foundation materials, a gradient of water pressure may be generated between different materials. This non-uniform distribution of liquid pressure will cause a sliding of fault and menace the stability of dam. In consequence, it is necessary to perform a coupled hydromechanical modelling of dam foundation.

In the numerical modelling realized, the rocks are considered as a saturated porous medium with two phases: solid (assemblage of grain) and liquid. The external solicitations are mechanical and hydraulic loading(Jia et al. 2010). The model proposed by Coussy (2004) is adapted here for the elastic description of saturated rock:

$$d\sigma_{ij} = \left(K_b - \frac{2}{3}G \right) d\varepsilon_v^e \delta_{ij} + 2G d\varepsilon_{ij}^e - b dp_{lq} \delta_{ij} \tag{4.1}$$

$$\frac{dm_{lq}}{\rho_{lq}} = M dp_{lq} + b d\varepsilon_v \tag{4.2}$$

In these equations, K_b and G is respectively drained bulk modulus and shear modulus of porous medium. σ_{ij} and ε_{ij}^e are respectively the components of Cauchy stress tensor and elastic strain tensor . The parameters b and M are respectively the Biot's coefficient and Biot's modulus of porous medium, characterizing the poroelastic coupling. Using the results from microstructure analysis, the two poroelastic coupling parameters can be expressed as functions of the properties of constituents:

$$b = 1 - \frac{K_b}{K_m}, \quad \frac{1}{M} = \frac{b - \phi}{K_m} + \frac{\phi}{K_{fl}} \tag{4.3}$$

The variable ϕ denotes the total porosity of porous medium. K_m and K_{fl} are respectively the compressibility modulus of solid matrix and fluid.

Under isothermal condition, the hydromechanical coupled system is composed of liquid diffusion equation and the mechanical equation (equilibrium). The linear momentum equation is written as follows:

$$div(\sigma_{ij}) + \rho_m \vec{g} = 0 \tag{4.4}$$

σ_{ij} is the Cauchy stress tensor. ρ_m and $\vec{g}$ are respectively the mean volumetric mass of rock and the gravity acceleration:

By applying Darcy's law (4.5) to the masse conservation equation (4.6) and combining the constitutive equations (4.1)-(4.2) in saturated porous media (Coussy, 2004), the generalized liquid diffusion equation (4.7) is obtained:

$$\frac{\vec{w}_{lq}}{\rho_{lq}} = \frac{k}{\mu_{lq}}\left(-\nabla p_{lq} + \rho_{lq}\vec{g}\right) \tag{4.5}$$

$$\frac{\partial m_{lq}}{\partial t} = -div(\vec{w}_{lq}) \tag{4.6}$$

$$\frac{k}{\mu_{lq}} div(\nabla p_{lq}) = \frac{1}{M}\frac{\partial p_{lq}}{\partial t} + b\frac{\partial \varepsilon_{kk}^{e}}{\partial t} \tag{4.7}$$

Here p_{lq} represent the pore water pressure, ε_{ij}^{e} is respectively the elastic strain tensor and the temperature, $\vec{w}_{lq}$ denotes the vector of fluid flow rate, ρ_{lq} the volumetric mass of fluid, k is the intrinsic permeability and μ_{lq} is the dynamic viscosity of fluid. By applying Galerkin's residual method to the generalized diffusion equations and to the momentum equation (Lewis and Schrefler 1998), a fully coupled finite element computer code has been developed for modelling nonlinear hydromechanical boundary value problems in Lille Mechanics Laboratary.

4.4. Numerical model and parameters

According to the specific geological engineering conditions of bedrock in hydropower Station, the dam section in the middle of the riverbed is simulated. Numerical modelling has been performed in plan strain conditions. In order to reduce the disturbances of the initial conditions on the outside boundary, the exterior boundary of the studied domain is taken as large as possible. As the emphasis of this study is to estimate the long term stability of dam function, the concrete dam is simulated by a poroelastic model. Moreover, according to the exterior loading, the foundation is generally subjected to the gravity force of dam and reservoir water as well as water pressure related to the weight of reservoir water. In the present study, we will study the case where the largest liquid pressure gradient is observed in the dam structure. Therefore, the reservoir is filled the water while no water is presented in the downstream area.

As the emphasis is put on the influence of cataclastic sandstone zone on the stability of bedrock, for the sake of simplicity, the material of foundation are considered as one host massif. Therefore, a perfect contact is assumed at the interfacs of silty mudstone/cataclastic sandstone and the interface between bedrock and concrete dam. Accordingly, only three geological domaines are

taken into account: concrete dam, silty mudstone and cataclastic zone (i.e fracture zone). The maximum elevation of stored water level may reach to 380m.

The dam is initially saturated by liquid water with an atmospheric pressure and subjected to its gravity force. According to the foundation rocks (i.e. silty mudstone and cataclastic sandstone), they are considered initially saturated by water and the water pressure filed, created by the weight of liquid, is applied.

The geometry and the boundary conditions of numerical model are shown in Fig. 4.3 Geometrical domain and boundary conditions of studied field. The mesh for foundation consists of 4344 quadrilateral elements with 4 nodes (Fig. 4.4). As the emphasis of this study is put on the long-term stability of bedrock, the construction phase of dam, impoundment phase and operation phases are simulated. The loading path of numerical simulation can be synthesized as follows:

- Dam construction phase: the weight of dam is applied progressively on the foundation utile the achievement of dam; the dam is build but no water impoundment. In this step, the self-weight of the bedrock and concrete dam is considered;
- Impoundment phase: the stress and liquid pressure due to the weight of reservoir water is applied on the upstream board of dam (AB) as well as the upper board of upstream bedrock. According to the downstream side of dam and foundation, an atmospheric pressure is applied;
- Operation phase: the hydromechancial behavior of the foundation is predicted numerically utile the lifetime (500 year) of hydropower station.

The hydromechanical parameters for the concrete and silty mudstone are given in Table 4.1. The parameters for cataclastic sandstone was obtained in chapter 3. According to the silty mudstone, the experimental investigation exhibits that it processes the same mechanical behavior as the cataclasic sandstone, but having a greater mechanical strength. Therefore, the constitutive model proposed in the chapter 3 is also adopted for silty mudstone. The model's parameter is identified by using the experimental data obtained by Li (2009) and given in the Table 4.2.

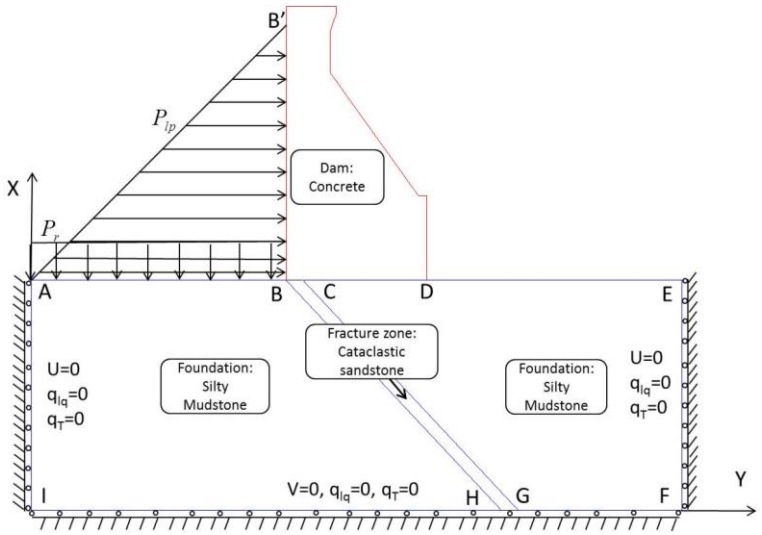

Fig. 4.3 Geometrical domain and boundary conditions of studied field

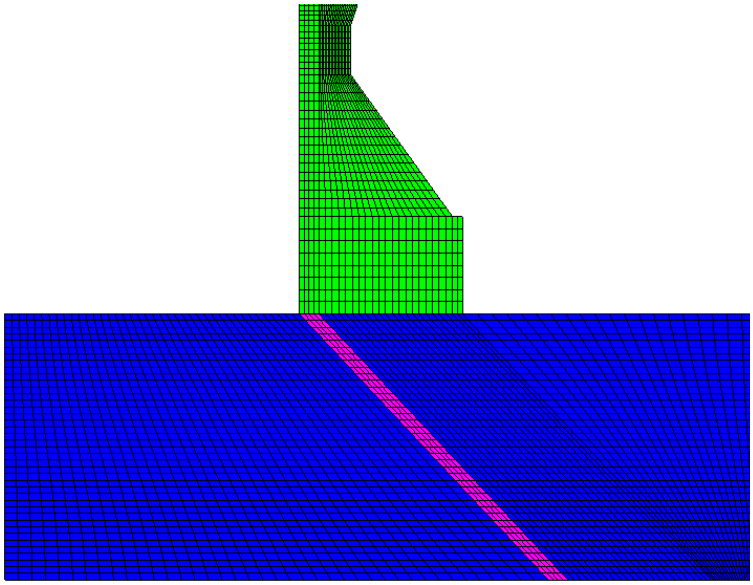

Fig. 4.4 Detail of two dimensional finite-element grid of zone studied

Table 4.1 Physical and elastic model's parameters for various materials of geometrical model

Materilas	Natural density (kN/m^3)	Porosity (%)	Elastic modulus (GPa)	Poisson ratio	Permeability coefficient (10^{-4}cm/s)	Biot coefficient
Dam body	24.2	10.3	30.07	0.2	0.001	0.6
Cataclastic sandstone	23.60	17.83	0.43	0.2	4.87	0.6

Silty mudstone	23.90	13.6	18	0.18	0.46	0.6

Table 4.2 Plastic model's parameters for various materials of geometrical model

Materilas	Failure parameters		α_p^0	η	B	γ
	A	C_0(MPa)				
silty mudstone	2.23	1.79	0.25	1.0	2200	0.00001

4.5. Numerical analysis of the stability of dam foundation

Due to the limited space in this chapter, only representative numerical results of foundation are presented in this section, which include the displacement, liquid pressure, stress and plastic hardening parameters in the foundation. The evolutions of different parameter are, respectively, given on the upper and lower board of bedrock as well as in the middle of bedrock. The emphasis is put on the influence of cataclastic sandstone on the long term stability of bedrock. In the numerical results, the tensile stress is positive; compressive stress is negative.

4.5.1. Numerical results of dam construction phase

As the dam construction phase, no water is presented in the reservoir. As a result, the liquid pressure is not presented in this section.

Fig. 4.5 and Fig. 4.6 illustrates the distributions of horizontal displacement of the dam foundation after the achievement of dam construction. During the construction of gravity dam, the self-weight of the rock mass and concrete structure applied progressively on the foundation. The numerical results show that under the self-weight stress of dam, the maximum horizontal displacements of the dam foundation is observed on the bottom of the fracture zone with a value of order 10.1mm while a negative displacement of order -12.4mm is obtained on the downstream of dam (Fig. 4.5). As a result, the dam moves slightly towards the downstream side.

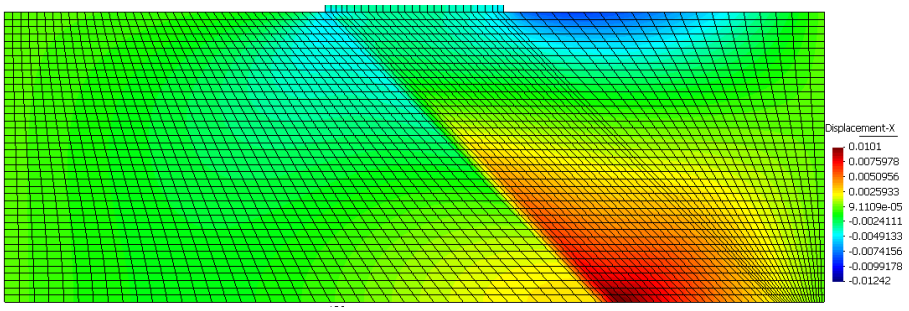

Fig. 4.5 Distribution of horizontal displacements in the foundation at the end of construction phase

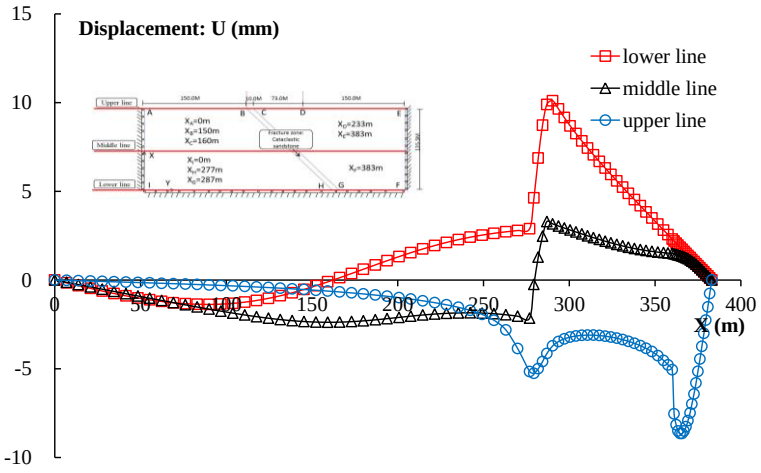

Fig. 4.6 Evolution of horizontal displacements on the upper and lower boards and in the middle of foundation at the end of construction phase

According to vertical displacement, the maximum value of vertical displacements is obtained on the bottom of dam (Fig. 4.7 and Fig. 4.8). On the other hand, no vertical displacement is observed on the lower board. This observation is due to the fact that a blockage of displacement is imposed. Generally, significant vertical displacement is essentially concentric under the dam (Fig. 4.8). Furthermore, the vertical displacement decreases with the depth.

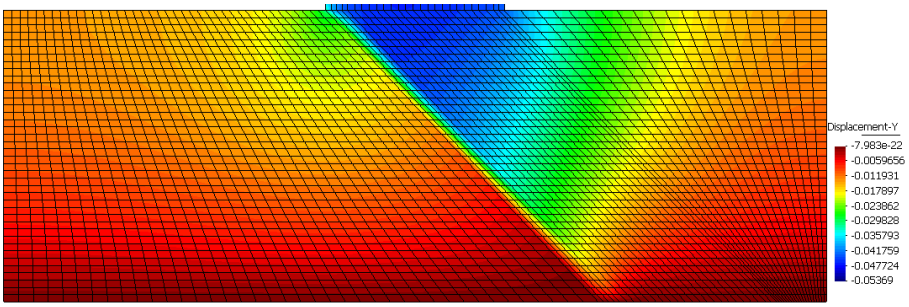

Fig. 4.7 Distribution of vertical displacements in the foundation at the end of construction phase

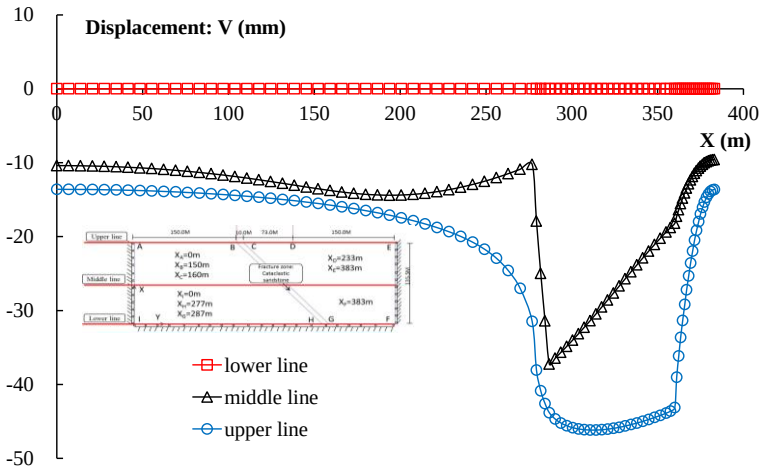

Fig. 4.8 Evolution of vertical displacements on the upper and lower boards and in the middle of foundation at the end of construction phase

The evolutions of horizontal stress σ_{xx} and σ_{yy} are given in Fig. 4.9-Fig. 4.12. According to the horizontal stress σ_{xx}, due to the sliding of cataclastic sandstone in the foundation, an important traction zone is observed on the lower board of the foundation(Fig. 4.10). As the tensile strength of studied rock is very low, it is suggest that the fracture zone plays a negative role in the dam foundation stability. This traction is due to the fact that a perfect contact is assumed between cataclastic sandstone and silty mudstone and the sliding at the interface isn't taken into account. However, if the sliding at the interface is taken into account in the numerical simulation, no tensile stress would be observed. However, the vertical stress is generally in compression.

On the other hand, due to the self-weight of the dam, the foundation is compacted strongly on the upper surface of foundation. Therefore, important compressions are observed at two points B and D (Fig. 4.10 and Fig. 4.12) which are the intersection points of the dam body and foundation.

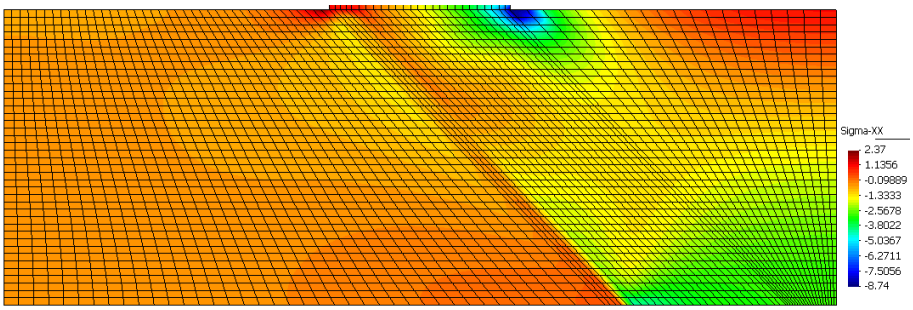

Fig. 4.9 Distribution of horizontal stress σ_{xx} in the foundation at the end of construction phase

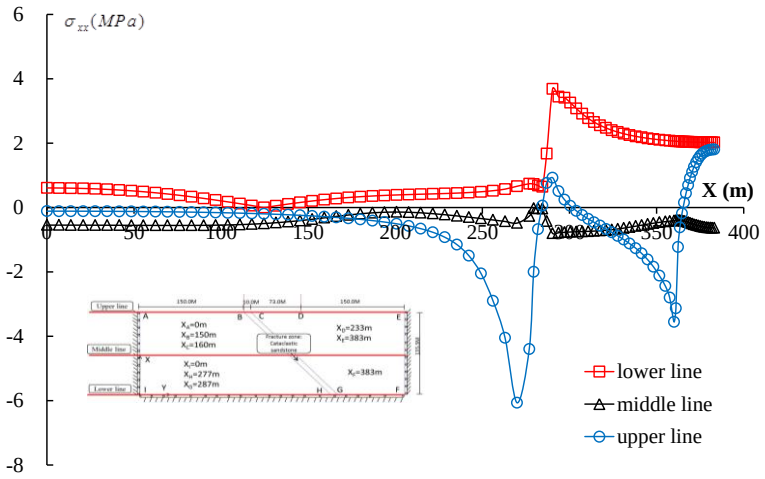

Fig. 4.10 Evolution of horizontal stress σ_{xx} on the upper and lower boards and in the middle of foundation at the end of construction phase

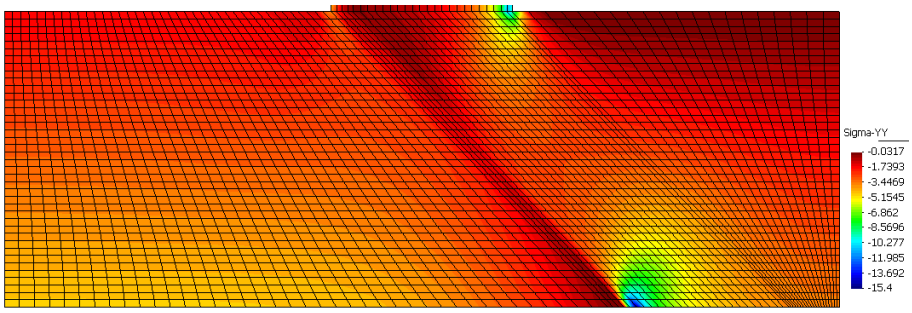

Fig. 4.11 Distribution of vertical stress σ_{yy} in the foundation at the end of construction phase

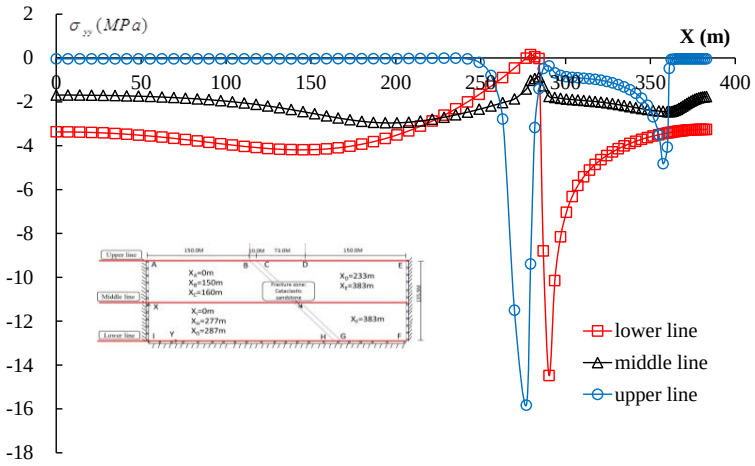

Fig. 4.12 Evolution of vertical stress σ_{yy} on the upper and lower boards and in the middle of foundation at the end of construction phase

In the present study, the mechanical behaviours of foundation rocks are characterized by a visco-elasto-plastic model. Therefore, the evolution of the inelastic zone can be determined by using the hardening parameter of the proposed model (Fig. 4.13-Fig. 4.14). It is observed that the plastic zone is limited essentially in cataclastic sandstone zone of a maximum value of 0.671 . This phenomenon is due to the shear deformation of dam foundation, and leads to a foundation failure after a long time loading. Moreover, it is observed that the maximum value of hardening parameter α_p decreases with the depth.

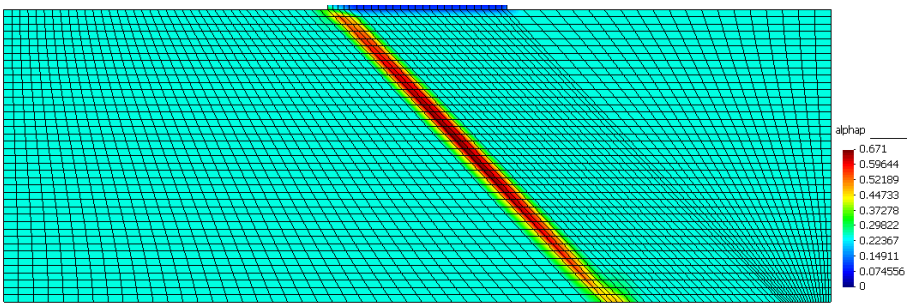

Fig. 4.13 Distribution of hardening parameter α_p in the foundation at the end of construction phase

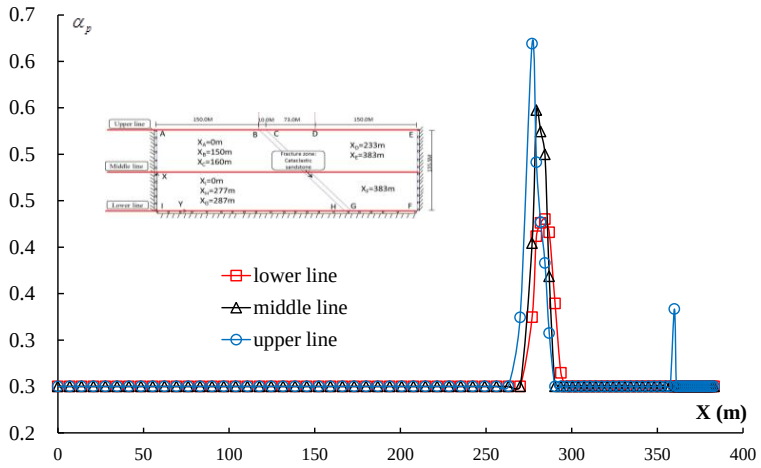

Fig. 4.14 Evolution of hardening parameter α_p on the upper and lower boards and in the middle of foundation at the end of construction phase

4.5.2. Numerical results of water impoundment phase

The distributions of horizontal and vertical displacements of the dam foundation are firstly presented at the end of water impoundment phase. During the water impoundment phase, the

upstream hydraulic load is applied progressively on the upstream board of dam and foundation.

The liquid pressure is firstly studied in this section. According to the imposed boundary condition, a liquid pressure of 1.54 MPa is found on the upstream surface of foundation while an atmospheric pressure is observed on the downstream surface of foundation. The liquid pressure in the foundation of upstream side increases also with the increase of reservoir water. Moreover, the amplitude of liquid pressure increase decrease with the depth. Therefore, the obtained liquid pressure on the middle line is greater that of lower liner. On the other hand, in the foundation of downstream side, the liquid pressure is less disturbed by the reservoir water and a liquid pressure state is close to the nature one. Finally, due to the permeability difference between silty mudstone and cataclastic sandstone, a change curvature is observed in the liquid pressure curve.

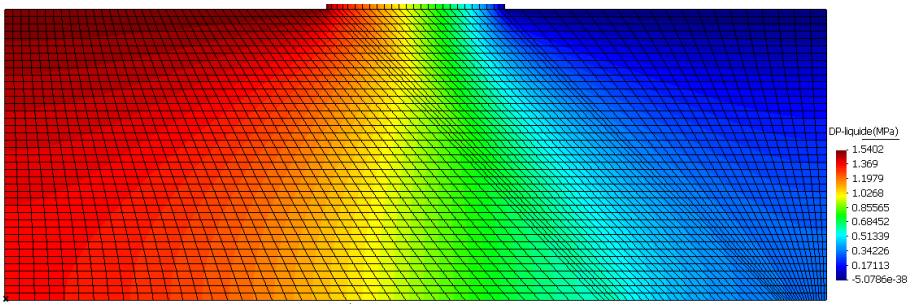

Fig. 4.15 Distribution of liquid pressure P_w in the foundation at the end of water impoundment phase

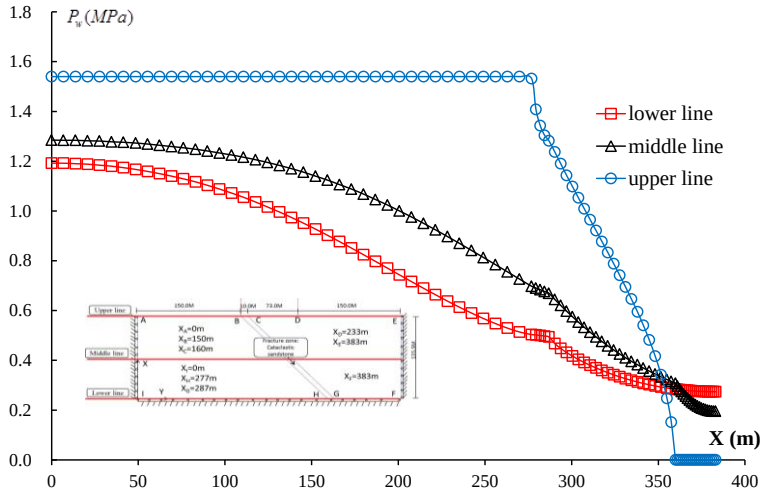

Fig. 4.16 Evolution of liquid pressure P_w on the upper and lower boards and in the middle of foundation at the end of water impoundment phase

Under the combinative action of evolution of liquid pressure and the self-weight of materials, the horizontal displacement of foundation increase progressively. Generally, the foundation moves toward downstream side. Great horizontal displacements are observed in the cataclastic sandstone zone (Fig. 4.17 and Fig. 4.18). A maximum value of order 14mm is observed on the lower board of foundation. However, on the upper board of foundation, due to the subsidence of foundation, a horizontal displacement towards upstream side is observed.

According to the vertical displacement, its maximum value of order 55mm is observed on the intersection point between dam and the downstream foundation. Moreover, the vertical displacement of the base of dam is not homogenous. This fact may induce the inclination of dam. Generally, the evolution of vertical displacement decreases with the depth. A blockage of vertical displacement on the lower board of foundation is related to the imposed boundary condition.

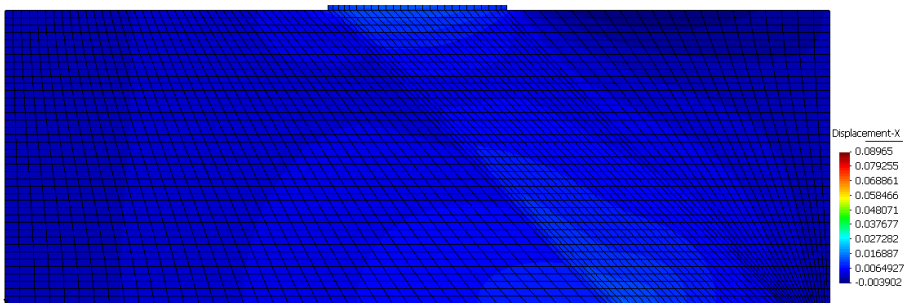

Fig. 4.17 Distribution of horizontal displacement in the foundation at the end of water impoundment phase

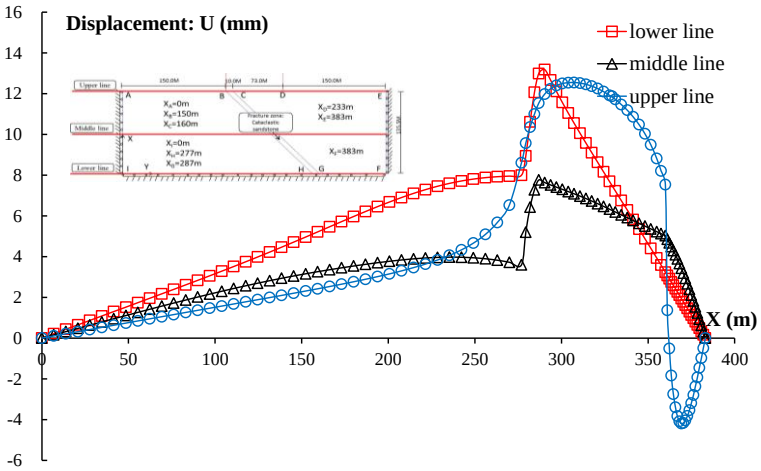

Fig. 4.18 Evolution of horizonta displacement on the upper and lower boards and in the middle of foundation at the end of water impoundment phase

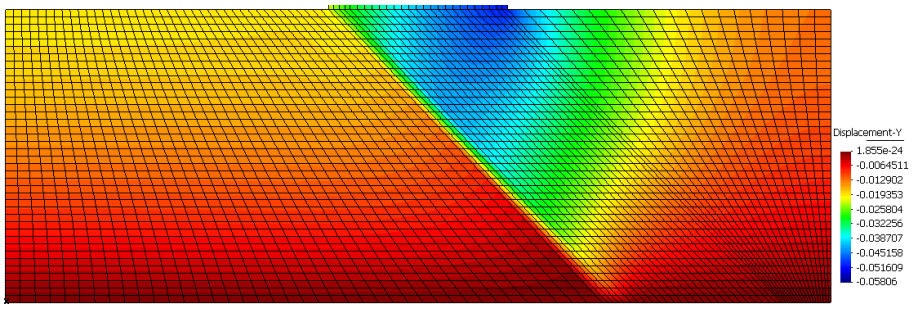

Fig. 4.19 Distribution of vertical displacement in the foundation at the end of water impoundment phase

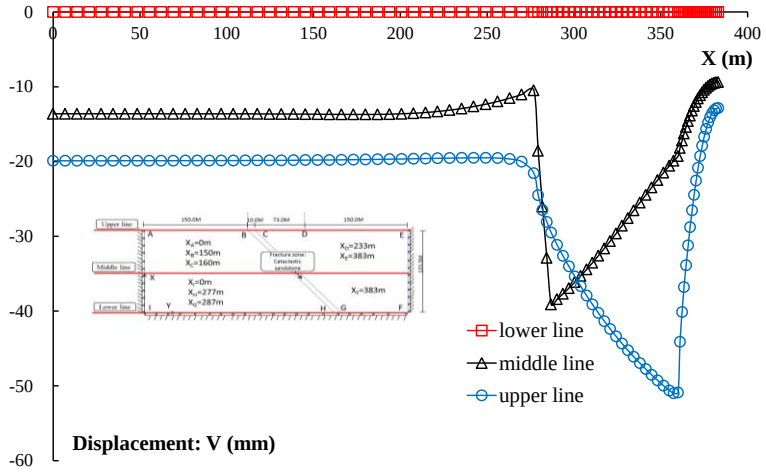

Fig. 4.20 Evolution of vertical displacement on the upper and lower boards and in the middle of foundation at the end of water impoundment phase

Fig. 4.21-Fig. 4.24 presents the distributions of horizontal stress and vertical stress in the studied structure. The results indicates that the stress significantly change at the intersection point of the dam body and the surface of fracture zone. On the upper line, important compression is observed (Fig. 4.22 and Fig. 4.24) due to important subsistence of bedrock. On the other hand, an important traction zone is also observed on the lower board. It indicates that the slippage may occur between cataclastic sandstone and silty mudstone. The stability of bedrock may be influence by this slippage.

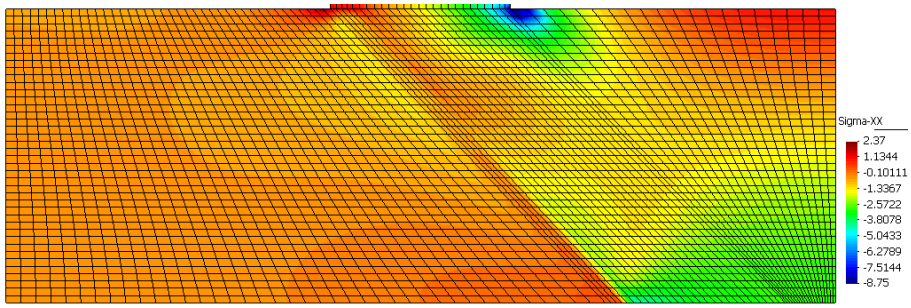

Fig. 4.21 Distribution of horizontal stress σ_{xx} in the foundation at the end of water impoundment phase

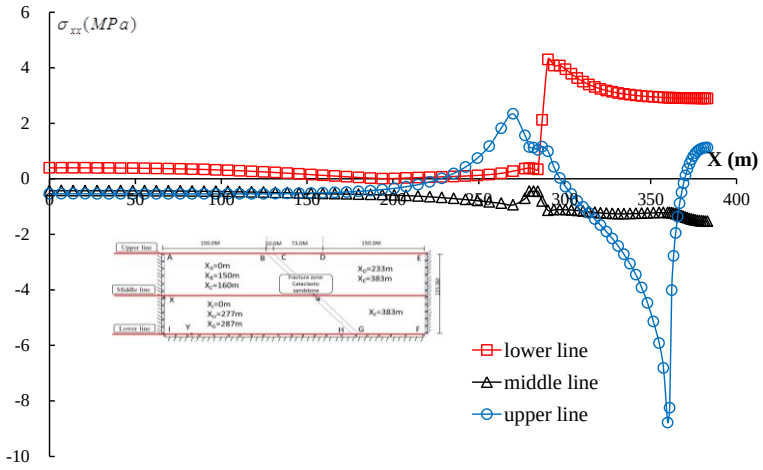

Fig. 4.22 Evolution of horizontal stress σ_{xx} on the upper and lower boards and in the middle of foundation at the end of water impoundment phase

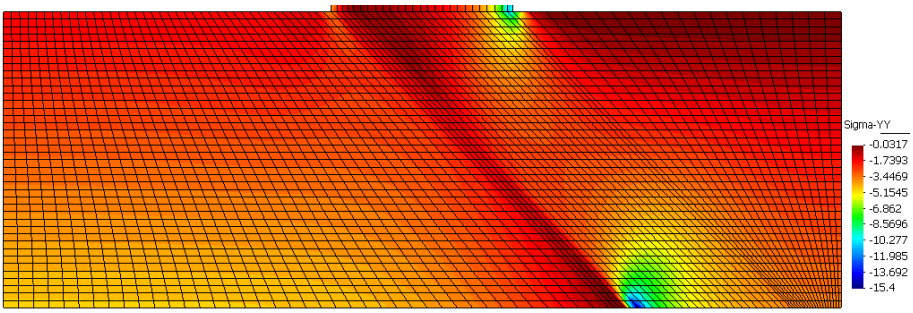

Fig. 4.23 Distribution of vertical stress σ_{yy} in the foundation at the end of water impoundment phase

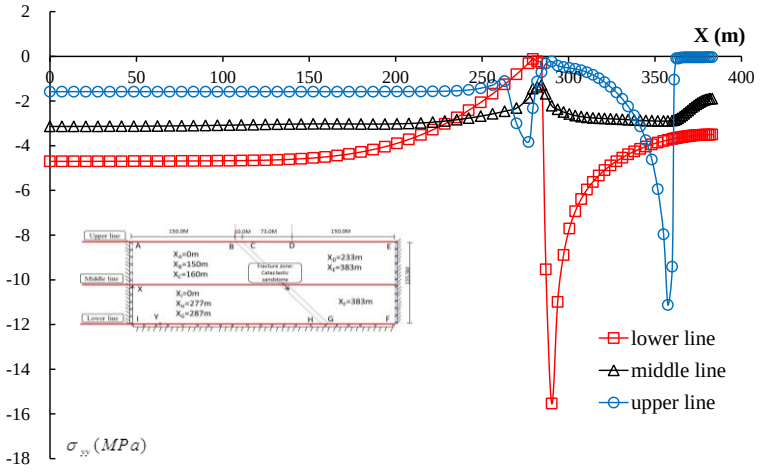

Fig. 4.24 Evolution of vertical stress σ_{yy} on the upper and lower boards and in the middle of foundation at the end of water impoundment phase

The evolution of hardening parameter α_p is finally studied (Fig. 4.25-Fig. 4.26). It is observed that the plastic zone is essentially limited in the cataclastic sandstone zone with a maximum value of order 0.677. This plastic zone may induce an important slippage on the interface of cataclastic sandstone and silty mudstone and then disturbs the stability of bedrock.

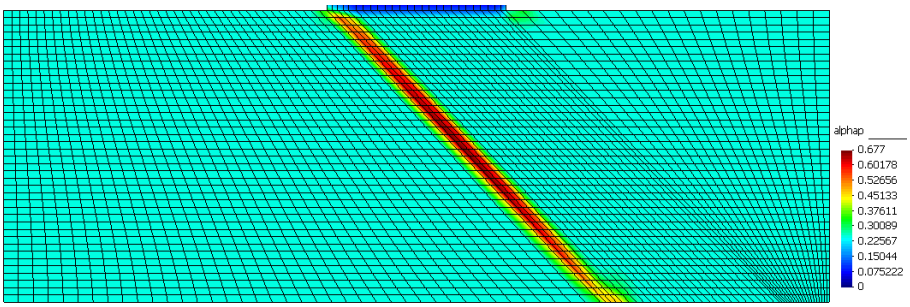

Fig. 4.25 Distribution of hardening parameter α_p in the foundation at the end of water impoundment phase

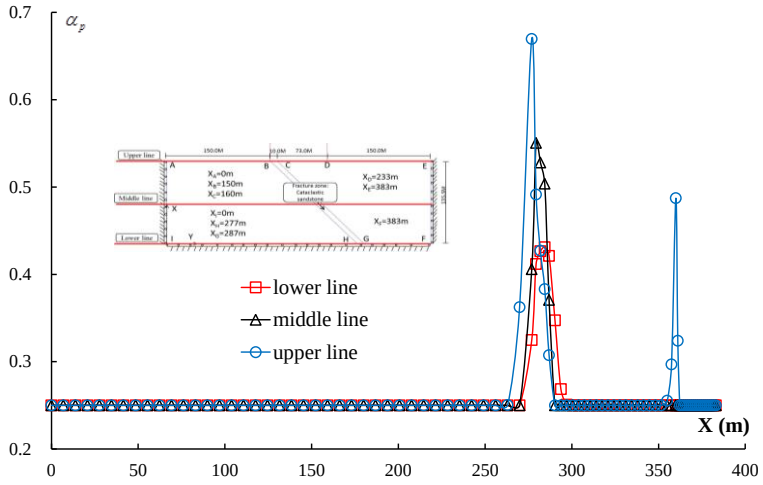

Fig. 4.26 Evolution of hardening parameter α_p on the upper and lower boards and in the middle of foundation at the end of water impoundment phase

4.5.3. Numerical results of operation phase

The principal results of operation phases are presented in this section. The evolutions of horizontal and vertical displacements of bedrock are firstly presented. In this phase, the applied load keeps constant. On the other hand, the hydromechanical coupling processes occurring in the bedrock are also disturbed by the viscoplasticiy of bedrock. With the development of viscoplasticity in the bedrock, the displacement increase with the time. On the other hand, the creep releases the stress in the skeleton of the rock and cause a redistribution of stress in rock. As a result, the pore pressue decrease with the time. However, due to the poor mechanical property and large permeability of cataclastic zone, the presence of cataclastic sandstone play an important role on the stability of bedrock.

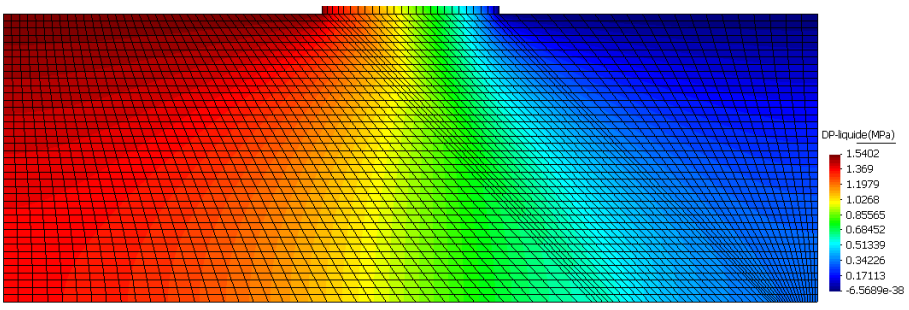

Fig. 4.27 Distribution of liquid pressure P_w in the bedrock at 500 years

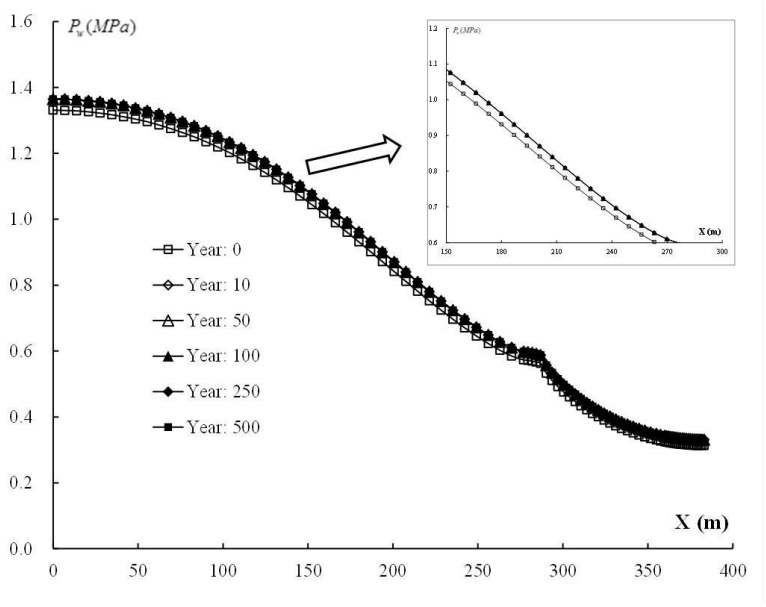

Fig. 4.28 Evolution of liquid pressure P_w on the lower line of bedrok

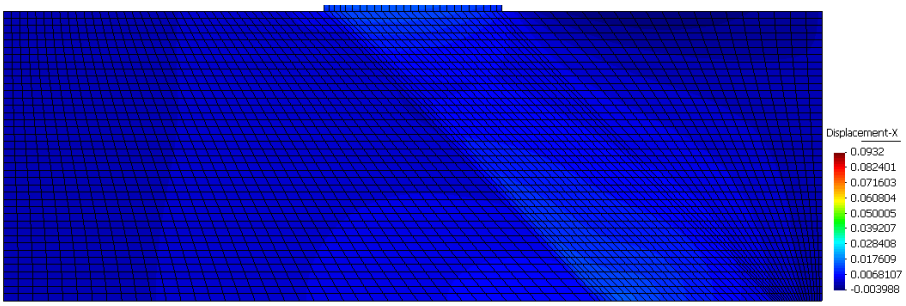

Fig. 4.29 Distribution of horizontal displacement in the bedrock at 500 years

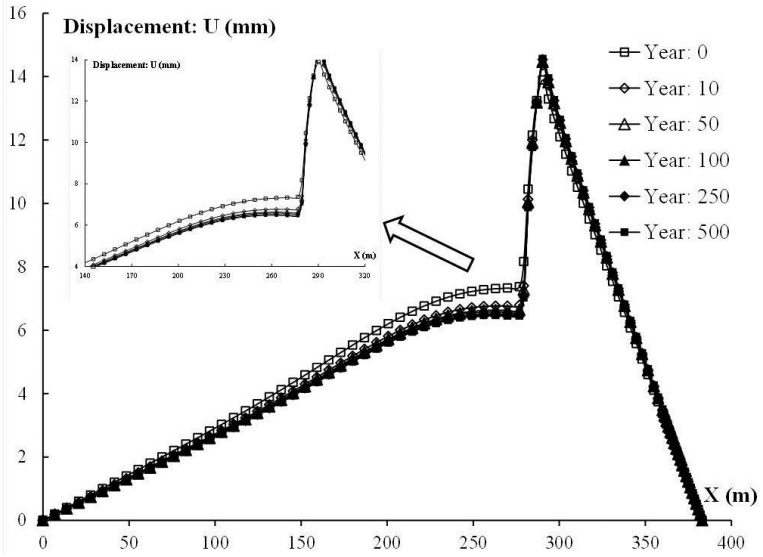

Fig. 4.30 Evolution of horizontal displacement on lower line of the bedrock

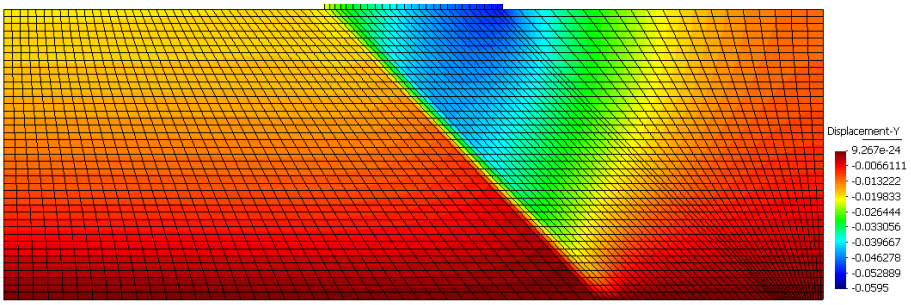

Fig. 4.31 Distribution of vertical displacement in the bedrock at 500 year

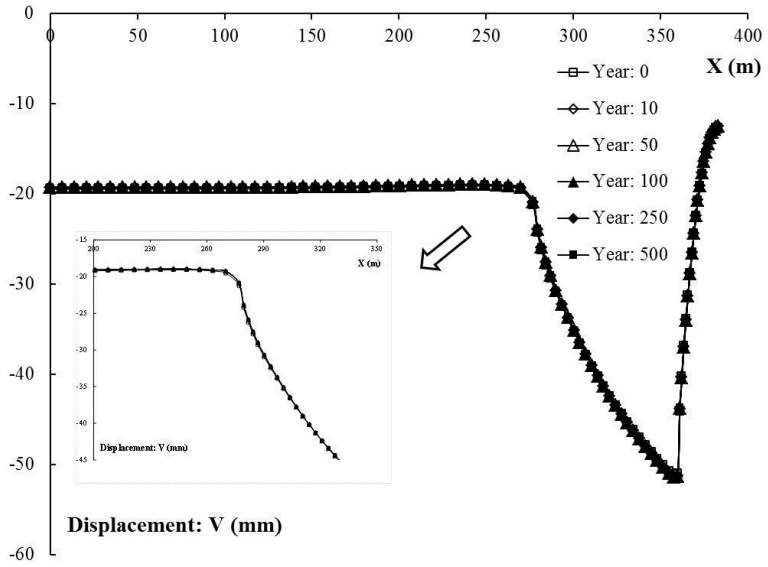

Fig. 4.32 Evolution of vertical displacement on the upper line of the bedrock

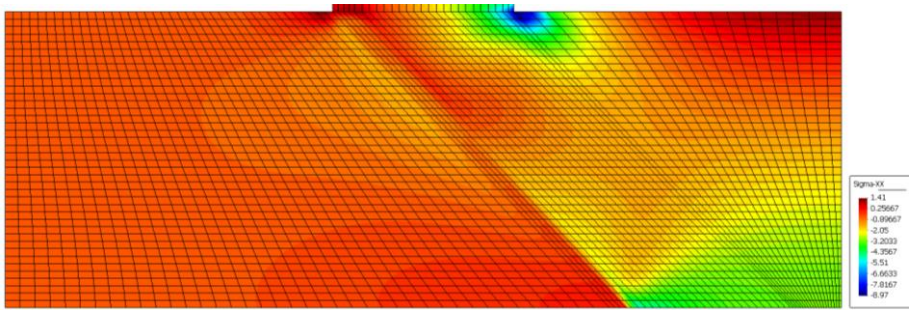

Fig. 4.33 Distribution of horizontal stress σ_{xx} in the bedrock at 500 year

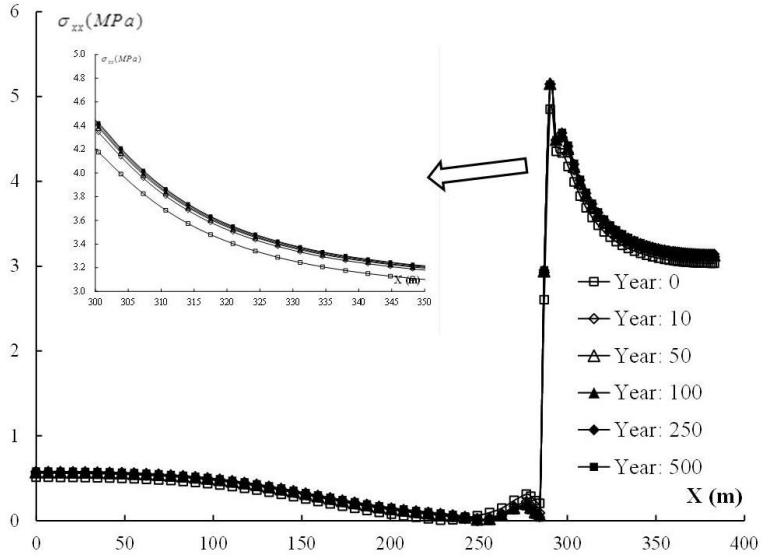

Fig. 4.34 Evolution of horizontal stress σ_{xx} on the lower board of the bedrock

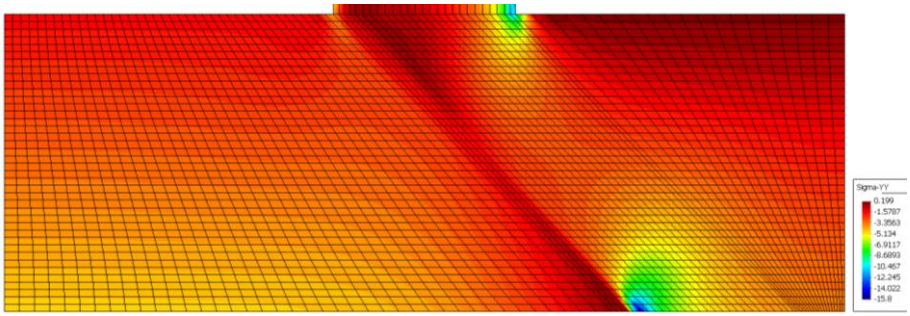

Fig. 4.35 Distribution of vertical stress σ_{yy} in the bedrock at 500 year

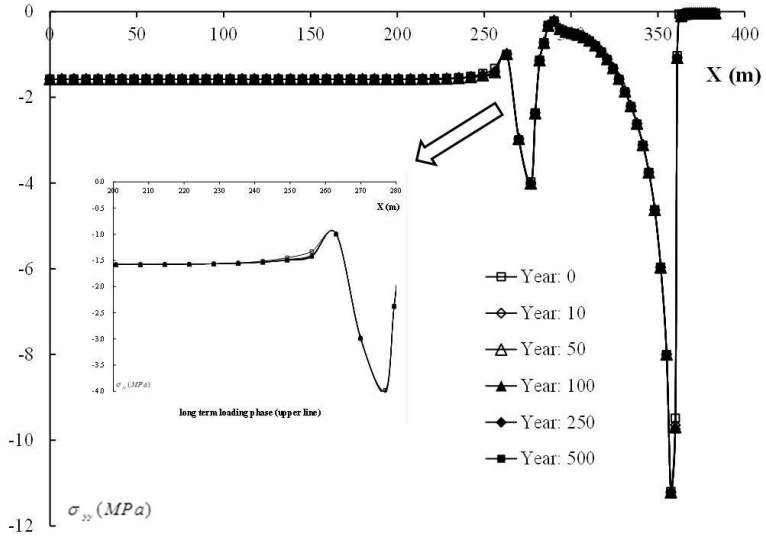

Fig. 4.36 Evolution of vertical stress σ_{yy} on the upper board of the bedrok during the operation phase

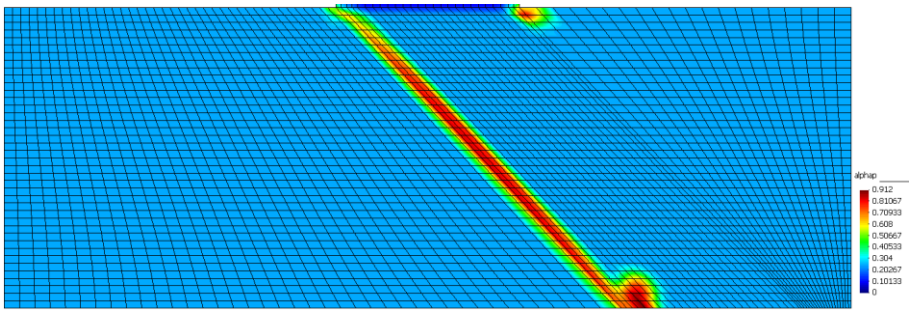

Fig. 4.37 Distribution of hardening parameter α_p in the bedrock at 500 year

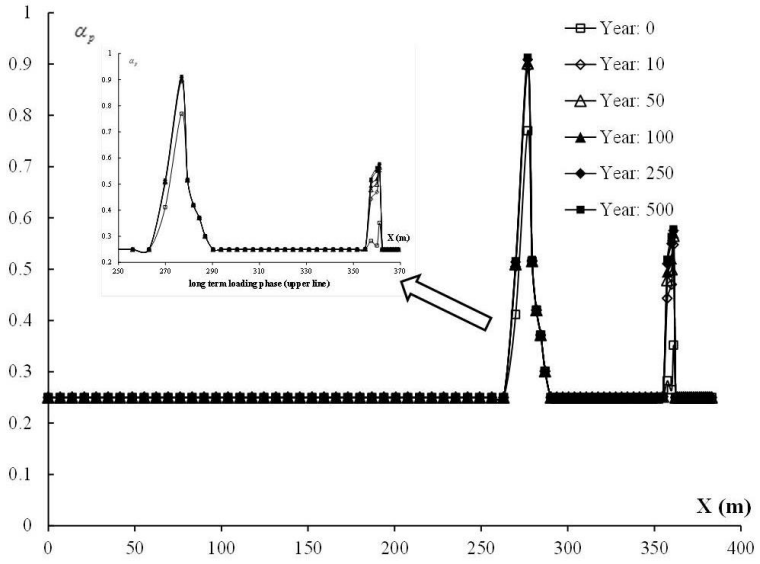

Fig. 4.38 Evolution of hardening parameter α_p on the upper board during the operation phase

4.6. Parametric study

Based on the numerical results obtained in the previous section, one observes that an important slippage is induce in bedrock due to the presence of cataclastic sandstone zone where is strongly damaged by the coupling hydromechanics coupling processes. In order to guarantee the long-term stability of bedrock, it is necessary to take some treatment to strengthen the cataclastic zone. For

this reason and in order to capture of the influences of some main parameters in hydromechanical responses of bedrock, it is proposed to perform some parametric studies in the following.

According to the parametric study, a reference study is firstly carried out. The calculation was done using an elatoplastic model with constant permeability for the cataclastic sandstone. A number of main parameters are chosen in the parametric studies and comparative calculations have been performed by changing one of these parameters. All these calculations are then compared with the reference case. The different cases are given in Table 4.3.

Table 4.3 Definition of different calculations in parametric study for the cataclastic sandstone

Influence of parameter	Case	Content
Reference		E= 0.43MPa, A=0.72, P_w=4.87E^{-5}cm/s
Mechanical	1a	E= 5.43MPa
	1b	E= 10.43MPa
	2a	A=0.42
	2b	A=0.12
Hydraulic conductivity	3a	P_w=4.87E^{-7}cm/s
	3b	P_w=4.87E^{-9}cm/s
Mechanical behavior	4	Elastoplastic + viscoplastique ($\gamma = 0.0001$)

Based on the numerical results presented in the previous section, it is observed that the maximum horizontal displacement is obtained on the lower liner while the maximum vertical displacement is observed on the upper liner. Therefore, only the evolutions of horizontal displacement of lower liner and vertical displacement of upper liner are compared in the section. According to the stress evolution, the evolutions of horizontal stress on the lower line and vertical stress on the upper line are then compared. Finally, as the maximum value of the hardening parameter α_p is observed on the upper line of bedrock, the evolution of hardening parameter α_p of upper line of bedrock is used for the comparison.

4.6.1. Influence of Young's Modulus E

Influence of Young's Modulus is firstly studied. Two cases are considered: case 1a with drained Young's module of order 5.43MPa which case 1b with a value of order of 10.43MPa. The values of the other parameters are the same as those in case reference. The influence of another mechanical parameter A which controls the failure surface is also carried out in cases 2a and 2b.

By comparing four calculations with different mechanical properties with the case reference, the influence of mechanical parameters is discussed. Fig. 4.39 and Fig. 4.40 show that the displacement increases significantly in the cataclastic zone. This phenomenon is due to the fact that the deformability of rock increases when the drained Young's modulus decreases. As a result, the stress increases also with the increase of displacement (Fig. 4.41 and Fig. 4.42). The cataclastic sandstone is strongly damaged in the case where the small drained Young's modulus is used (Fig. 4.43). However, the drained Young's modulus has a negligible effect on the evolution of the liquid pressure which is essentially controlled by the material's permeability (Fig. 4.44).

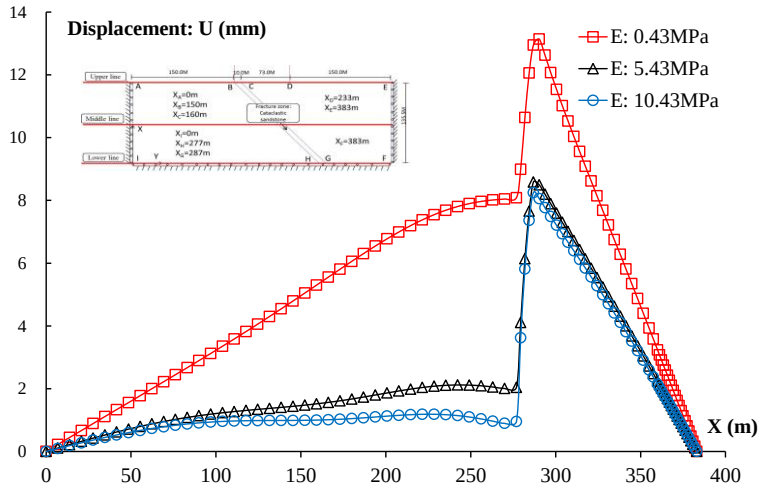

Fig. 4.39 Influence of the drained Young modulus of cataclastic sandstone on the horizontal displacement (lower line of bedrock)

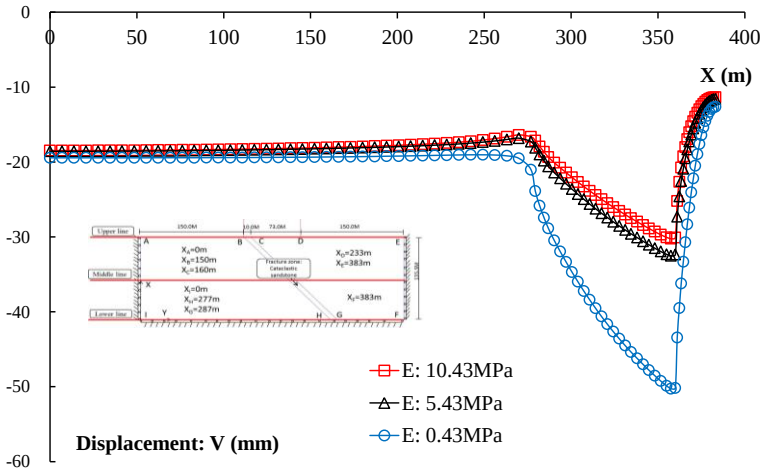

Fig. 4.40 Influence of the drained Young modulus of cataclastic sandstone on the vertical displacement (upper liner of bedrock)

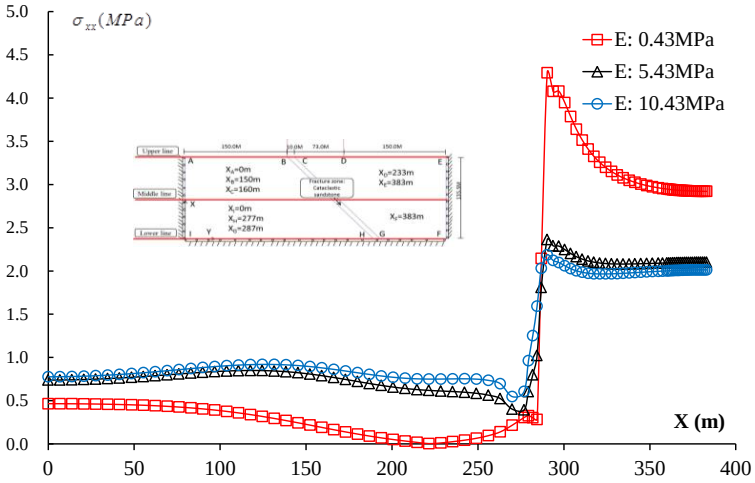

Fig. 4.41 Influence of the drained Young modulus of cataclastic sandstone on the horizontal stress (lower line of bedrock)

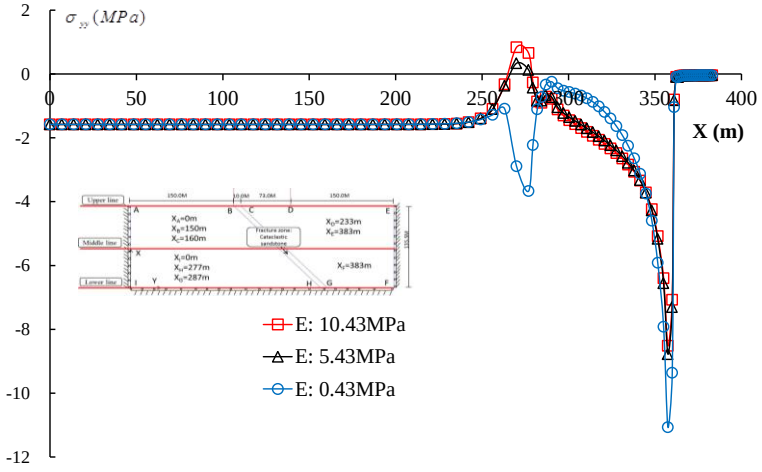

Fig. 4.42 Influence of the drained Young modulus of cataclastic sandstone on the vertical stress (upper line of bedrock)

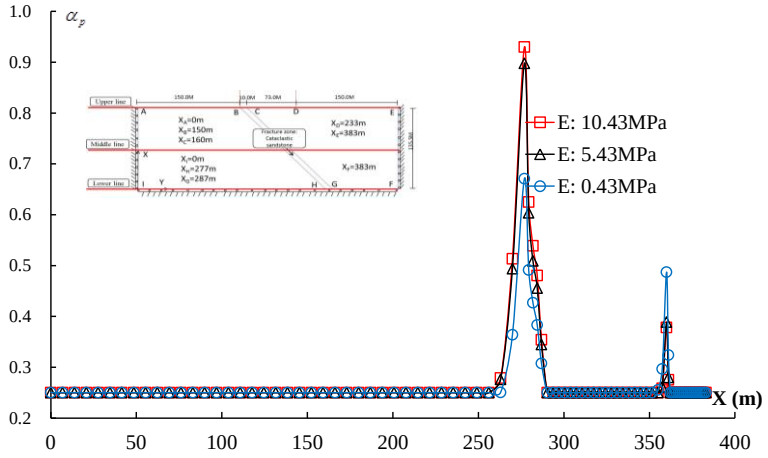

Fig. 4.43 Influence of the drained Young modulus of cataclastic sandstone on the hardening parameter α_p (upper line of bedrock)

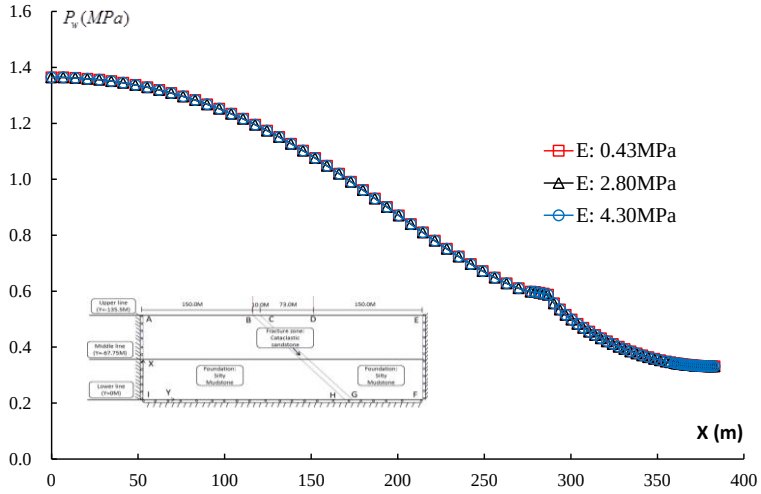

Fig. 4.44 Influence of the drained Young modulus of cataclastic sandstone on the liquid pressure in bedrock (lower line of bedrock)

4.6.2. Influence of parameter A

In addition, the displacements in bedrock are slightly perturbed by the variation of the parameter A of failure surface (Fig. 4.45 and Fig. 4.46). According to failure surface of proposed model, the parameter A affects the failure surface and plastic potential of material. With a smaller value of parameter A, the rock will have smaller strength and yield stress. As a result, a higher stress and greater plastic zone are generated in rock(Fig. 4.47-Fig. 4.48). However, the influence of

parameter A on pore water pressure seems to be relatively small with a constant permeability(Fig. 4.50).

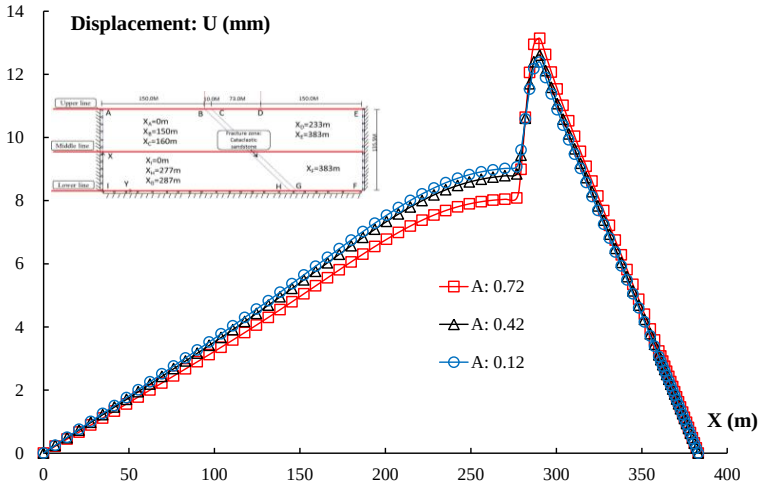

Fig. 4.45 Influence of the parameter A on the horizontal displacement(lower line of bedrock)

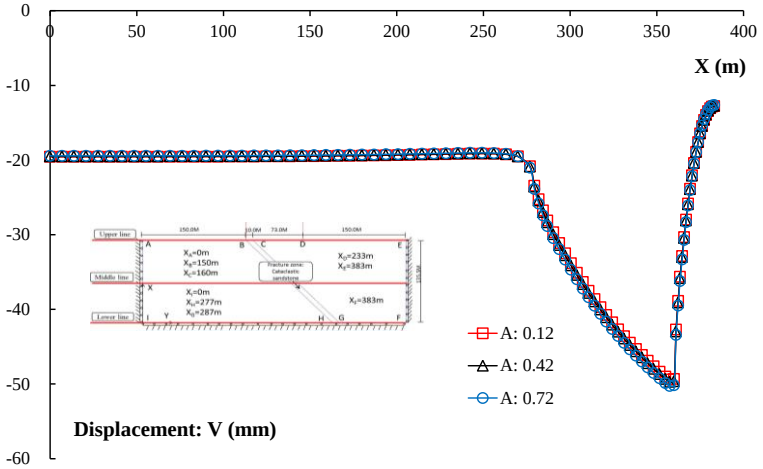

Fig. 4.46 Influence of the parameter A on the vertical displacement (upper line of bedrock)

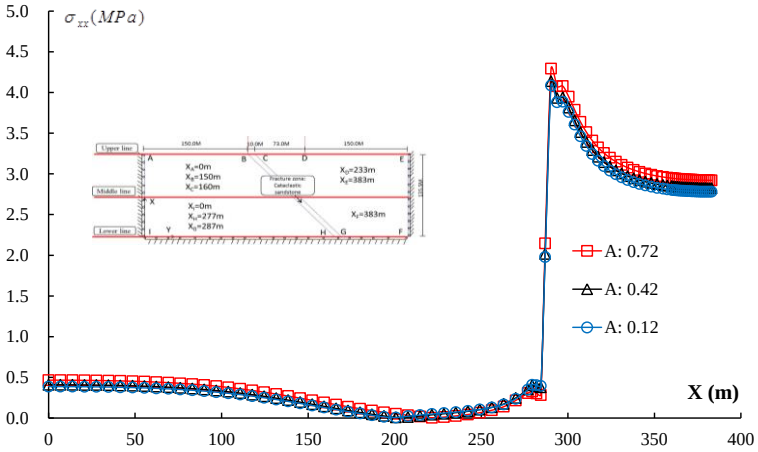

Fig. 4.47 Influence of the parameter A on the horizontal stress (lower line of bedrock)

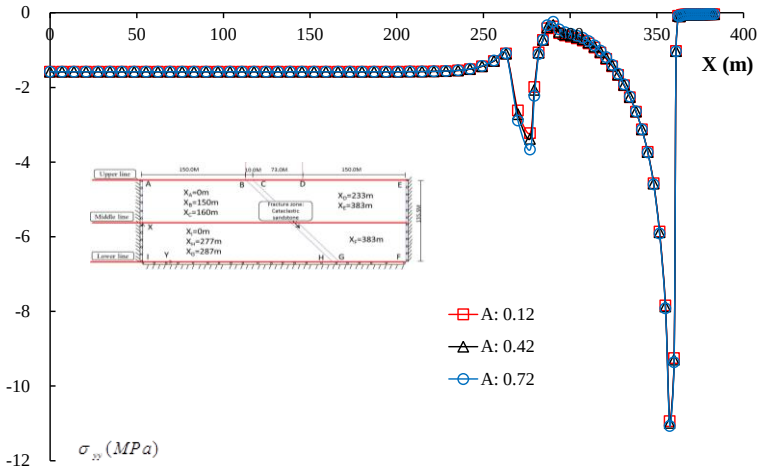

Fig. 4.48 Influence of the parameter A on the verticalstress (upper line of bedrock)

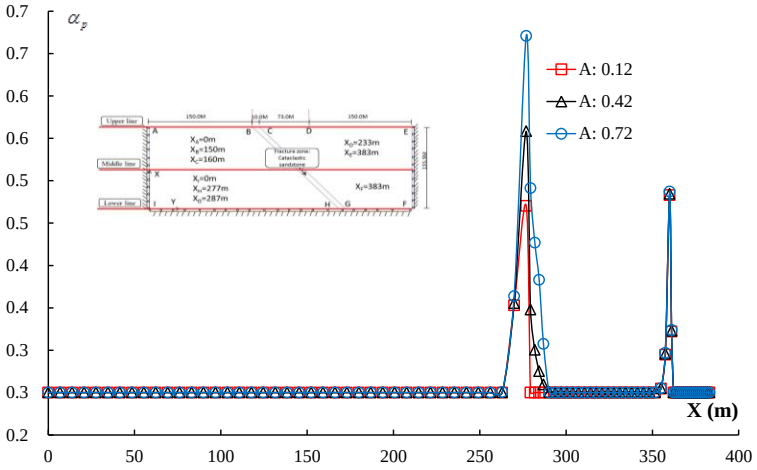

Fig. 4.49 Influence of the parameter A on the hardening parameter α_p (upper line of bedrock)

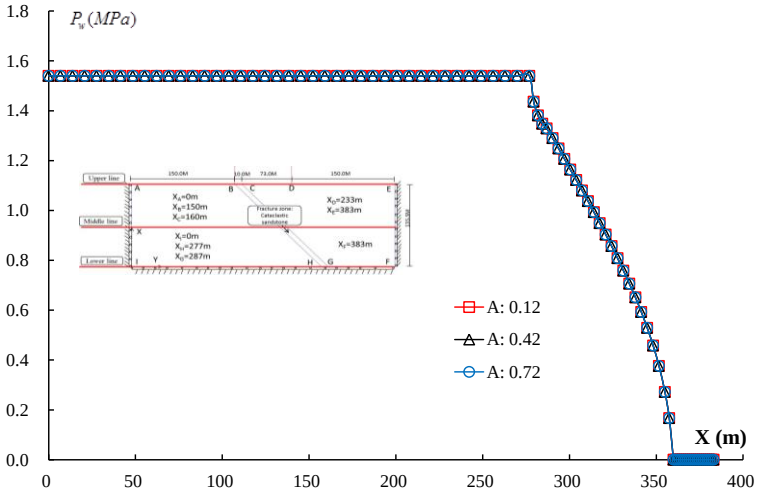

Fig. 4.50 Influence of the parameter A on the liquid pressure (lower line of bedrock)

4.6.3. Influence of permeability parameter P_w

In order to capture the influences of permeability, a sensitivity study has been performed. Two calculations have been done with different value of permeability. The numerical results are presented in Fig. 4.51-Fig. 4.56. With a greater value of permeability, the liquid water escapes more quickly from the rock mass. As result, it leads a greater decrease of pore water pressure. This feature is clearly illustrated by numerical prediction (Fig. 4.51). However, variation of the permeability has a negligible influence on the displacement and stress of studied rock .

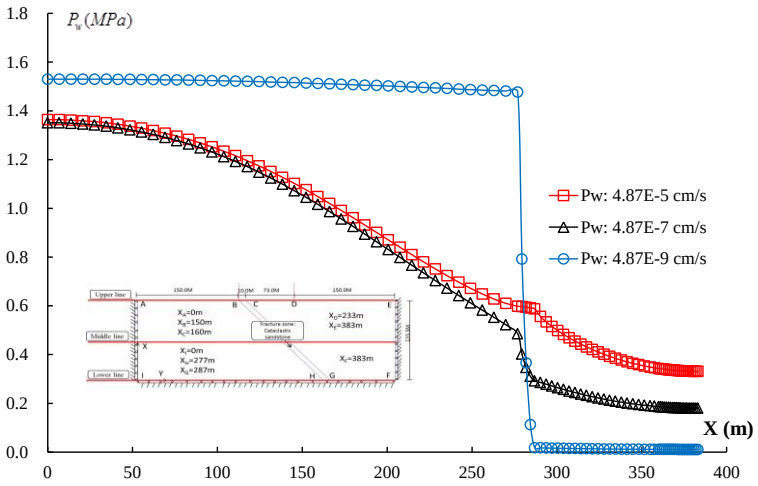

Fig. 4.51 Influence of the permeability of cataclastic sandstone on the liquid pressure (ower line of bedrock)

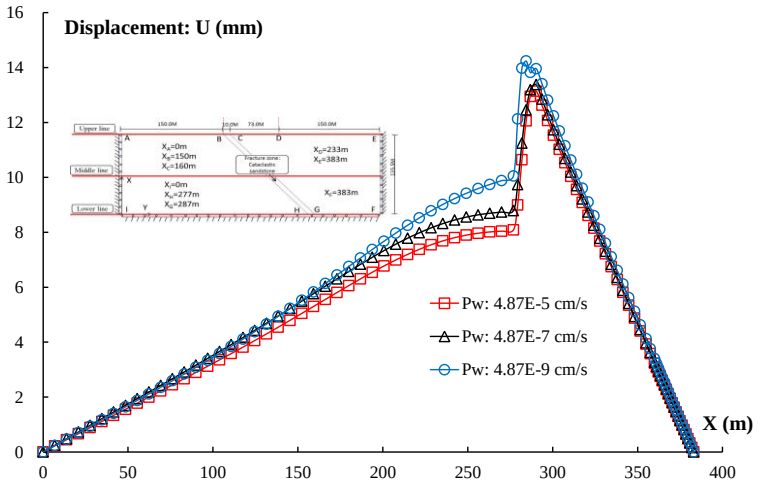

Fig. 4.52 Influence of the permeability of cataclastic sandstone on the horizontal displacement lower line of bedrock)

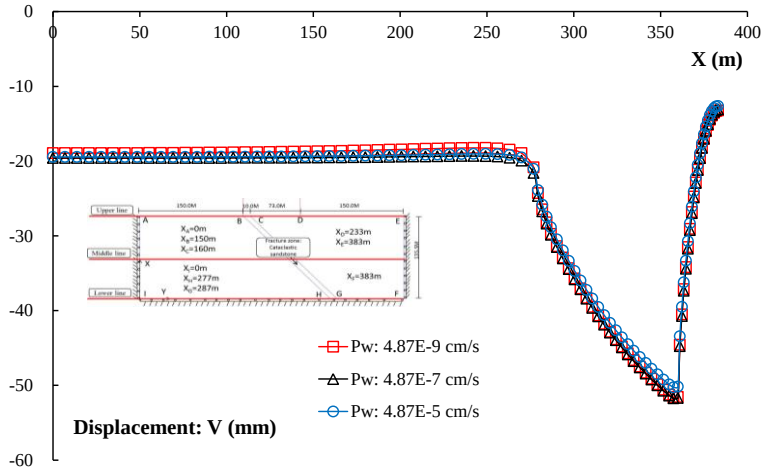

Fig. 4.53 Influence of the permeability of cataclastic sandstone on the vertical displacement (upper line of bedrock)

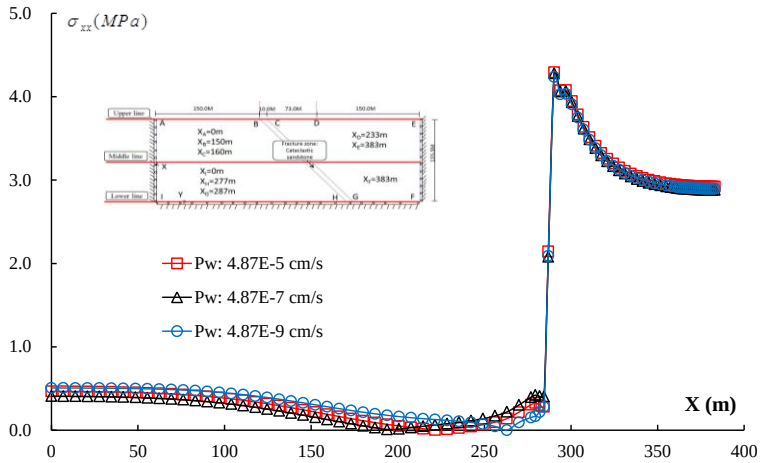

Fig. 4.54 Influence of the permeability of cataclastic sandstone on the horizontal stress (lower line of bedrock)

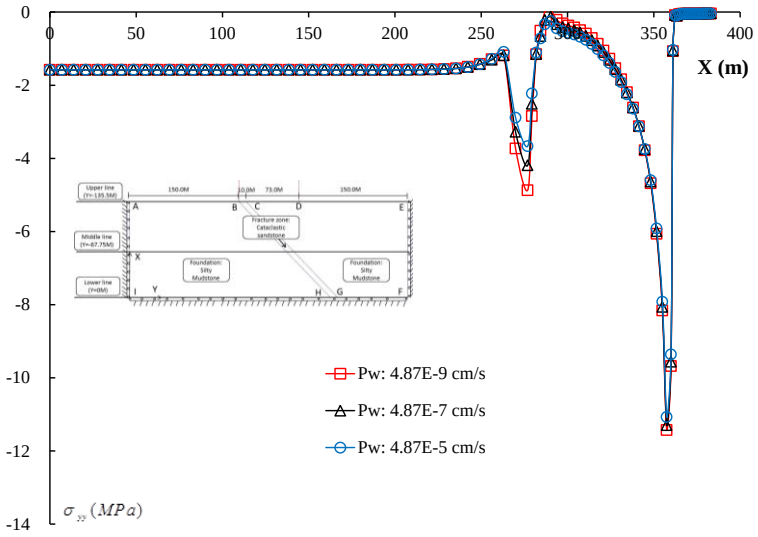

Fig. 4.55 Influence of the permeability of cataclastic sandstone on the vertical stress (upper line of bedrock)

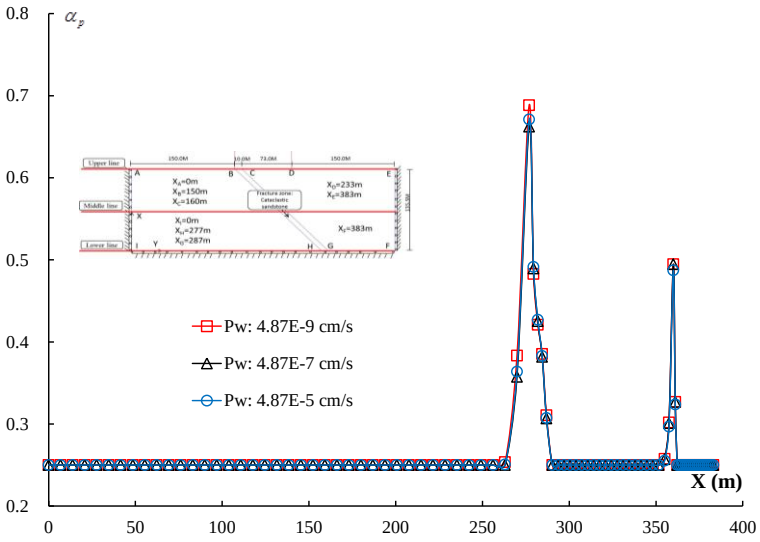

Fig. 4.56 Influence of the permeability of cataclastic sandstone on the hardening parameter α_p (upper line of bedrock)

4.6.4. Influence of creep rate γ

The creep will increase the deformation of the host rock and generate a redistribution of stress and strain field. In this section, the emphasis is put on the influence of viscoplastic behavior. A calculation with different creep rates ($\gamma = 0.0001$) are conducted. The results are compared with that

of reference case. It can be observed that greater displacement and plastic strain are generated in the bedrock when the viscoplastic behavior of material was taken into account. The comparison between different creep rate shows that the amplitude of displacement depends strongly on the creep rate: material deforms more significantly with a greater creep rate (Fig. 4.57-Fig. 4.58). On the other hand, the viscoplastic behavior has significant influence on the evolutions of liquid pressure (Fig. 4.59).The creep releases the stress in the skeleton of the pore media and cause a redistribution of stress in rock(Fig. 4.60-Fig. 4.61). In consequence, the pore pressure decreases more clearly with the increase of creep rate.

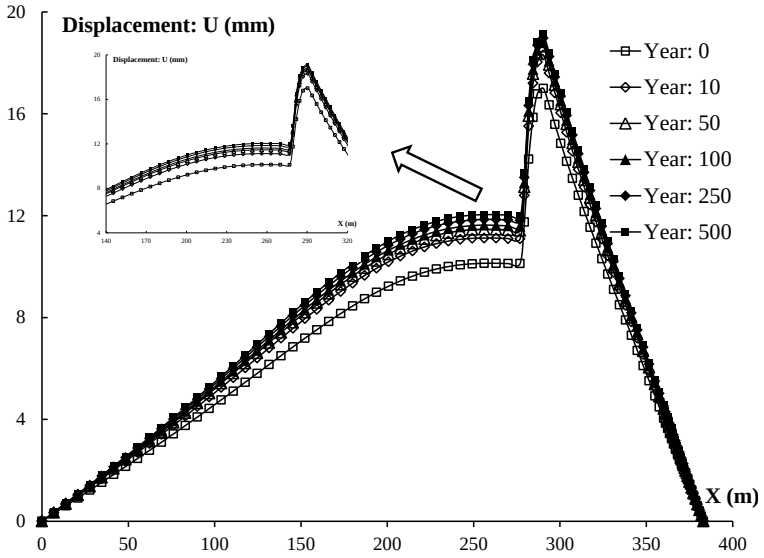

Fig. 4.57 Evolution of horizontal displacement on lower line of the bedrock under high creep rate

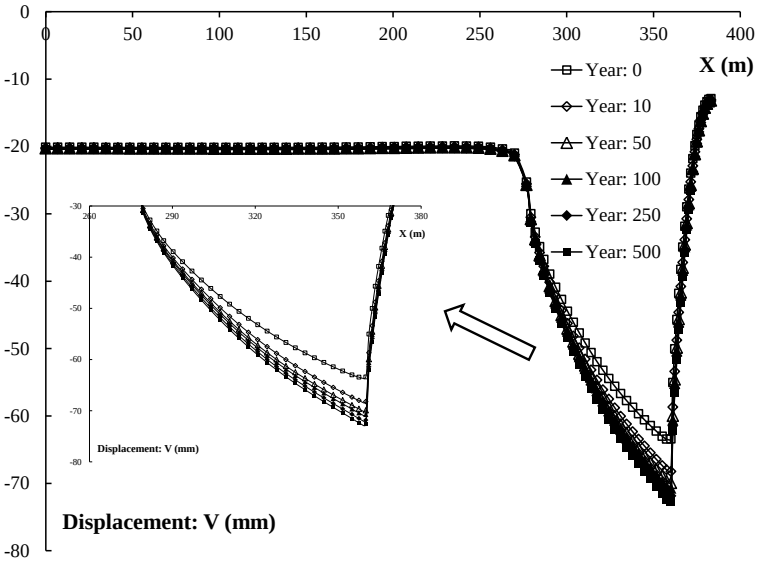

Fig. 4.58 Evolution of vertical displacement on upper line of the bedrock under high creep rate

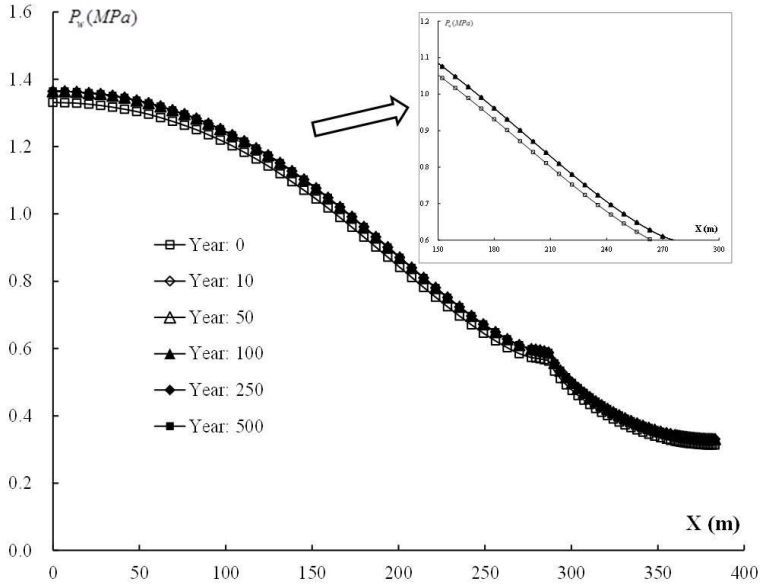

Fig. 4.59 Evolution of liquid pressure on lower line of the bedrock under high creep rate

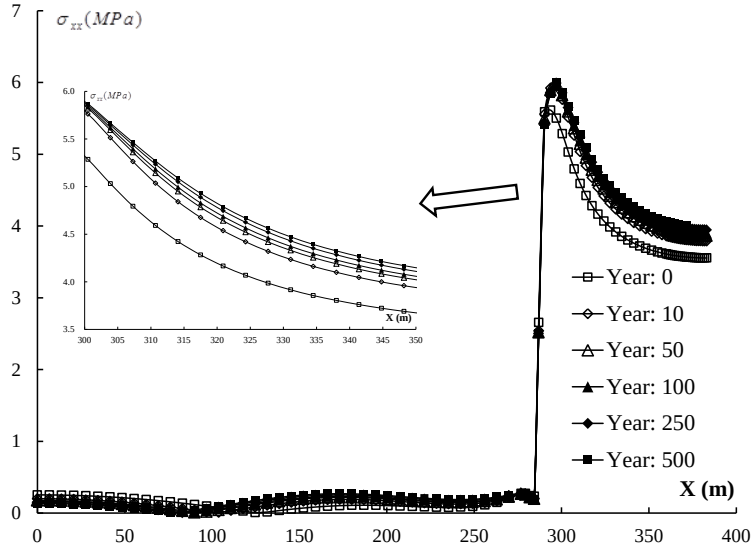

Fig. 4.60 Evolution of horizontal stress on lower line of the bedrock under high creep rate

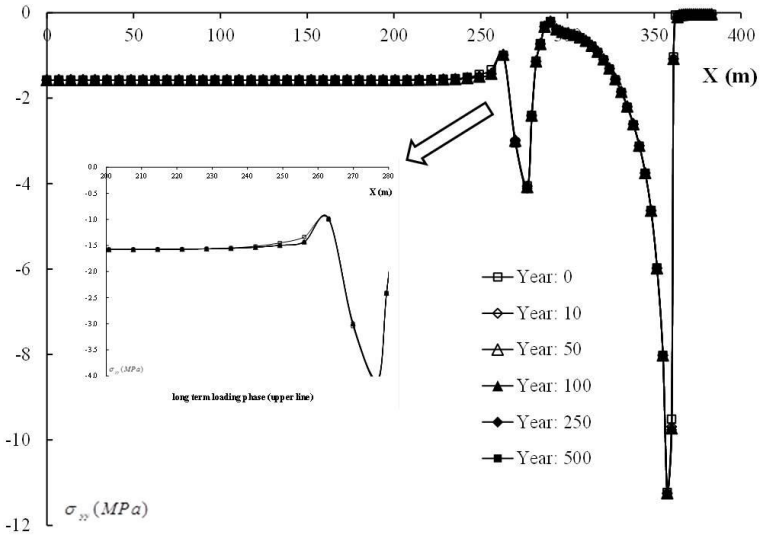

Fig. 4.61 Evolution of vertical stress on upper line of the bedrock under high creep rate

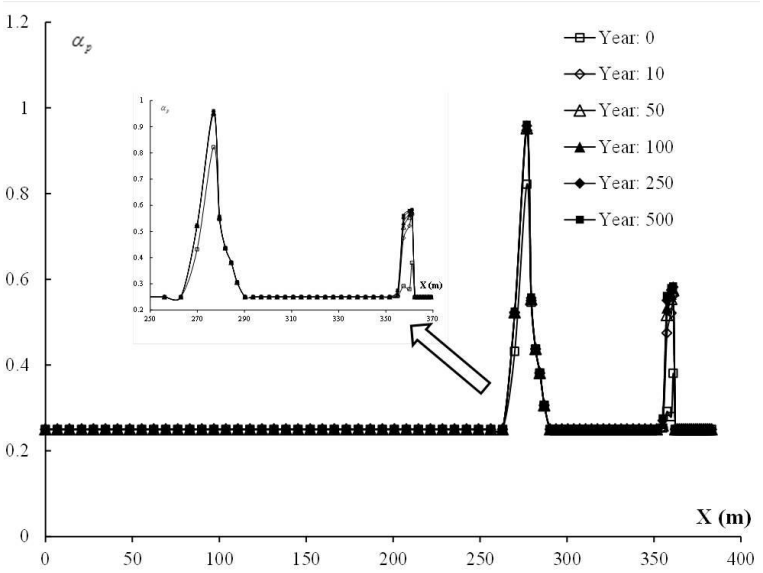

Fig. 4.62 Evolution of hardening parameter α_p on upper line of the bedrock under high creep rate

4.7. Conclusion

The influence of cataclastic sandstone on the stability of dam foundation is studied in this chapter. Based on the numerical analysis and parametric study, one can see that the evolution of pore water pressure in rock is essentially dominated by the permeability and ventilation. The evolution of displacement of rock is essentially controlled by mechanical properties such as elastic modulus, failure surface and imposed stress field. Finally, the consequences of viscoplastic

deformation play an important role on the stability of bedrock.

To ensure the long term stability and safety of the hydropower station, the mechanical strength and stiffness should be enhanced while its permeability should be very low in order to guarantee the good performance of reservoir. In generally, the catacalsitc sandstone can be replaced by a concrete. The numerical results of parametric study can provide some advices on the choice of concrete. Finally, a final numerical calculation has been performed by replacing the cataclastic sandstone by a concrete material. The numerical results of this calculation demonstrate that after replacement the dam foundation and concrete dam body are stable (presented in the annex).

Chapter 5. Conclusions and Perspectives

The study on the short term and long mechanical behaviour of cataclastic sandstone is an important issue in the framework of stability of hydropower station. In this thesis, the mechanical behavior of cataclastic sandstone has been investigated using a series of laboratory tests and numerical simulations. Experimental studies on physical properties and conventional mechanical behaviors of cataclastic sandstone are firstly presented. The creep behavior of cataclastic sandstone is then experimental investigated. Next, the influences of different mechanical properties of rock on the numerical results are discussed. Finally, the obtained series of parameters, which correctly reproduce the experiment measurement, are used to simulate the laboratory tests. The numerical simulation of laboratory tests shows a good agreement with experimental data. Finally, a long term stability of a foundation of hydropower station is analyzed. Based on this study, the following conclusions can be drawn:

It's considered that such rock which belongs to small porosity sandstone has an extremely complex microstructure. The principal mineral compositions are quartz, feldspar and sericite while principal chemical constituent is SiO_2. The chemical erosion is not significant;

According to the short term behaviour of cataclastic sandstone, an important closing of internal micro-cracks is observed in the hydrostatic test. The studied material exhibit a low uniaxial compression strength of order 2.6MPa. In triaxial compression tests,the applied load have a great influence on the rheological fundamental of studied material: increase of peak stress, transition between volumetric compaction and dilatancy and important irreversible deformations. The . The strain-stress curves can be decomposed into three stages: a linear elastic response, a plastic hardening phase and post-peak softening phase.

The cataclastic sandstone presents important time-dependent deformation and the magnitude of creep strain attains 2%. The complete creep curve generally exhibits three phases: a transient creep, steady creep and accelerated creep phase. Moreover, the applied load has an important impact on the kinetic of creep deformation: the strain rate increases with the increase of applied stress while it decreases with the increase of confining pressure.

The obtained permeability coefficient of the studied material is between $2.54*10^{-5}$cm/s and

$1.63*10^{-4}$cm/s under natural state. Moreover, it varies with the evolution of sample deformation. Generally, the permeability of rock decreases progressively with the increase of applied stress and tends to a constant value when applied stress reaches up to a certain level. This phenomenon is related to the volumetric transition from compaction to dilatancy observed in studied material. Furthermore, the permeability change shows some mutation during creep test. But the overall change is decreasing slowly and quasi-linearly at different applied stress owing to continued compaction. The curve of permeability variation is composed of an instantaneous part due to applied stresses and a steady fluid flow part during creep process induced.

Based on the experimental investigation, a unified model is proposed for the descrption of instantaneous and creep behavior of cataclastic sandstone. The instantaneous behaviour of studied material is described by an elastoplastic model while a creep model for time dependent behavior is logically formulated from the extension of elastoplastic model. The creep behavior is numerically simulated by a progressive degradation of elastoplastic properties and failure coefficient of microstructure of studied material. The proposed model contains a small number of parameters which can be determined from conventional triaxial compression tests and a creep test. Comparisons between numerical simulations and test data have been presented for various laboratory tests. In general, a good concordance is obtained between the experimental data and numerical simulations. The main features of studied material have been satisfactorily reproduced by the proposed model, such as irreversible deformations, pressure sensitivity, plastic compressibility-dilation transition and creep. It shows that the proposed model describes the mechanical behavior of cataclastic sandstone quite well. In the further, the proposed model can be extended and used for the description of other time dependent behavior, such as relaxation test, unloading creep test and constant strain rate test of similar rocks.

The long term stability of the bedrock of a hydropower station is studied. The numerical results exhibit that the stability of bedrock is strongly disturbed by the presence of cataclastic sandstone. An important slippage is observed at the interfaces between the cataclastic sandstone and silty mudstone. Moreover, the bedrock is strongly damaged in and around the cataclastic sandstone zone. As the permeability of bedrock material is great, the reservoir water of upstream can reach easily the downstream side. In order to guarantee the long-term stability of the bedrock, it is necessary to

reinforce the cataclastic sandstone zone. In view of this, a series of parametric study have been performed in order to capture the mains parameters for the coupling hydromechanical process in the bedrock. Based on the parametric study, it is suggested to replace the calaclastic sandstone by a concrete.

- As a continue research for the present work, it is possible to suggest a number of perspectives for further experimental, theoretical and applied research along this line:

Accruing to the laboratory tests, the present study mainly focuses on the influence of applied load on the short term and long term mechanical behaviour of cataclastic sandstone. As the studied rock is located in the foundation of hydropower station, it may be interesting to study the influence of other factors, such as hydro-mechanical properties, scale effect and tectonisation degrees on the mechanical behavior of cataclastic sandstone. These tests are quite difficult in laboratory but of practical interests to many engineering problems.

During the exploration phase of hydropower station, the water pressure related to the reservoir varies with climate changes. Moreover, the in-situ observation exhibits an important temperature evaluation in the concrete dam. The results obtained in these tests will be used as basic data in the formulation of the long term thermo-hydro-mechanical coupling constitutive model. For the numerical aspects, only uniform laboratory tests have been simulated in the present work. As most of these tests have been used in the determination of parameters, the comparisons presented between the simulations and experimental data represent only a first phase of validation of the model. Further advanced tests; in particular boundary value problems like hollow cylinder tests and in situ investigations, are still needed to check the general validity of the proposed model.

References:

Andreev G.E. (1995) Brittle failure of rock materials: test results and constitutive models. Rotterdam: Balkema, Netherlands

Bai M., Meng F., Elswroth D., Abousleiman Y., Roegiers J.C. (1993) Numerical modeling of coupled flow and deformation in fractured rock specimens. Int J Numer Anal Methods Geomech. 23: 141-160

Barla G., Debernardi D., Sterpi D. (2012) Time-dependent modeling of tunnels in squeezing conditions. International Journal of Geomechanics 12(6): 697-710

Barton N., Bandis S., Bakhtar K. (1985) Strength, deformation and conductivity coupling of rock joints. Int J Rock Mech. Min. Sci. and Geomech. Abstr. 22(3): 121-140

Bazant Z.P., Xi Y. (1994) Drying creep of concrete: constitutive model and new experiments separating its mechanism. Materials and Structures 27(1): 3-14.

Billiotte J., Yang D.S., Su K. (2008) Experimental study on gas permeability of mudstones. Physics and Chemistry of the Earth 33: 231-236

Brantut N., Heap M.J., Meredith P.G., Baud P. (2013) Time-dependent cracking and brittle creep in crustal rocks: A review. Journal of Structural Geology, 52:17-43

Briffaut M., Benboudjema F., Torrenti J.M., Nahas G. (2012) Concrete early age basic creep: Experiments and test of rheological modelling approaches. Construction and Building Materials, 36: 373-380.

Bodas F.T.M., Potts D.M., Zdravkovic L. (2011) A time dependent constitutive model for soils with isotach viscosity. Computers and Geotechnics 38(6): 809-820.

Bonini M., Debernardi D,. Barla M., Barla G. (2009) The mechanical behaviour of clay shales and implications on the design of tunnels. Rock Mechanics and Rock Engineering 42(2):361-388

Boukharov G.N., Chanda M.W., Boukharov N.G. (1995) The three processes of brittle crystalline rock creep. International Journal of Rock Mechanics & Mining Sciences 32 (4): 325-335.

Bojesen K., J.A., Bjerager, M., Piasecki, S. (2009) Shallow core drilling and petroleum geology related field work in East and North-East Greenland. Geol. Surv. Denmark Greenland Bull.

17: 53-56

Bourgeois F., Shao J.F., Ozanam O. (2002) An elastoplastic model for unsaturated rocks and concrete. Mechanics Research Communications 29: 383-390

Budiansky B., O'Connell R.J. (1976) Elastic moduli of a cracked solid. Int. J. Solids Struct. 12: 81-97

Burgi C. (1999) Cataclastic fault rocks in underground excavations: a geological characterisation. Dissertation, EPF-Lausanne

Burgi C., Parriaux A., Franciosi G., Rey J.-Ph. (1999) Cataclastic rocks in underground structures-terminology and impact on the feasibility of projects (initial results). Engineering Geology 51: 225-235

Caine J.S., Evans J.P., Forster C.B. (1996) Fault zone architecture and permeability structure. Geology 24: 1025-1028

Carter N.L. (1993) Rheology of salt rock. Journal of Structural Geology 15(10): 1257-1272

Chandler Neil A. (2013) Quantifying long-term strength and rock damage properties from plots of shear strain versus volume strain. International Journal of Rock Mechanics and Mining Sciences 59: 105-110

Chan K.S. (1997) A damage mechanics treatment of creep failure in rock salt. International Journal of Damage Mechanics 6(1): 122-152

Chen H., Hu Z.Y. (2003) Some factors affecting the uniaxial strength of weak sandstones. Bulletin of Engineering Geology and the Environment 62: 323-332

Chen X., Liao Z.H., Peng X. (2012) Deformability characteristics of jointed rock masses under uniaxial compression. International Journal of Mining Science and Technology 22: 213-221

Chen Y.J. (2003) Study on the rheological constitutive model of rock and its intelligent identification. Dissertation, Changsha: Central South University, 2003: 1-2. (in Chinese)

Chen Y.L., Azzam R. (2007) Creep fracture of sandstones. Theoretical and Applied Fracture Mechanics 47:57-67

Coussy O (2004) Poromechanics. John Wiley & Sons,UK

Dahou A., Shao J.F., Bederiat M. (1995) Experimental and numerical investigations on transient creep of porous chalk. Mechanics of Materials, 21(1):147-58.

Damjanac B., Fairhurst C. (2010) Evidence for a Long-Term Strength Threshold in Crystalline Rock. Rock Mechanics and Rock Engineering 43: 513-531

David C., Menendez B., Zhu W.L., Wong T. F. (2001) Mechanical Compaction, Microstructures and Permeability Evolution in Sandstones. Phys. Chem. Earth (A) 26(1-2): 45-51

David C., Wong T.F., Zhu W.L. Zhang J.X. (1994) Laboratory measurement of compaction-induced permeability change in porous rocks: Implications for the generation and maintenance of pore pressure excess in the crust. Pure Appl. Geophys. 143: 425-456

De Gennaro V., Delage P., Priol G., Collin F., Cui Y.J. (2004) On the collapse behavior of oil reservoir chalk. Géotechnique 54: 415-420

Dusseault M.B., Fordham.C.J. (1993) Time dependent behaviour of rocks, Comprehensive Rock Engineering: principles, practice and projects. Oxford: Pergamon Press, 119-149.

Elodie S., Christopher A.J. W. (2010) Evolution of cataclastic faulting in high-porosity sandstone, Bassin du Sud-Est, Provence, France. Journal of Structural Geology 32(11): 1590-1608

Fabre G, Pellet F. (2006) Creep and time-dependent damage in argillaceous rocks. International Journal of Rock Mechanics & Mining Sciences, 43 (1): 950-960

Fischer G.J., Paterson M.S. (1989) Dilatancy during rock deformation at high temperatures and pressures. J. Geophys. Res. 78: 607-617

Fujii Y., Kiyama T., Ishijima Y., Kodam J. (1999) Circumferential strain behavior during creep tests of brittle rocks. International Journal of Rock Mechanics and Mining Sciences 36: 323±337

Gudmundsson A., Simmenes T. H., Belinda L., Sonja L.P. (2010) Effects of internal structure and local stresses on fracture propagation, deflection, and arrest in fault zones. Journal of Structural Geology 32: 1643-1655

Gutierrez M., Lewis R. (2002) Coupling of fluid flow and deformation in underground formations. J. Eng. Mech. 128(7): 779-787

Habimana J., Labiouseb V., Descoeudres F. (2002) Geomechanical characterisation of cataclastic rocks: experience from the Cleuson-Dixence project. International Journal of Rock Mechanics & Mining Sciences 39: 677-693

Haimson B. (2006) True triaxial stresses and the brittle fracture of rock. Rock Damage and Fluid Transport, Part I 163, 1101-1130

Haupt P., Kersten T. (2003) On the modelling of anisotropic material behaviour in viscoplasticity. International Journal of Plasticity 19, 1885-1915.

Heiland J. (2003) Laboratory testing of coupled hydro-mechanical processes during rock deformation. Hydrogeology Journal 11: 122-141

Heiland J., Raab S. (2001) Experimental investigation of the influence of differential stress on permeability of a Lower Per mian (Rotliegend) sandstone deformed in the brittle deformation field. Phys Chem Earth. 26(1-2): 33-38

Hicks T.W., Pine R.J., Willis R.J. (1996) A hydro-thermomechanical numerical model for HDR geothermal reservoir evaluation. Int J Rock Mech Min Sci Geomech Abstr. 33(5): 499-511

Homand S., Shao J.F. (2000). Mechanical behavior of a porous chalk and water/chalk interaction., Part I: Experimental study. Oil Gas Sci. Technol. 55: 591-598

Homand F., More E., Henry J.P., Cuxac P., Hammade E. (1993) Characterization of the moduli of elasticity of an anisotropic rock using dynamic and static methods. International Journal of Rock Mechanics and Mining Sciences & Geomechanics Abstracts 30(5): 527–535

Horsrund P., Holt R.M., Sonstebo E.F.. (1994) Time dependent borehole stability: laboratory studies and numerical simulation of different mechanism in shale[C]//. Proc. Eurock SPE/ISRM 94. Rotterdam: Balkema, 259-266.

Hudson J.A., Harrison J.P. (1997) Engineering rock mechanics: an introduction to the principles. Oxford, Elsevier, 106-111

Jaeger J.C., Cook N.G.W., Zimmerman R.W. (2007) Fundamentals of rock mechanics, 4th edition. Blackwell, Oxford

Jiang T., Shao J.F., Xu W.Y., Zhou C.B. (2010) Experimental investigation and micromechanical analysis of damage and Permeability variation in brittle rocks. International Journal of Rock Mechanics & Mining Sciences 47: 703-713

Jia Y., Bian H.B., Su K., Kondo D., Shao J.F. (2010) Elastoplastic damage modeling of desaturationand resaturation in argillites. International Journal for Numerical and Analytical Methods in Geomechanics 34 (2): 187-220

Kiyama T, Kita H, Ishijima Y, Yanagidani T, Aoki K, Sato T. (1996) Permeability in anisotropic granite under hydrostatic compression and triaxial compression including post-failure

region. In: Aubertin M, Hassani F, Mitri H, editors. Rock mechanics tools and techniques, NARMS'96, Rotterdam: Balkema, 1643-1650.

Lewis R.W, Schrefler B.A (1998) The Finite Element Method in the Static and Dynamic Deformation and Consolidation of Porous Media. John Wiley

Li L.Q. (2009) Study on rhelolgical mechanics characteristics and rhelolgical deformation of rocks in large-scale underground caverns of hydropower station. Dissertation, hohai university (in chinese)

Li D.Y., Wong L.N.Y., Liu G., Zhang X.P. (2012) Influence of water content and anisotropy on the strength and deformability of low porosity meta-sedimentary rocks under triaxial compression. Engineering Geology 126: 46-66

Li Y.P., Wang Z.Y., Tang M.M., Wang Y. (2008) Relations of complete creep processes and triaxial stressstrain curves of rock. Journal of Central South University of Technology, 15(1): 311-315.

Li Y.S., Xia C.C. (2000) Time-dependent tests on intact rocks in uniaxial compression. International Journal of Rock Mechanics & Mining Sciences 37(1): 467-475

Lori A. K., James K. R. (2012) Cataclastic production of volcanic ash at Mount Saint Helens. Physics and Chemistry of the Earth, Parts A/B/C 45:40-49

Lu Y.F., Tian B., Huang W.J., Shao J.F. (2005) Laboratory study of sandstone with large porosity. J. of Hust. (Urban Science Edition) 22: 56-58

Maranini E., Brignoli M. (1999) Creep behaviour of a weak rock: experimental characterization. International Journal of Rock Mechanics & Mining Sciences 36(1): 127-138

Ma L. (2004) Experimental investigation of time dependent behavior of welded Topopah Spring tuff. Dissertation, University of Nevada

Ma L., Daemen J. J. K. (2006) An experimental study on creep of welded tuff, International Journal of Rock Mechanics & Mining Sciences 43(1): 282-291

Martin CD. (1993) The strength of massive Lac du Bonnet granite around underground openings. PhD thesis. Winnipeg: University of Manitoba; 1993.

Martin C.D., Chandler N.A. (1994) The progressive fracture of Lac du Bonnet granite Int J Rock Mech Min Sci, 31 (6) :643–659

Meerea P. A., Mulchrone K.F. (2003) The effect of sample size on geological strain estimation from passively deformed clastic sedimentary rocks. Journal of Structural Geology 25: 1587-1595

Millard A., Rejeb A., Chijimatsu M., Jing L., De Jonge J., Kohlmeier M., Nguyen T.S., Rutqvist J., Souley M., Sugita Y. (2005) Numerical study of the THM effects on the near field safety of a hypothetical nuclear waste repository-BMT1 of the DECOVALEX III project. Part 2: Effects of THM coupling in continuous and homogeneous rocks. Int J Rock Mech Mining Sci & Geomech Abstr. 42: 731-744

Mogi K. (2007). Experimental Rock Mechanics. Taylor & Francis, London

Ngwenya B.T., Kwon O., Elphick S.C., Main I.G. (2003) Permeability evolution during progressive development of deformation bands in porous sandstones. J Geophys Res. 108 (B7): 2343-2357

Nur A., Yilmaz O. (2006) SP profiles in fractured rocks. Geophys. Prospect. 42(6): 493-714.

Pacheco A. (1990) A method for evaluating transient creep. Dissertation, Canada: University of Alberta.

Pietruszczak S., Lydzba D., Shao J.F. (2002) Modelling of inherent anisotropy in sedimentary rocks. International Journal of Solids and Structures 39:637-648.

Pietruszczak S., Lydzba D., Shao J.F. (2004) Description of creep in frictional materials in terms of microstructure evolution. Journal of Engineering Mechanics 130 (6): 681-690

Read R.S. (2004) Twenty years of excavation response studies at AECL's Underground Research Laboratory Int J Rock Mech Min Sci, 41 (8): 1251-1275

Renner J., Rummel F. (1996) The effect of experimental and micro-structural parameters on the transition from brittle failure to cataclastic flow of carbonate rocks. Tectonophysics 258: 151-169

Rudnicki J.W., Rice. J.R. (1975) Conditions for the localization of detormation in pressure-sensitive dilatant materials. J. Mech. Phys. Solids 23: 371-394

Saleeb A.F., Arnold S.M. (2004) Specific hardening function definition and characterization of a multi mechanism generalized potential-based viscoelastoplasticity model. International Journal of Plasticity 20: 2111-2142

Shao J.F., Zhou H., Chau K.T. (2005) Coupling between anisotropic damage and permeability

variation in brittle rocks. Int J Numer Anal Methods Geomech 29: 1231-1247

Shao J.F., Zhu Q.Z., Su K. (2003) Modeling of creep in rock materials in terms of material degradation. Computers and Geotechnics 30: 549-555.

Shao J.F., Jia Y., Kondo D., Chiarelli A.S. (2006) A coupled elastoplastic damage model for semi-brittle materials and extension to unsaturated conditions. Mechanics of Materials 38 218-232

Song I., Suh M., Woo Y.K., Hao T.(2004) Determination of the elastic modulus set of foliated rocks from ultrasonic velocity measurements. Engineering Geology 72,(3-4): 293-308

Souley M., Homand F., Pepa S., Hoxha D. (2001) Damage-induce permeability change in granite: a case study at the URL in canada. Int J Rock Mech Min Sci, 38(2):297-310.

Tang C.A., Tham L.G., Lee P.K.K., Yang T.H, Li L.C. (2002) Coupled analysis of flow, stress and damage(FSD) in rock failure. Int. J. Rock Mech. & Min. Sci. 39: 477-489.

Tsai L.S., Hsieh Y.M., Weng M.C., Huang T.H., Jeng F.S. (2008) Time-dependent deformation behaviors of weak sandstones. International Journal of Rock Mechanics & Mining Sciences 45: 144-154

Uehara S., Shimamoto T. (2004) Gas permeability evolution of cataclasite and fault gouge in triaxial compression and implications for changes in fault-zone permeability structure through the earthquake cycle. Tectonophysics 378: 183-195

Voyiadjis G., AlRub R., Palazotto A. (2004) Thermodynamic framework for coupling of non-local viscoplasticity and non-local anisotropic viscodamage for dynamic localization problems using gradient theory. International Journal of Plasticity 20, 981-1038

Wang H.X., Wang G., Chen Z.X., Wong R.C.K. (2010) Deformational characteristics of rock in low permeable reservoir and their effect on permeability. Journal of Petroleum Science and Engineering 75: 240-243

Wang H.L., Xu W.Y., Shao J.F. (2013) Experimental Researches on Hydro-Mechanical Properties of Altered Rock Under Confining Pressures. Rock Mech Rock Eng DOI 10.1007/s00603-013- 0439-y

Wang H.L., Xu W.Y.. (2013) Permeability evolution laws and equations during the course of deformation and failure of brittle rock. Journal of Engineering Mechanics. doi:10.1061/(ASCE) EM.1943-7889.0000608

Wibberley C.A.J., Shimamoto T. (2003) Internal structure and permeability of major strike-slip fault zones: the Median Tectonic Line in Mie Prefecture, Southwest Japan. Journal of Structural Geology 25: 59-78

Xie S.Y., Shao J.F. (2006) Elastoplastic deformation of a porous rock and water interaction. International Journal of Plasticity 22: 2195-2225

Xie S.Y., Shao J. F. (2014) An Experimental Study and Constitutive Modeling of Saturated Porous Rocks. Rock Mechanics and Rock Engineering DOI 10.1007/s00603-014-0561-5

Xiong Y.B., Chen J.J., Hu Y.L. , Wang W.P. (2012) Study on the key parameters of the Johnson-Holmquist constitutive model for concrete. Engineering mechanics. 29(1): 121-127.

Xu W.Y., Nie W.P., Zhou X.Q., Shi C., Wang W., Feng S.R. (2011) Long-term stability analysis of large-scale underground plant of Xiang-jiaba hydro-power station. Journal of Central South University of Technology, 18(1): 511-520.

Xu W.Y., Wang R.B., Wang W., Zhang Z.L., Zhang J.C., Wang W.Y. (2012) Creep properties and permeability evolution in triaxial rheological tests of hard rock in dam foundation. Journal of Central South University of Technology, 19(1): 252-261.

Yin J. H., Graham J. (1994) Equivalent times and one dimensional elastic viscoplastic modeling of time dependent stress strain behavior of clays. Canadian Geotechnical Journal 31: 42-52

Yin, J.H., Tong, F. (2011) Constitutive Modelling of the Time-dependent Stress-strain Behaviour of Saturated Soils Exhibiting both Creep and Swelling. Canadian Geotechnical Journal 48(12): 1870-1885

Yang C.H., Daemen J. J. K., Yin J.H. (1999) Experimental investigation of creep behavior of salt rock. International Journal of Rock Mechanics & Mining Sciences 36(2): 233-242

Yang D.S., Billiotte J., Su K. (2010) Characterization of the hydro-mechanical behavior of argillaceous rocks with effective gas permeability under DS Engineering Geology 114: 116-122

Yang S.Q., Jiang Y.Z., Xu W.Y., Chen X.Q. (2008) Experimental investigation on strength and failure behavior of pre-cracked marble under conventional triaxial compression. International Journal of Solids and Structures 45: 4796-4819

Yang S.Q., Jiang Y.Z. (2010) Triaxial mechanical creep behavior of sandstone. Mining Science

and Technology 20(3): 339-349

Yang W.D., Zhang Q.Y., Li S.C., Wang S.G. (2014) Time-Dependent Behavior of Diabase and a Nonlinear Creep Model. Rock Mechanics and Rock Engineering DOI 10.1007/s00603-013-0478-4

Yasuhara H., Polak A., Mitani Y., Grader A., Halleck P.M., Elsworth D. (2006). Evolution of fracture permeability through fluid-rock reaction under hydrothermal conditions. Earth and Planetary Science Letters 244: 186-200

Zhang H.B., Wang Z.Y., Zheng Y.L., Duan P.J., Ding S.L. (2012) Study on tri-axial creep experiment and constitutive relation of different rock salt. Safety Science 50: 801-805

Zhang J., Standifird W.B., Roegiers J.C., Zhang Y. (2007) Stress dependent fluid flow and permeability in fractured media: from lab experiments to engineering applications. Rock Mech Rock Eng 40(1):3-21

Zhao Y.L., Cao P., WANG W.J., Wan W., Liu Y.K. (2009) Viscoelasto-plastic rheological experiment under circular increment step load and unload and nonlinear creep model of soft rocks. Journal of Central South University of Technology, 16(1): 488-494.

Zhang Y., Xu W.Y., Gu J.J., Wang W. (2013) Triaxial creep tests of weak sandstone from the deflection zone of high dam foundation. Journal of Central South University of Technology 20: 2528-2536.

Zhang Z.L., Xu W.Y., Wang W. (2012) Triaxial creep tests of rock from the compressive zone of dam foundation in Xiang-jiaba Hydropower Station, International Journal of Rock Mechanics and Mining Sciences 50(1): 133-139

Zhou H. (2003) Mechanical and hydraulic behaviour of salt in the excavation disturbed zone around underground facilities. Int J Rock Mech Min Sci 40(5): 725-738

Zhou H., Bian H.B., Jia Y., Shao J.F. (2013) Elastoplastic damage modeling the mechanical behavior of rock-like materials considering confining pressure dependency. Mechanics Research Communications 53: 1-8

Zhou H.W., Wang C.P., Han B.B., Duan Z.Q. (2011) A creep constitutive model for salt rock based on fractional derivatives. International Journal of Rock Mechanics&Mining Sciences 48: 116-121

Zhu W., Wong T. (1997) The transition from brittle faulting to cataclastic flow: permeability evolution. J Geophys Res 102: 3027-3041.